Innovative Design of a Soft Robotic Gripper for In-hand Manipulation

Amir Pagoli

Université Clermont Auvergne

École Doctorale Sciences Pour l'Ingénieur

Thèse

Presented by

Amir Pagoli

Required for the Degree of

Docteur d'Université

Specialty: Génie Mécanique

Innovative Design of a Soft Robotic Gripper for In-hand Manipulation

---

Publicly presented on 07, 12, 2021 before the jury composed of:

Dr. Pierre Renaud	Professor, INSA Strasbourg	Rapporteur
Dr. Jean-Pierre Gazeau	Research Engineer HDR, CNRS	Rapporteur
Dr. Véronique Perdereau	Professor, Sorbonne Université	Examiner
Dr. Kaspar Althoefer	Professor, Queen Mary University	Examiner
Dr. Frédéric Chapelle	Assoc. Prof., HDR, Clermont Auvergne INP	Co-supervisor
Dr. J. Corrales-Ramón	Assoc. Prof., Universidade de Santiago de Compostela	Co-supervisor
Dr. Youcef Mezouar	Professor, Clermont Auvergne INP	Co-supervisor
Dr. Yuri Lapusta	Professor, Clermont Auvergne INP	Co-supervisor

Institut Pascal - M3G/ISPR departments

UMR 6602 CNRS/UCA/SIGMA Clermont, F-63000 Clermont-Ferrand, France

Lovingly dedicated to
my beautiful wife, **ELI**

Résumé

Ce document est une dissertation en format multi-articles sur la conception, l'optimisation et la fabrication d'actionneurs pneumatiques souples pour des applications robotiques souples. Introduite comme une nouvelle technologie ces dernières années, la robotique souple ouvre de nouveaux horizons dans le domaine de la robotique grâce à des caractéristiques prometteuses telles que l'adaptabilité, la légèreté, la facilité d'assemblage et le faible coût pour réaliser des configurations complexes dans divers environnements. Même s'il existe une grande diversité d'applications pour les SFA, de nombreux défis subsistent dans ce domaine, notamment le contrôle de la rigidité et de la forme de flexion. Pour illustrer les applications méthodologiques et théoriques actuelles des systèmes robotiques souples, le premier article présente une revue systématique des actionneurs fluidiques souples qui ont tenté de relever les défis critiques en matière de matériaux souples et actifs, de méthodes de traitement, d'architectures de préhension, de capteurs et de méthodes de contrôle. Différents modèles constitutifs de matériaux en silicone proposés et testés dans la littérature sont régénérés par le logiciel ABAQUS afin de comparer les données de déformation et de contrainte réelles issues des modèles constitutifs avec les données d'essai de traction standard basées sur la norme ASTM412. Cet article montre que la plupart de ces modèles peuvent prédire le modèle du matériau de manière acceptable dans une petite gamme de données de contrainte-déformation. Mais pour de grandes valeurs de contrainte-déformation, quelques-uns d'entre eux prédisent le comportement du matériau silicone avec précision. Le deuxième article présente un nouveau type de doigt souple avec une articulation mobile à commande pneumatique basée sur le contrôle du point de flexion et une rigidité variable. Le doigt proposé est plus flexible que les solutions précédentes en termes d'espace 3D atteignable et de forces de contact applicables au bout du doigt en changeant la position de son articulation, et donc, le point de flexion. La méthode des éléments finis et l'algorithme NSGA-II sont appliqués

pour optimiser la géométrie de l'articulation afin de maximiser l'angle de flexion et de minimiser les dimensions de l'articulation. Le troisième article de cette thèse se concentre sur le développement d'un nouveau type de pince souple dextre avec trois doigts reconfigurables et une paume active améliorant les capacités de manipulation manuelle. Dans chaque doigt, le point de flexion et la longueur de manipulation effective peuvent être modifiés et contrôlés en déplaçant une tige rigide insérée dans le trou central du doigt. La capacité de manipulation manuelle de cette pince robotique souple est validée par différents tests expérimentaux, notamment la rotation, le saisir et le roulement. Par conséquent, deux types de palmes à vide (ventouse et particules granulaires) sont utilisés pour garantir une large gamme de tâches de manipulation d'objets que les préhenseurs souples proposés précédemment ne peuvent pas complètement réaliser. Dans le dernier chapitre de cette thèse, le quatrième article propose un capteur tactile peu coûteux et facile à fabriquer pour une application de robot souple. Il est très flexible et facile à utiliser, ce qui en fait un choix approprié pour les applications de robots mous. La plupart des matériaux (encre conductrice, silicone, carte de contrôle) utilisés dans la fabrication de ce capteur sont peu coûteux et peuvent être trouvés facilement sur le marché. Le capteur capacitif proposé peut détecter la position et la force appliquée en mesurant la charge électrique des électrodes. En raison des incertitudes et des bruits, un réseau neuronal artificiel est proposé pour calibrer la force correspondant à la tension produite.

ABSTRACT

This document is a multiple-article format dissertation investigating the design, optimization, and fabrication of soft pneumatic actuators (SFAs) for soft robotic applications. Introduced as a novel technology in recent years, soft robotics broadens new horizons in robotics thanks to promising characteristics such as adaptability, lightweight, less assembly, and low cost to perform complicated configurations in various environments. Even though there is a large diversity of applications for SFAs, many challenges remain in this field, including stiffness and bending shape control. To illustrate the current methodological and theoretical applications of soft robotic systems, the first article presents a systematic review of soft fluidic actuators that tried to address the critical challenges in soft and active materials, processing methods, gripper architectures, sensors, and control methods. Different constitutive models of silicone materials proposed and tested in the literature are regenerated by ABAQUS software to compare the engineering and true strain-stress data from the constitutive models with standard uniaxial tensile test data based on ASTM412. This paper shows that most of these models can predict the material model acceptably in a small range of stress-strain data. But for large strain-stress values, a few of them predict the behavior of the silicone material accurately. The second article presents a novel type of soft finger with a pneumatic-actuated movable joint based on bending point control and variable stiffness. The proposed finger is more flexible than previous solutions in terms of the attainable 3D space and applicable contact forces at the fingertip by changing the position of its joint, and thus, the bending point. The finite element method (FEM) and NSGA-II algorithm are applied to optimize the

joint geometry to maximize the bending angle and minimize the joint dimensions. The third article in this dissertation is focused on developing a new type of dexterous soft gripper with three reconfigurable fingers and an active palm enhancing in-hand manipulation capabilities. In each finger, the bending point and the effective manipulation length can be changed and controlled by moving a stiff rod inserted inside the center hole of the finger. The in-hand manipulation capability of this soft robotic gripper is validated by different experimental tests, including rotation, regrasping, and rolling. Therefore, two types of vacuum palms (suction cup and granular particles) are utilized to guarantee a wide range of object manipulation tasks that previously suggested soft grippers cannot completely perform. In the final chapter of this dissertation, the fourth article proposed a low-cost, easy fabrication tactile sensor for soft robot application. It is very flexible and easy-use which make it an appropriate choice for soft robot application. Most of the materials (conductive ink, silicone, control board) used in the fabrication of this sensor are inexpensive and can be found easily in the market. The proposed capacitive sensor can detect the position and applied force by measuring the electric charge of the electrodes. Due to the uncertainties and noises, an Artificial neural network is suggested to calibrate the force corresponding to the produced voltage.

Acknowledgment

I would like to express my sincerest gratitude to my supervisors, Professor Yuri Lapusta, Prof. Youcef Mezouar, Dr. Frédéric Chapelle and Dr. Juan-Antonio Corrales-Ramón for their valuable guidance, motivating and inspiring advice, remarkable support and patience on my way through exploring this exciting project. Their encouragement and reliable support helped me overcome all the difficulties throughout this research. The completion of this project would not have been possible without their guidance and assistance.

I would like to thank all my dissertation committee members: Prof. Pierre Renaud, Dr. Jean-Pierre Gazeau, Prof. Kaspar Althoefer and Prof. Véronique Perdereau. I sincerely appreciate your constructive and thoughtful feedback on my dissertation. Each member of my committee provided guidance in their respective areas of expertise that helped bolster both my dissertation and interests in new fields. I am extremely grateful for the time they committed to helping me shape the focus of my work.

Special acknowledgements are extended to the French government research program (CAP2025) for the financial support of this project.

I would like to extend my gratitude to my parents and sisters. Your love, support, and encouragement have been a blessing throughout this process. Thank you for your love, support, guidance, comfort, and protection throughout the years.

Most of all, I would like to acknowledge the support of my wife, Eli, Thank you for your love, encouragement, and support throughout this process. You believed in me, and I am grateful for that! Your accomplishments, hard work, dedication, and intelligence are inspiring.

Table of contents

Table of figures

Table of tables

Chapter 1: General Introduction

1.1. Foreword

This dissertation has received funding from the French government research program “Investissements d'Avenir” through the IDEX-ISITE initiative 16-IDEX-0001 (CAP20-25). It was prepared at the Institut Pascal laboratory within the M3G department (Mechanics, Mechanical Engineering, Civil Engineering, Industrial Engineering) and ISPR (Image, Systèmes de Perception, Robotique). It is a multidisciplinary thesis, which is part of four themes of the department: MACCS (Modélisation, Autonomie et Contrôle dans les Systèmes Complexes), MRSI (Machines, Robots, and Industrial Systems), MatInn (Innovative Materials). The objective is to design a soft robotic gripper with innovative materials capable of in-hand manipulation. The thesis work was carried out at Institut Pascal and SIGMA Clermont, which allowed exploiting the machines available at the CTT (Centre de Transfert Technologique: mechanical platform of SIGMA Clermont) to manufacture the prototype. Various fruitful contributions have already been highlighted by a journal article in Smart Materials and Structures (SMS), Robotics & Automation Magazine (RAM), IEEE Robotics and Automation Letters (RAL), and presented in ICRA2021 and IROS2021 conferences. There are also contributions to the 29th international workshop on computational mechanics of materials workshop 2019 in Croatia and the French Robotics Workshop 2019 organized by the GDR Robotique.

1.2. Introduction and Motivation

Soft robots open a new era in the robotic field. For many decades, scientists tried to bring their robot design closer to the human body's performance. Conventional robots are rigid and rough. They are designed to work in specific environments and satisfy a task recurrently with high precision. Though these manipulators are very effective in many industries such as the automotive area, they have some limitations, such as low maneuverability or insufficient DOFs (Degrees of Freedom), restricting their movements in a given workspace. Inspired by nature, soft robots emerged and reduced the gap of human interaction in robotic environments. Additionally, they provide new interesting capacities compared to the other robotic architectures; for instance, soft robots are more deformable and capable of maneuvering through congested spaces without inducing stress concentrations or damaging. One of the most widely used actuating technologies for soft robotics is Fluid Elastomer Actuation (FEA), powered by a pressurized fluid (gas or

liquid) [1]. Due to many advantages of FEAs, including easy fabrication, producing high forces, large strokes, and low-cost elastomer materials [2], they have been used in numerous configurations for various purposes, such as locomotion [3], manipulation [4], medical applications [5], and wearable devices [6]. FEAs can generate high forces proportional to the pressure of the fluid and the surface area where the active pressure is applied. Large strokes, very little friction, and distributed forces can be produced [7], also thanks to 3D printing technology to enhance mold design with the advantages of fast and precise fabrication [8]. Employing 3D printing technology, faster and more reliable molds can be developed. Even though these soft actuators have various applications, many challenges remain in this field, including stiffness control and shape configuration. Several types of research have increased the performance of these kinds of actuators by integrating them with other types of actuation methods that help FEAs in terms of shape control and variable stiffness. Consequently, it is necessary to advance, innovate and optimize a low-cost, soft actuator to accomplish various tasks, as will be conducted in this thesis.

1.3. Principal Contributions

This study presented several contributions in the field of soft pneumatic actuators. Different tasks such as design, fabrication, and experimental evaluation tests have been conducted. The overall research technical insights and contributions methodology during the various stages of this thesis can be outlined as follows

- Conduct a comprehensive literature review considering soft materials, soft actuators, sensing technology, modeling, and control in the field of soft robotic systems. This study helps to recognize profoundly current research efforts.
- We characterized a new classification of soft fluidic actuators (SFAs) based on the applied pressure for three mains categories: soft pressurized fluidic actuators (SPFAs), soft vacuumed fluid actuators (SVFAs), and hybrid mechanisms including a combination of SFA with the other existing types of soft actuators
- The mechanical behaviors of hyperelastic materials were studied theoretically to characterize differences between the constitutive equations. ABAQUS software was utilized to regenerate the strain-stress data of each article and depicted it in two different graphs, representing engineering strain-stress and true strain-stress for the

most popular silicone rubbers. We then compare them with standard uniaxial tensile test data based on ASTM412.

- An innovative variable stiffness soft finger with a fluid-actuated movable joint was introduced and optimized in terms of its main characteristics. The variable length of the finger with the capability of bending in different directions results in more dexterity of the finger dealing with a target inside its 3D workspace by increasing the number of possible configurations. Furthermore, the finger can apply a wide range of force to the fingertip thanks to the movable joint design.
- The finite element method (FEM) and experiments were conducted to optimize the joint geometry, maximize the bending angle, and minimize the joint dimensions. Furthermore, the sensitivity of each design parameter and the consequent effects on the optimization objectives are also analyzed.
- Design and fabrication of a dexterous soft robotic gripper with three fingers and an active palm capable of performing in-hand manipulation purposes were leaded. The effective length of each finger can be changed. This reconfigurability provides a more accessible workspace than conventional soft grippers. Besides, a large diversity of the finger's shape configurations results in more dexterity and in-hand manipulation capability.
- Design of an active palm for secure grasping like human manipulation, significantly enhancing in-hand manipulation capabilities. An active palm enables us to complete the in-hand manipulation task without taking advantage of the ground or gravity to fix or support the object when the palm is above the object, which is more like human in-hand manipulation. Besides, the palm provides a reliable grasping approach of the broader range of objects weights.
- A soft, low-cost, large-area covering capacitive sensor was proposed to expand fully compliant soft robotics applications.

1.4. The Organization of the Manuscript

This manuscript is organized into five chapters based on the accepted papers, as shown in Figure 1.1. Following this introductory chapter, an extensive literature review paper is presented in Chapter 1, which reviews soft fluidic actuators: classification and materials modeling analysis. This paper is published in the Smart Materials and Structures (SMS) journal. Chapter 2 presents the second paper with the design and optimization of a

soft reconfigurable robotic finger with a sliding, rotating, and bending pneumatic actuator, published in IEEE Robotics & Automation Magazine (RAM) and presented at ICRA2021 conference. Chapter 3 presents the third paper with the title of a soft robotic gripper with an active palm and reconfigurable fingers for fully dexterous in-hand manipulation. This paper is accepted for IEEE Robotics and Automation Letters (RAL) journal and presented at the IROS2021 conference. Chapter 4 demonstrates a large area covering soft capacitive sensor for soft robot applications. Finally, Chapter 5 presents the major findings and conclusions of this work, alongside suggestions for future research.

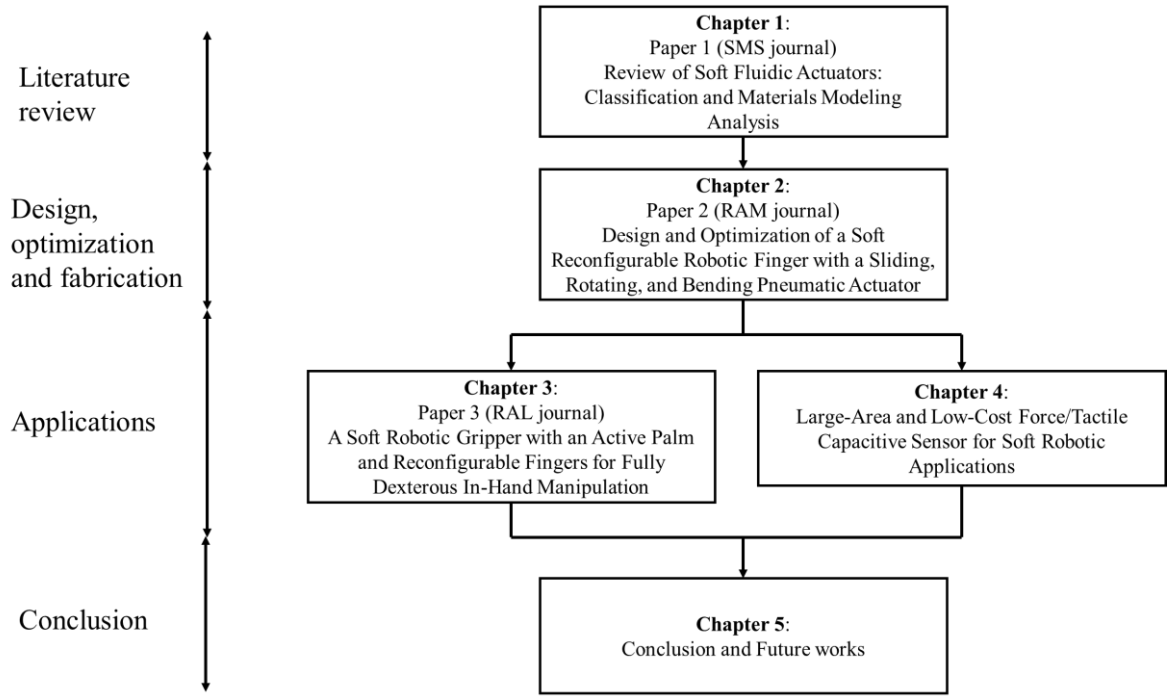

Figure 1.1. Flowchart of the thesis outline

I

Chapter 2: Paper #1

Review of Soft Fluidic Actuators: Classification and Materials Modeling Analysis

DOI:

https://doi.org/10.1088/1361-665X/ac383a

Published in:

Smart Materials and Structures journal

2.1. Abstract

Soft actuators can be classified into five categories: tendon-driven actuators, electroactive polymers (EAPs), shape-memory materials, soft fluidic actuators (SFAs), and hybrid actuators. The characteristics and potential challenges of each class are explained at the beginning of this review. Furthermore, recent advances especially focusing on soft fluidic actuators (SFAs) are illustrated. There are already some impressive SFA designs to be found in the literature, constituting a fundamental basis for design and inspiration. The goal of this review is to address the latest innovative designs for SFAs and their challenges and improvements with respect to previous generations, and help researchers to select appropriate materials for their application. We suggest seven influential designs: pneumatic artificial muscles (PAM), PneuNet, continuum arm, universal granular gripper, origami soft structure, vacuum-actuated muscle-inspired pneumatic (VAMPs), and Hydraulically amplified self-healing electrostatic (HASEL). The hybrid design of SFAs for improved functionality and shape controllability is also considered. Modeling SFAs, based on previous research, can be classified into three main groups: analytical methods, numerical methods, and model-free methods. We demonstrate the latest advances and potential challenges in each category. Regarding the fact that the performance of soft actuators is dependent on material selection, we then focus on the behaviors and mechanical properties of the various types of silicone which can be found in the SFA literature. For a better comparison of the different constitutive models of silicone materials which have been proposed and tested in the literature, ABAQUS software is here employed to generate the engineering and true strain-stress data from the constitutive models, and compare them with standard uniaxial tensile test data based on ASTM412. Although the figures presented show that in a small range of stress-strain data, most of these models can predict the material model acceptably, few of them predict it accurately for large strain-stress values. Sensor technology integrated into SFAs is also being developed, and has the potential to increase controllability and observability by detecting a wide variety of data such as curvature, tactile contacts, produced force, and pressure values.

Keywords: soft robotics, fluidic elastomer actuators, constitutive models, soft materials, FEM analysis

2.2. Introduction

For many decades, scientists have tried to bring their robot designs closer to human body performances. Advances in materials and soft components are expanding the range of new types of robots that perform complex tasks and interact more closely with humans. They have pushed back the boundaries in the field of robotics with their remarkable capabilities, including lightweight, hyper redundancy, fast assembly and cost-effective materials [9]. Furthermore, soft robots can be actuated using different strategies, such as pneumatic or hydraulic fluids, electric motors, heat, chemical reactions, etc. [10]. Unlike soft robots, conventional robots are rigid and consist of a number of links connected together by joints; they are designed to work in specific environments and satisfy recurrent high-precision tasks [11]. Although these manipulators are very common in many industries such as automotive and food, they have some limitations, such as limited dexterity and an insufficient number of degrees of freedom (DOFs). These limitations restrict their movements in arbitrary workspaces. Inspired by nature, soft robots have emerged and reduced the gap between human interaction and robotic environments. Additionally, they provide interesting new capacities in comparison with other robotic architectures; for instance, soft robots are capable of maneuvering through congested environments with minimum inducing stress concentrations or damage.

Many classification approaches have been used to characterize satisfactorily their structures and performances. Trivedi et al. divided robots into two classes, according to their materials and degrees of freedom: soft and hard robots [12]. Soft robots were categorized as a subset of continuum robots. This means that soft robots are able to act with continuous deformation, but not all continuum robots are soft. For instance, some of them include several hard links and joints, creating more DOFs. A number of DOFs largely higher than the number of actuators puts them in the hyper redundant robot class. Although many DOFs are not controllable, they increase the shape configuration adaptability of a robot with various objects. Several reviews on soft robots have been carried out and can be found in the literature; most of them are focused on the recent advances in this field [13], [14], [15], [16], [17], [18]. Shintake et al. [2] classified soft grippers in three separate groups based on their grasping technology: actuation, adhesion control and variable stiffness control. Boyraz et al. [10] presented a comprehensive comparison of soft robot actuators and mentioned their challenges. Gorissen et al. [19] and Walker et al [20] separately reviewed the design, manufacturing and control of soft

pneumatic actuators. They focused on soft pneumatic actuators with positive pressure, while SFAs with negative pressure play a significant role in achieving soft robot milestones. In this study, we classify soft robots based on their actuation mechanism into 5 classes: 1- tendon-driven actuation, 2- electroactive polymers (EAPs): dielectric elastomer actuators (DEAs) and ionic polymer-metal composites (IPMC), 3- shape-memory materials: shape memory alloys (SMAs) and shape memory polymers (SMPs), 4- soft fluidic actuators (SFAs, see Figure 2.1), 5- hybrid actuators. Although additional soft actuators such as a soft magnetic robot [21], soft grippers using gecko-adhesion [22], fishing line actuator [23], Electrorheological Fluids (ER) [24], and Magnetorheological Fluids (MR) [25] are reported in the literature, due to their rare usage, in this study, we have focused on reviewing these five mentioned classes of soft actuators.

We first position SFAs in relation to other soft actuation technologies, then we suggest a general classification of the soft fluidic actuator domain by considering all pressurized and vacuum technologies. We then summarize the most effective SFA designs that could be a source of inspiration for future approaches. Furthermore, SFA functions are strongly dependent on the type and properties of the selected material. Silicone is the most commonly-used material in SFAs. Due to its highly nonlinear behavior, modeling and operating prediction are the main challenging aspects of SFAs. In this paper, we study a wide variety of silicones and review the different modeling methods.

2.3. Soft Actuation Technologies and SFAs

As mentioned, this review paper is focused on SFAs as one of the most common actuation mechanisms in the field of soft robots, but it is necessary to explain briefly the other actuation methods to help to clarify the reason for choosing SFAs to review as one of the soft robot actuator approaches. Moreover, in hybrid designs, SFAs can be integrated with other actuation types to enhance robot performance. Figure 2.1 shows the most representative actuator technologies in soft robots based on previously published results. The major advantages and challenges of each actuation method are summarized in Table 2.1 and explained in the remaining part of this section. The first category concerns tendon-driven actuation. It is widely used in continuum soft robots. This technology enables them to reach the desired position with many different configurations, so they have high dexterity and superior performance in congested environments [18], [19], [15].

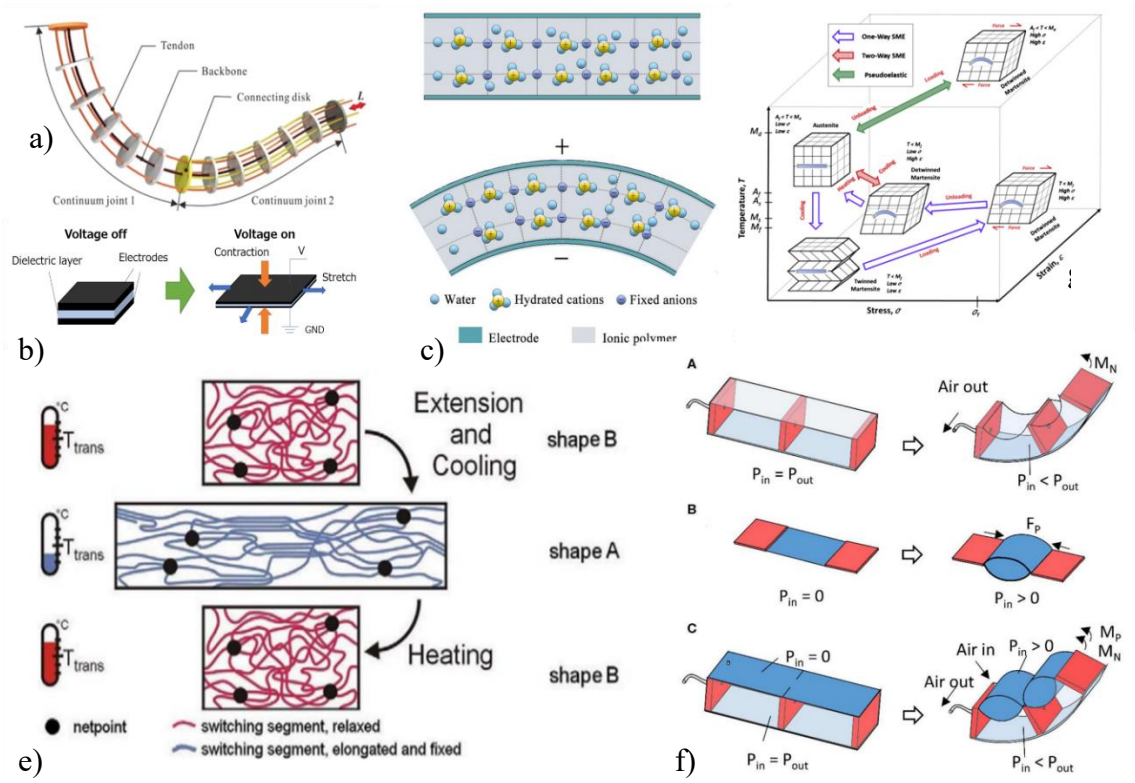

Figure 2.1. Different types of actuations in soft robots. a) Tendon-driven mechanisms [29], b) Dielectric elastomer actuators (DEAs) [30], c) Ionic polymer-metal composites (IPMCs) [31], d) Shape memory alloys (SMAs) [32], e) Shape memory polymers (SMPs) [33], f) Soft fluidic actuators (SFAs) [34].

Table 2.1. Different types of soft robot actuators

Design Parameters	***Power supply***	***Advantages***	***Challenges***
Tendon driven mechanisms	Electric motor	Large stroke bending with a high produced force	Require external motors
Dielectric elastomer actuators (DEAs)	Electric	Large actuation strokes, self-sensing capability, fast response time, requiring small currents	Require high voltages; difficult fabrication procedure for complex geometry
Ionic polymer-metal composites (IPMCs)	Electric	Bending in both directions, variable stiffness, large bending strokes with low actuation voltages, self-sensing	Slow response and low produced force
Shape memory alloys (SMAS)	Electric or thermal	High active stress, high elastic modulus, conductivity without the need for an external heater, act as a strain sensor at the same time	Slow response and speed, hysteresis, require high currents
Shape memory polymers (SMPs)	Thermal electric	Variable stiffness capability	Low produced force
Fluidic actuators	Pneumatic or hydraulic	High force generation, large stroke bending	Require external pumps, bulky and heavy

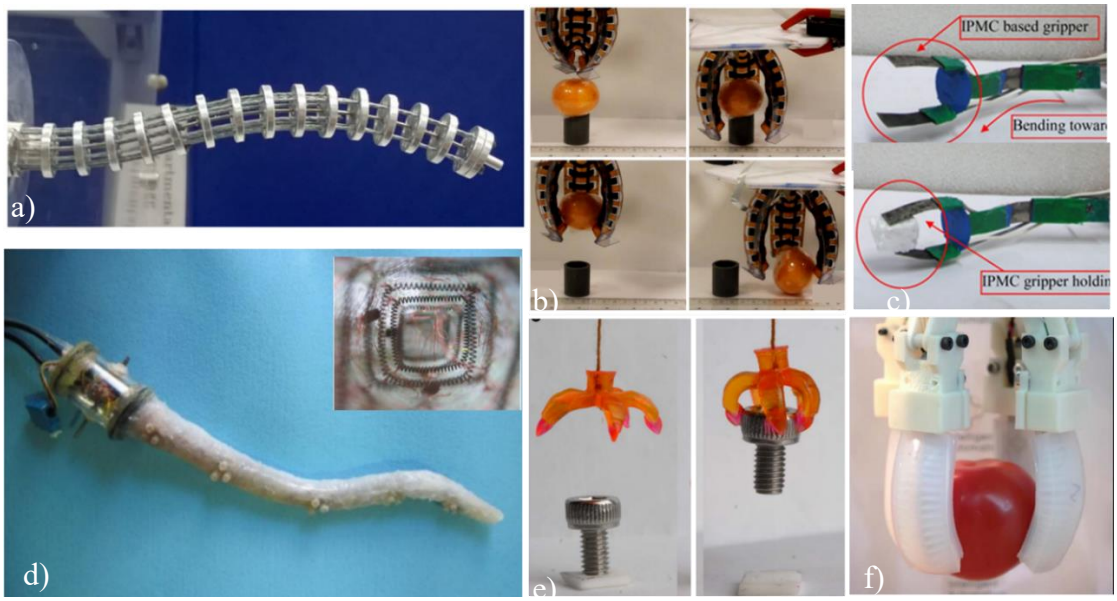

Figure 2.2. Examples of different actuation types in the soft robotics field: a) Surgery robot using a tendon-driven mechanism [35], b) DEA soft gripper [36], c) IPMC gripper for manipulating the object [37], d) SMA spring soft actuator. [38], e) SMP soft gripper [39], f) Soft pneumatic actuator [40].

In a continuum soft robot, a moment is applied at the tip of the arm with the tendon mechanism, then the whole arm deforms smoothly and continuously (Figure 2.1a). It can transmit compressive forces which enabling it to perform perfectly in complex conditions or when encountering obstacles. Due to their inherent design, continuum robots can grasp objects by using whole arm manipulation, and carry payloads without causing damage. Recently, a variety of actuators, joints, and mechanisms inspired by nature have been built, such as those connecting several small links [41], Serpentine Robot [42], and elephant trunks with a single flexible backbone actuated by wires [43]. Xu and Simaan designed human body surgery robots with multiple flexible backbones actuated in push-pull mode [44], applicable for tele-operated surgery in the throat and upper airways [45]. Figure 2.2a shows the snake-like robot design by Ouyang et al. [35]. This design is composed of a base disk, an end disk, several spacer disks, and four arranged super-elastic NiTi tubes. The central tube is the primary backbone, while the remaining three tubes are the secondary backbones. By pulling two of these three secondary backbones in each section and changing their lengths, the end disk can be oriented in any required direction in space. To study more about the other types of tendon-driven soft robots, the reader may refer to [12], [33], [34]. The second class of soft robot actuators is EAPs. They respond to electrical stimulation with significant changes in dimension or shape [48]. DEAs and IPMCs are the two most well-known EAP technologies, especially in the robotics field

[49], [50], [51], [52]. DEAs consist of a thin elastomer membrane between two compliant electrodes (Figure 2.1b) [30]. By applying a voltage, the elastomer starts to deform, and consequently mechanical actuation appears [53]. The main performance advantages of DEAs can be highlighted by large deformation [54], high energy density, fast responses [55], lightweight and low cost [56]. Moreover, DEAs self-sensing [57], [58] and variable-shape configuration capabilities make them a wise choice in soft robotic actuators [59], [60]. Anderson et al. [61] reviewed DEA applications as artificial muscle to generate many translational and rotational degrees of freedom, especially for soft machines. The DEAs' multifunctionality in actuation and sensing capability provide feedback control in the closed-loop system without requiring any external sensor. In addition, they remarked the most important self-sensing potential factors in DEAs, namely material development, reliability, manufacturability, and miniaturizing. Araromi et al. [62] proposed a small-scale gripper consisting of a pre-stretched elastomer DEA actuator. By applying a voltage, the 0.65 g gripper can bend up to 60 degrees and produce a 2.2 mN gripping force. As shown in Figure 2.2b, a stiff layer of Polyvinyl chloride (PVC) sheet can be added to DEA elastomer [36]. This layer increases the generated grasping force to 168 mN. The potential challenge of DEAs is that they require high voltages in the kV range. which not only raises the cost and size of the kV control electronics but also increases the risk of electrical discharge, undesirable in many applications, especially with human interaction [63], [64], [65]. A potential solution to this problem is decreasing the dielectric membrane thickness. The optimum range of DEA thickness is between 20–100 μm, whereby reducing more than this range increases fabrication challenge [66]. Ji et al. [67] presented low-voltage stacked DEAs (LVSDEAs) with an operating voltage below 450 volts to fabricate an ultralight (1 g) insect-sized (40 mm long), and fast (30 mm/s tethered, 12 mm/s untethered) device. Moreover, the operating voltage of DEAs can also be decreased by increasing the elastomer permittivity [68], [69] or reducing the elastic modulus [70]. Gu et al. reviewed recent works in the DEA-driven soft robot field; they tried to summarize the challenges and opportunities for further mechanism design, dynamics modeling and autonomous control [71].

Hydraulically amplified self-healing electrostatic (HASEL) is a similar mechanism to DAE which has been advanced recently by Acome et al. [72]. Like DEA, HASEL actuators include two flexible layers but use liquid dielectric instead of elastomers. The electric field applies electrostatic force to drive shape change in a soft fluidic architecture by transporting fluid through a system of channels. Unlike DEAs, HASEL actuators are

fabricated without a pre-stretch layer or rigid frames, making them suitable for building soft actuators [73]. Moreover, liquid dielectric provides an electrically self-healing capability in the event of a dielectric breakdown. As a result, HASEL actuators generate large strains and fast response while having self-sensing capabilities, especially for developing closed-loop control of soft robots [74]. However, the potential challenges of HASEL actuators similar to DEA, for achieving fats response required very high voltages (≈20 kV). Besides, for sealing fabrication of the elastomers for the layers, two standard molding cast or metal die methods are used, which are time-consuming processes for different geometries and designs [75]. Recent techniques have focused on miniaturizing high-voltage dc-dc converters as a promising solution for both HASEL and DEA actuation [76]. The XP Power and Pico Electronics are two famous commercial converters that can produce up to 10 kV using a 5-V input [77]. Although the functionality of the HASEL actuators is more similar to the DEAs, due to the pressurizing the fluid, some applications with HASEL can be classified as a soft pressurized fluidic actuator (SPFAs). More details about these types of actuators in soft robots are explained in the corresponding section.

Another widespread type of EAP material is IPMC, which bends in response to electrical activation [78]. A typical IPMC consists of chemically-plated gold or platinum on a perfluoro sulfonic acid membrane, which is known as an ion-exchange membrane. When an input voltage is applied to the metal layers, the cations move toward the cathode. This translation generates strain and the IPMC starts to bend toward the anode [31] (Figure 2.1c). Shahinpoor et al. [79] classified their IPMC study in a series of four reviews to present a summary of the fundamental properties and characteristics: various techniques and experimental procedures in manufacturing [80], modeling and simulation analysis [81], and finally industrial and medical applications for IPMC [82]. Due to several advantages, including a low activation voltage (1∼3 V), self-sensing capability, ease of miniaturization, and operation in wet conditions, IPMC technology has been used in actuators and sensors in soft robotics for the last two decades. Kashmery [37] fabricated grippers composed of an IPMC membrane actuator to manipulate a small object by applying 5 V DC (Figure 2.2c). Slow actuator response and low produced stress are the most challenging issues when using IPMC as an actuator [2]. Recent technologies and applications of IPMCs are reviewed in [83], [84], [85]. Hao et al. reviewed the latest advances in IPMCs for soft actuators and sensors, especially in the field of soft robotics [86].

Shape memory materials are another actuation method widely used in soft robotics, due to their deformation in response to electrical stimuli or temperature. Shape memory alloys (SMAs) and shape memory polymers (SMPs) are the two kinds of materials which exhibit these characteristics. Figure 2.1d shows the two well-known properties of SMAs. The first is the phenomenon of phase transformation between martensite and austenite, which leads to mechanical actuation and subsequent return to their original shape [87]. The second feature of SMAs is the superelastic effect, which is the ability of the material to recover its large elastic deformations upon removal of the load [88]. As is the case for tendon-driven actuation, this second property of SMAs is widely used in continuum robots to push/pull cables. This kind of SMA is a nickel-titanium alloy known as Nickel-titanium. The amount of deformation and stroke produced during a heating/cooling cycle is depended on the shape of the SMA and its thermomechanical treatment. Nowadays, the use of SMAs as actuators in soft robots is growing because of the promising advantages of being able to significantly reduce actuator size, the available rapid manufacturing techniques, the large actuation force, and the displacement. Cianchetti et al. [38] designed soft actuators with a combination of SMA springs and braided sleeves for multi-purpose applications in water (Figure 2.2d). The conductivity features of SMAs enable them to utilize the direct Joule heating technique without needing an external heater [89]. However, the potential challenges of using SMAs as actuators remain; for instance, their slow operation frequency, controllability, accuracy, energy efficiency, and recovery speed are important issues [32].

SMPs are considered as memorized polymers that can change shape under heat or light stimulation and transform from a temporary shape to a memorized permanent shape [39], [90] (Figure 2.1e). Because of low recovery speed and hysteresis, few works can be found using SMPs as the main actuators of soft robots [91]. Figure 2.2e shows a SMP small-scale gripper with four fingers. The gripper can hold small objects such as a screw after heat actuation [39]. SMPs are usually integrated into other technologies such as SMAs [92] and SFAs [93] to vary the stiffness of the robot. These hybrid mechanisms will be discussed in more detail in the dedicated section. Recent progress on SMPs and their potential challenges are reviewed in [90], [94], [95], [96].

The soft fluidic actuator is one of the most ubiquitous actuation mechanisms in soft robotics due to its many advantages, including simple assembly, cost-effective materials, large deformation, and high generated force [34], [1] (Figure 2.1f). These unique characteristics make them promising candidates for various applications, such as gripping

Figure 2.3. Timeline showing major production advances in the field of SFAs: a) PAM mechanism developed by Suzumori et al.[97], b) OctArm [98], c) PneuNets [99], d) Universal gripper [100], e) Origami soft structure [101], f) VAMPs design [102], and g) HASEL actuator [72].

[2],[103], [104] , [105], mobility [3], robotic manipulation [4], [106], [107] medical applications [108], [109], and rehabilitation and assistive robotics [6], [110]. By applying positive or negative pressure inside the chamber, the soft actuator, depending on the type of surface where the pressure is applied, starts to bend, extend, twist, or contract [111] (Figure 2.2f). Moreover, in hybrid designs SFAs can be integrated with other actuation types to enhance robot performance [10].

As seen in this section, each actuation strategy has some capability which differs drastically in terms of performance from the others, such as response speed, stroke, amount of force produced, and variable stiffness. SFAs have particularly wide application areas and are reported frequently [112]. Due to the huge potential of SFAs, we focus in this review paper on some of the developments in their various applications in soft robotics and discuss the recent progress of soft robots using SFAs. In the following sections we review recent developments in the field of SFA regarding classification, design, computational procedures, and the history of the most effective SFAs design mechanisms which have inspired many works over the last two decades.

2.4. History and Classification of SFAs

We classify SFAs based on the applied pressure in three main categories: soft pressurized fluidic actuators (SPFAs), soft vacuumed fluid actuators (SVFAs), and hybrid mechanisms including a combination of SFA with the other existing types of soft actuators explained in the soft actuation section. In SPFAs, positive pressure is used to inflate channels in a soft material and cause the desired deformation, while in SVFAs, vacuuming the air inside the chamber causes contraction. We review the most significant research based on these three categories. Figure 2.3 shows the timeline.

2.4.1. *Soft Pressurized Fluidic Actuators (SPFAs)*

Pneumatic artificial muscles (PAMs) [113], also known as McKibben actuators, are one of the first generations of SPFAs. This soft actuator is composed of hollow elastomer tubes reinforced by fiber stiffness layers. Depending on their design, they will either expand or contract when pressure is applied. The invention of this artificial muscle is generally attributed to Richard H. Gaylord (1958), but it was popularized at the beginning of the 1960s by Joseph L McKibben [114]. The first SFA gripper, with four fingers, was demonstrated by Suzumori et al. [97] in 1989 (Figure 2.3a). These fingers include three chambers that give them 3 degrees of freedom and can bend in any direction. This gripper can grasp a wide range of objects. There is a lot of research on soft robots that can be found using this actuation mechanism. For instance, Polygerinos et al. [6] suggested a flexible glove for robot-assisted rehabilitation. The device utilized the McKibben mechanism not only to support precise functional grasping but also to remain light and low profile (Figure 2.4a). Some approaches tried to combine multiple McKibben actuators to increase SFA functionality with more complex motions. As an example, Al Abeach et al. [115] developed McKibben muscles for a three-fingered gripper. Both extensor and contractor McKibben designs were deployed to provide the form and efficient force for grasping ability, respectively.

PAM elastomer actuators exhibit complex nonlinear snap-through instabilities. This behavior allows the actuator to gradually store elastic energy, before releasing it suddenly to exert rapid motion or high force [116]. As shown in Figure 2.4b, Overvelde et al. [117] developed this kind of nonlinear mechanism to exert high force and trigger large geometrical changes by sequential steps. Rothemund et al. [118] designed a bistable soft valve. They calculated the required switching pressure as a function of the geometry and valve’s material (Figure 2.4c). McKibben's muscles are also employed in the actuation of continuum robots. Tsukagoshi et al. [119], presented an elephant trunk-type manipulator named Active Hose, consisting of a spiral tube turned around the manipulator backbone like a coil, to generate bending moment. This can be useful in rescue operations.

The other type of manipulator which benefited from PAM actuators is OctArm. It was first presented by Grissom et al. [98] (Figure 2.3b) and consists of three serial sections that are actuated separately. By applying pressure inside the chamber of each section, the arm starts simultaneously to bend and extend longitudinally for the whole-arm grasping of objects [120]. A large manipulator continuum robot with McKibben actuators

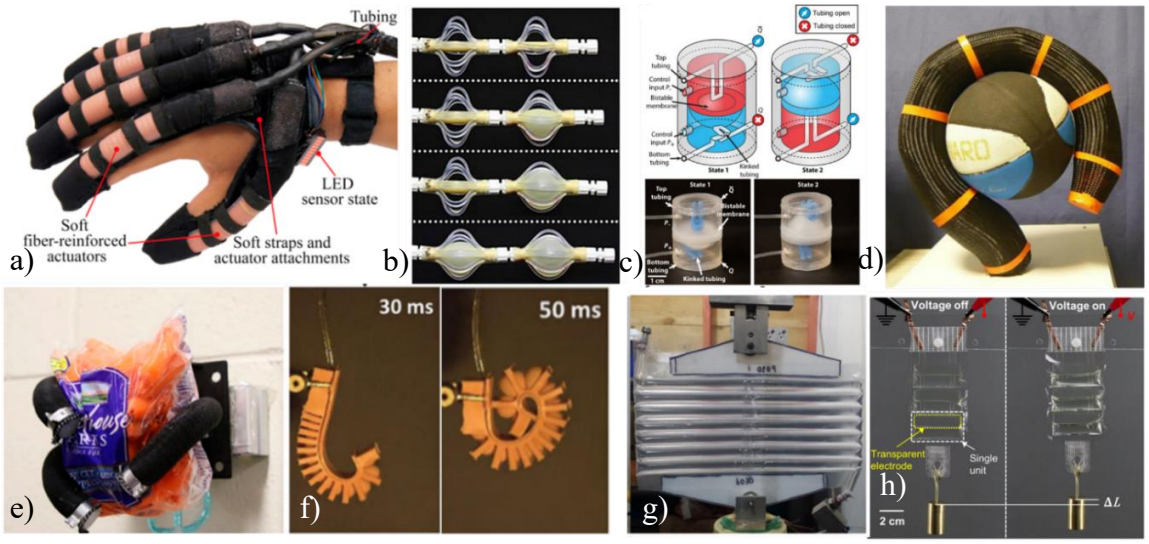

Figure 2.4. Some examples of SPFAs: a) PAM mechanism used for rehabilitation gloves [6], b) Snap-through instabilities mechanism changes by sequential shape changes [117], c) Bistable soft valve in SFA applications [118], d) Large manipulator continuum robot with McKibben's muscles [121], e) Soft pneumatic artificial sleeved muscles [122], f) PneuNets actuator developed by Mosadegh et al. [123], g) Peano-fluidic muscle [124], and h) Peano-HASEL actuator [77].

consisting of 6 sections is reported by [121] (Figure 2.4d). Applying air pressure of around 4 bars causes a 66% extension in section and 380° rotation in less than 0.5 s. Walker et al. [120] in 2005 developed cephalopod robots incorporating 12 McKibben actuators. The considerable length of the robots (120 cm), acting like a manipulator, achieves more kinematic DOFs than in previous pneumatic arms and is more similar to the real biological inspiration. SPFAs can be made using highly extensible elastomer materials such as silicones. With these materials, highly deformable and adaptable soft actuators appeared. In these kinds of actuators, one or more embedded chambers are actuated and deformed by applying pressurized fluid, which can be operated pneumatically [125], [126], [127], [3], or hydraulically [128], [129], [130]. On account of their light-weight and cleanness, pneumatic systems in most cases are preferred over hydraulic designs especially in gripper design (Figure 2.4e) [122].

Pneumatic networks (PneuNets) are a famous pneumatic version of these actuators working as a gripper. This was first presented by Needleman [131] in 1977. He demonstrated that PneuNets, comprising a series of channels in an elastomer, can inflate like balloons for actuation. This mechanism was later developed and used as a soft gripper by Ilievski in 2011 [99] (Figure 2.3c). This gripper consists of six legs for grasping soft fragile objects like an egg or even a live small animal like a mouse. In an interesting work, Mosadegh et al. [123] developed the PneuNets architecture, achieving rapid

response and more durable actuation cycles by proposing a gap layer between the walls of each chamber. Inextensible fibers are added to the FEAs to boost local stiffness and consequently the weight-object ratio in the grasping application (Figure 2.4f). In reference [132], they employed polyaramid fibers to prevent the local weakening of the elastomer during repeated actuations. Deimel and Brock [133] developed a SPFA with a three-fingered hand and flexible palm. The fingers are made of fiber-reinforced silicone, and the palm has substantial passive compliance. The RBO Hand shows the capacity to grasp a wide variety of objects, including water bottles, eyeglasses, and sheets of fabric. Later, they presented the RBO Hand 2, composed of a five-finger and palm configuration with similar fiber-reinforced actuation technology to develop an SPFA hand [134]. It demonstrated dexterity similar to a human hand with the ability to perform most human grasping tasks.

Various types of PAMs have been developed in recent years. A famous one is a Peano-fluidic muscle presented by Veale et al. [135]. It consists of flat layers of thermoplastic, textile reinforced plastic, or textile/silicone composite. The intervals of these layers are bonded perpendicularly in the direction of contraction (Figure 2.4g). When air pressure is applied, the shapes of tubes become round with a contract ratio between 15% and 30%. The geometries of the tube affect the static and dynamic behavior of Peano-muscles [124]. The optimum channel should not exceed 20% for maximizing performance. The narrower channels increase flow restriction, subsequently, a damping force model was applied to Peano's muscle for high-accuracy controllability and further suitability in uncontrolled environments [136].

As discussed in the previous section, a similar mechanism to the Peano-muscle is the HASEL actuator. It was introduced in 2018 [72] and designed to produce linear contraction with stack (Figure 2.3g). Peano-HASEL is one type of HASEL actuator, exhibits fast and precise linear motion that closely resembles muscle-mimetic activation without stack, prestretch, or rigid frames. It was developed by Kellaris et al. [77] and made of a rectangular shell formed by flexible polymer films filled with a liquid dielectric, and planting a pair of electrodes on either side of the shell (Figure 2.4h). When a charge opposes the electrodes zip together due to the electrostatic force, hence the fluid squeezes into the volume of the shell which is not surrounded by the electrodes and creates linear contraction of the actuator. This linear actuator can lift more than 200 times its weight with a strain rate of 900% per second at 10 kV. The fast response speed, self-sensing and self-healing advantages of HASEL actuators make them a promising

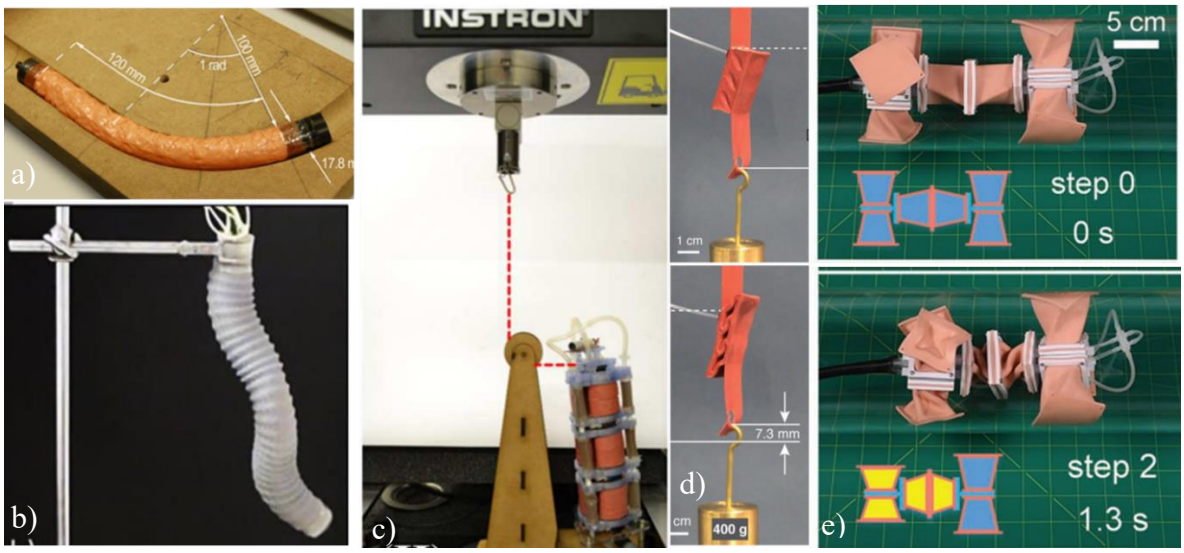

Figure 2.5. Some examples of SVFAs: a) Flexible endoscope [137], b) Soft multi-modulus manipulator for minimally invasive surgery [138], c) Multi-purpose SVFA with jamming-based stiffening [139], d) VAMPS actuator made by Yang et al. [140], e) Soft robot multi-task actuator application [141].

candidate for applications in different soft robotic mechanisms such as untethered soft robots for manipulation and continuum applications [142], tubular pump [143], and prosthetic finger driven by Peano-HASEL [144]. Rothemund et al. [75] reviewed the latest advances and future opportunities of HASEL in the soft actuators field.

2.4.2. *Soft Vacuumed Fluid Actuators (SVFAs)*

Vacuum mechanisms have also been widely employed in soft robots as actuators. Negative-pressure operations are safer, more compact and more robust compare to pressurized actuators. They cannot burst when the actuator collapse. Moreover, decreasing their volume enables them to go through congested or narrow areas compared to their nominal sizes. One of the representative examples of SVFAs is the universal soft gripper developed by Brown et al. [100] as shown in Figure 2.3d. Because of its simple structure, it is one of the earliest and most famous soft vacuum grippers. Unlike other soft robot actuation mechanisms, it is simply composed of a membrane filled with granular materials; the stiffness of the bag is changed by evacuating air and provides sufficient force for lifting and holding objects. It shows promising performance, especially when the shape or material properties of the object are unknown or when precise grasping is not required. This gripper was able to pick up a wide variety of objects of different sizes and shapes, such as a wooden hemisphere, spring, small LED, tube, cups, raw egg, shock absorber, etc. The device can rapidly grasp and release a wide range of objects; however,

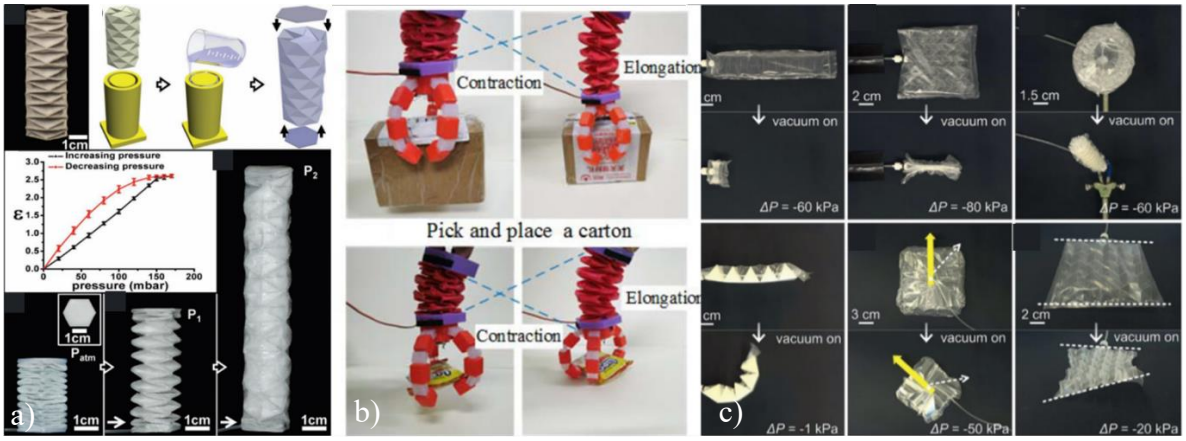

Figure 2.6. Origami fluidic soft actuators: a) Combining a stretchable elastomer with a non-stretchable bendable sheet [101], b) Soft origami gripper [145], c) Lightweight origami shell reinforcement with various applications [146].

it is not appropriate for grasping flat or soft objects. The universal gripper was commercialized in [147] and has inspired several research applications, such as a prosthetic jamming terminal device (PJTD) [148], human collaborative robot [149], universal hand for position adjusting and assembly tasks [150], deep-sea sample-collecting device [151], flexible endoscope [137] (Figure 2.5a), and soft multi-modulus manipulator for minimally invasive surgery [138] (Figure 2.5b). Amend and Lipson [152] presented two simple two-fingered configurations with pockets of granular material used as end-effectors at the fingertips. This design enables each of the fingertips to work separately as independent universal grippers, or to work together like a finger and a thumb. The variable stiffness, lightweight, and energy efficiency of granular jamming make it popular for use in the soft robotics field [139] (Figure 2.5c). The granule particles can be coffee, glass, plastic or beans. The application determines the grain size; for example, powder-like granular size is generally utilized in soft robotic grippers [137], [153]. Soft manipulators, which require greater stiffness, normally employ larger grains [154]. Sayadan et al. [155] studied the impact of various mechanical parameters (stiffness, curvature radius, applied moment, internal stresses, and defection) on the behavior of cantilever membrane beam samples by presenting a simplified formulation under different vacuum pressure conditions. They designed various experimental tests with latex membranes filled with granular materials such as hemp, sun-dried barberries, black peppers and datura seeds.

Another important class of SVFAs was created by Yang et al. [102] as a vacuum-

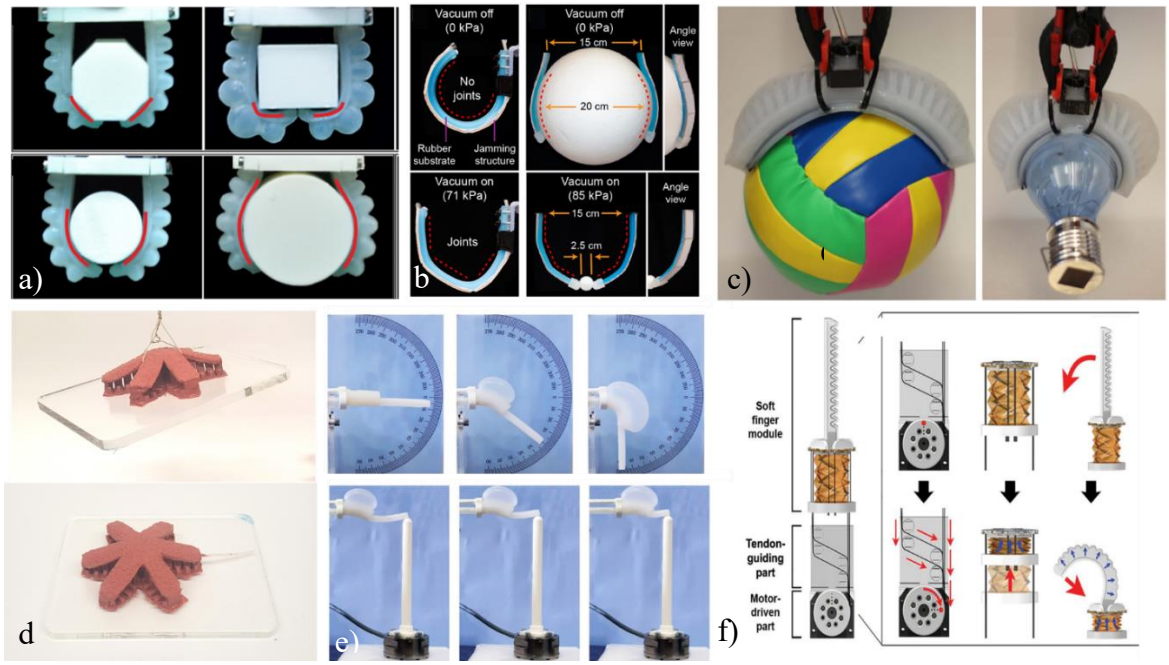

Figure 2.7. Hybrid design of SFAs: a) LMPA + SPFA [156], b) SFA + Layer jamming mechanism [157] c) Electro adhesion + SPFA [158], d) Gecko adhesion technique +SPFA [159], e) SFA+ hard: changing the bending point and variable stiffness [160], f) Tendon + SFPA [161].

actuated muscle-inspired pneumatic structure (VAMPs) (Figure 2.3f). It uses the buckling of elastomeric beams to generate muscle-like motions when negative pressure is applied. Its mechanism differs from those of previous elastomeric pneumatic actuators such as PneuNets or McKibben. They can generate a linear motion similar to biological muscles. This mechanism is very similar to the performance of human muscles. Unlike other pneumatic actuation such as McKibben and PneuNets, the deformation is not obtained from area expansion and occurs inside the structure. The VAMP actuator made by Yang was able to lift 400 g. Figure 2.5d shows the performance of the VAMP. They also built a muscle-like actuator to simulate a skeleton arm moving similarly within the human body. It can contract up to 40% of its length, with loading stresses up to 65 KPa. The final displacement of the muscle is nearly 5 times the primary length of the VAMP. With this design, the gripper can pick up a volleyball weighing 274 g. VAMPs actuators are fast, with low cost, are easy to fabricate, lightweight, and operate safely with human interactions [140]. Verma extended Yang's works by combining a pressurized and vacuum actuator for a soft robot climbing in a tube application [162]. This climbing robot is composed of a VAMP actuator for linear motion and two ring-shaped pneumatic actuators at its extremities to hold the robot in position inside the tube. These linear actuators integrated one DOF and provided one single motion. While Jiao et al. [141] proposed a multi-task actuator to offer many different types of motion at the same time,

such as twisting, radial and linear movement (Figure 2.5e). Their design included seven SVFAs to provide five crawl deformations.

Origamis are new innovative structures that have large potential use in soft robotics because of their lightweight, low-cost, easily available materials, and simple design for complex motions. They do not need hinges or joints and are actuated by applying positive or negative pressure. Therefore, according to their design and application, they can be SPFA or SVFA. Origami is the art of generating 3D structures by folding 2D sheets [163]. In [101], Martinez et al. proposed a wide range of origami soft actuators by combining a stretchable elastomer with a non-stretchable but easily bendable sheet (Figure 2.3e, 6a). These actuators can perform a range of complex motions that would be difficult to achieve with hard robots. Figure 2.6b shows the origami-based robotic grippers proposed by Hu et al [145]. They have been easily fabricated by 3D printing and included high foldability and damage tolerance. Li et al. [146] suggested fluid-driven origami-inspired artificial muscles (FOAMs) with multiaxial complex motions (Figure 2.6c). Their origami actuator is fast and powerful, with a very low manufacturing cost. A soft active origami robot with a self-actuation design without the assistance of any external actuators is reported in [164]. Paez et al. [165] presented a lightweight origami shell-reinforced bending module within the desired range of displacement and force requirements. Rus et al. reviewed the design, fabrication, actuation, sensing, and control of origami robots with their applications in the different robotic areas [166].

2.4.3. *Hybrid Mechanisms*

SFAs have been combined with other techniques to improve their performance, including constructability, variable stiffness, and operational range criteria. Table 2.2 summarizes various novel hybrid actuation approaches to address potential advances in the performance of SFAs. SMPs [167] and low melting point alloys (LMPAs) [156], [168] are deployed with SFAs to enhance shape configurability by changing and controlling the position and bending angle (Figure 2.7a). Particle jamming and layer jamming can be integrated by the SFA to increase the stiffness of soft robots [157], [169], [170] (Figure 2.7b). Adhesion technology such as electro-adhesive material [158] (Figure 2.7c) and Gecko adhesion technique [159] (Figure 2.7d) are added to SFA grippers to enhance grasping performance by increasing the lifting weight ratio and object shape diversity. Combining soft and rigid robot characteristics can build new capabilities for soft robots. For instance, Stokes et al. [171] proposed a hybrid soft robot consisting of a

wheeled robot (hard robot part) and PneuNet SPFA (soft robot part) to manipulate and grasp an object at the same time. Pagoli et al. [160] (Figure 2.7e) introduced the innovative variable stiffness soft finger. Its soft pneumatic sliding joint can move and rotate along with the finger by using two electric motors. The changing position of the bending point increases the capability of the finger in terms of shape control and variable configuration. The stiffness, and consequently the applied force, at the tipping point of the finger is controlled by the pneumatic pressure inside the soft silicone link. As explained in the previous section, the climbing robot designed by Verma et al. [162] includes two kinds of pressurized (SPFA) and vacuumed actuators (SVFA) and thus can also be classified in the hybrid design domain. Hybrid design can also be found in origami soft robots by using simultaneously positive (SPFA) and negative pressure (SVFA) to increase the actuating capability. A hybrid crawling soft robot is illustrated in [172] utilizing these characteristics for mobility. Li et al. [173] suggested a pre-charged hybrid gripper with a combination of SPFA and tendon-driven mechanisms. The pushing/pulling cable controls the bending angle of the SPFA, the advantage of the proposed mechanism being that controlling cable movement is much easier and more accurate than pneumatic pressure. Kim et al. [161] integrated SPFA with an origami pump which is controlled by a tendon-driven mechanism(Figure 2.7f). The main advantage of the proposed gripper is that it can work without needing an external pneumatic source such as a compressor. This design helps to miniaturize soft robot actuators.

2.5. Material and Fabrication Methods

2.5.1. *Materials of SFAs*

Advances in the field of soft robotics largely depend on the knowledge of material behavior in the design of soft robotic structures and the control of these robots. Silicone rubbers are the most common material used in soft robotic systems, because of their hyper-elastic properties, lightweight, low cost, and fast and simple fabrication. Several SFA design architectures that can be found in the literature use silicone rubbers. They produce high power-to-weight ratios, requiring small input air pressures yet generating large deformations. Furthermore, they can easily be shaped into different configurations which makes them suitable for building soft actuators with a complex design. The actuation performance, such as response time, stiffness and the amount of generated force,

is dependent on the type of silicone. The mechanical properties of widespread types of silicones used in soft robotic systems are listed in Table 2.3. Several companies producing elastomer silicone can be found on the market; the most well-known brands are Smooth-On [174], Gelest [175], Dow Corning [176], and Wacker [177]. Most applications of these materials in soft robotic systems, especially in SFAs, are reviewed in this section.

EcoFlex is one of the popular silicones that are frequently used. It is commercialized by Smooth-On with several Shore hardness ratings, ranging from 00–10 to 00–50. The mechanical properties of three widely-used EcoFlex Shores in soft robotic applications are listed in Table 2.3. They include hyperelasticity capability, which enables them to be stretched several times their original size without rupturing. This characteristic makes

Table 2.2. The hybrid design of SFAs with other actuation mechanisms

Hybrid Design	***The improvement goal***	***Application***	***Reference***
SFA + SMP	Changing the bending point, shape configuration, and variable stiffness	Soft gripper	[167], [178]
SFA + LMPAs	Changing the bending point and shape configuration	Soft gripper	[156], [168]
SFA + Gecko adhesion	Higher-strength grasps at lower pressures	Soft gripper	[22]
SFA + DEA	Handling soft and delicate target objects	Soft gripper	[179]
	Minimizing the size of SFAs with 2 DoFs	Soft actuator	[180]
SFA+ Tendon	Accurate control of the bending angle by servo motor	Quadrupedal, soft gripper	[173]
SFA+ Hard robot	Miniaturizing the actuator	Soft gripper	[161]
	Changing the bending point, shape configuration, variable stiffness	Dexterous finger, soft gripper	[160]
	Capable of multiple functions	Locomotion and grasping	[171]
SFA+ Electro adhesion	Gripping delicate, flat, and complex-shaped objects	Soft gripper	[158]
SFA + Layer jamming mechanism	Variable stiffness and shape control	Soft gripper	[170], [157]
SFA + Particle jamming mechanism	Variable stiffening of soft robotic actuators	Soft gripper	[169]
SPFA+SVFA	Variable stiffening of soft robotic actuators	Soft gripper	[181]
	Variable stiffening of soft robotic actuators	Minimally invasive surgery	[138]
	Linear motion	Soft climbing robot	[162]
	Increasing actuating and motion capability	Soft crawling robot	[172]

them convenient in soft applications. For instance, EcoFlex 00-50 and 00-30 are very useful for developing different types of soft sensors, including prosthetic strain sensors [182], hyperelastic pressure sensors [183], flexible and wearable pressure sensors [184], healthcare biomedical wearable sensors [185], and piezoresistive sensors for human motion detection applications [186]. Furthermore, their large elongation properties make them appropriate for actuation mechanisms. Elsayed et al. [187] studied the material properties of silicones and their effects on the bending angle of a soft pneumatic actuator. They designed and built the same geometry module with two different silicone materials, EcoFlex 00-30 and 00-50. Their experimental tests showed that the softer EcoFlex 00-30 module required a lower pressure of 0.1 bar, while the other material needed 0.32 bar to reach 90 degrees. Their approach shows that the behavior of the soft actuator is dependent on the type of silicone used. Studying and comparing different types of silicon in this review paper can thus help to select the proper material for SFA actuators. Several works on the use of EcoFlex materials in SPFAs can be mentioned. For instance, Calisti et al. [188] proposed an octopus with six flexible limbs made from EcoFlex 00-30 with the dual capability of locomotion and grasping objects. Flexible limbs are responsible for the stability and correct balancing of the octopus in water. They also provide an effective pushing force to move the robot forward and to grasp the object by wrapping themselves around it. Tian et al. [8] developed a SPFA human hand made of EcoFlex 00-30. It consisted of five fingers and a palm, with two joints in the thumb and three joints in the other four fingers. This soft hand can reach any point in a 3D workspace, using a variety of shapes and configurations. It also produces low resistance and carries fragile objects without damage [189].

Dragon Skin is another range of silicone commercialized by Smooth-on. Unlike the EcoFlex series, Dragon Skins have a higher Young's modulus and require more fluid pressure to actuate as SFAs. On the other hand, their greater hardness enables them to apply a larger force during actuation. Yap et al. [190] studied and characterized the curvature radius and the force in SPFAs with different material stiffnesses. They fabricated four types of silicone rubber (EcoFlex 00-30, EcoFlex 00-50, Dragon Skin 10, and Dragon Skin 20). They defined a ratio coefficient to compare the behavior of these materials in terms of stiffness and output force by dividing the curvature radius by the original length. Their experimental results showed that for SPFAs with a 10 mm thickness, EcoFlex 00-30 achieved a minimum ratio of 0.088 at 42 kPa, while EcoFlex 00-50 reached this ratio at 52 kPa. The required pressure for Dragon Skin 10 to attain the

minimum ratio of 0.092 was 180 kPa, and for Dragon Skin 20, the minimum ratio because of higher hardness was not lower than 0.199, when applying 380 kPa. On the other hand, the maximum force of the SPFA increased when the stiffness of the material increased. For example, the maximum force output for EcoFlex 00-10 and 00-50 was 2.33 at 42kPa and 3.98 at 52 kPa respectively. For Dragon Skin 10 and Dragon Skin 20, the output force ratio was higher, reaching 8.82 at 180 kPa and 9.96 at 380 kPa, respectively.

Another popular silicone rubber in soft robot applications is Sylgard 184, due to its characteristics, including optical transparency, low viscosity, average tear resistance, and

Table 2.3. Mechanical properties of the most commonly-used silicones in the soft robotics field

Material	*manufacturer*	*Shore hardness*	*100% Modulus (psi)*	*Tensile Strength (psi)*	*Elongation at break (%)*	*Viscosity (cp)*	*Pot life (min)*	*Cure time (min)*
Silicone								
EcoFlex 00-10 [174]	Smooth-On	00–10	8	120	800	14000	30	240
EcoFlex 00-20 [174]	Smooth-On	00–20	8	160	845	3000	30	240
EcoFlex 00-30 [174]	Smooth-On	00–30	10	200	900	3000	45	240
EcoFlex 00-50 [174]	Smooth-On	00–50	12	315	980	8000	18	180
Dragon Skin 10 [174]	Smooth-On	10A	22	475	1000	23000	4-20	30-300
Dragon Skin 20 [174]	Smooth-On	20A	49	550	620	20000	25	240
Dragon Skin 30 [174]	Smooth-On	30A	86	500	364	20000	45	960
Sylgard 184[176]	Dow Corning	43A	-	980	100	5100	90	2880
Elastosil M4601 [177]	Wacker	28A	75 [140]	943	700	10000	90	720
ExSil 100 [175]	Gelest	15A	29	870-1015	4000-6000	12000-14000	1440	240 at 80 °C
Sil 940 [174]	Smooth-On	40A	200	600	300	35000	30	1440
Sil 950 [174]	Smooth-On	50A	272	725	320	35000	45	1080
Sil 960 [174]	Smooth-On	60A	280	650	270	30000	45	960
Mold Star 30 [174]	Smooth-On	30A	96	420	339	12500	45	300
RTV615[191]	Momentive	44A	-	920	120	4000	240	6-7 days
RTV-KE-1603 [192]	ShinTsu	28A	-	508	450	-	90	1440
3D Printer Materials								
FilaFlex [193]	Recreus	82A		-	700 (DIN 53504)			
NinjaFlex [194]	NinjaTek	85A		580	660 (ASTM D638)			
Agilus30 [195]	Stratasys	30-35A		348-450	220-270 (ASTM D 412)			
		30-40A		305-377	185-230			

the ability to be sealed by plasma-activated surface bonding [196]. It is commercialized by Dow Corning [197]. The viscosity and Young's modulus of this silicone are 3500 cp and 3.9 MPa respectively. The high modulus of Sylgard 184 makes it a stiff and inappropriate choice for SFA applications, since it requires a higher pressure than EcoFlex to function as an actuator. However, it can be useful, especially in soft grippers if integrated with other actuation methods such as DEA [198] or Gecko adhesion [199]. It is also found in a wide range of sensor products, e.g. capacitive strain sensor [200], pressure sensor [201], and tactile sensor [202]. White et al. [203] fabricated Sylgard 184 silicone layers with gallium–indium alloy as a resistant sensor to measure the geometry changes due to deformations. They were deployed to build a sensor for soft robots. This sensor was able to measure uniaxial strain and curvature, and could be applicable in soft skin sensors. In a similar approach, Markvica et al. [204] studied the mechanical behavior of an elastomer composite with four different blends of Sylgard 184 and Sylgard 527 containing liquid metal droplets. It ruptured when mechanical damage occurred and could be a suitable sensor for damage detection in soft robots with self-healing properties.

In recent years, self-healing materials have been developed to recover their structure entirely from mechanical damage, without using external stimuli [205]. This autonomous capability increases the commerciality of SFAs, especially in unstructured environments. On the other hand, self-healing polymers are usually more expensive and require more synthetic steps and chemical modification processes [206]. Diels–Alder (DA) networks are popular thermo-reversible polymers deployed by Terryn et al. [207] to heal SFAs ripped, perforated, or scratched by sharp objects. Later they have shown the safe healing ability of SFA's applications in safe human-robot interactions such as social robots, household robots, and hand rehabilitation devices. Shepherd et al. [132] developed a soft fluid actuator integrated with polyaramid fibers (Kevlar) reinforcement. After actuating with positive pressure, this SFA could seal itself after being punctured with a 14-gauge needle. Even after removing the needle, the pressure was retained inside the chamber [208]. Bilodeau et al. [209] reviewed recent advanced and future self-healing applications and damage-resilient materials in soft robotic systems.

Elastosil M4601 is commercialized by the Wacker Chemical company and can be found in some of the soft robotics literature. As shown in Table 2.3, its Shore hardness and Young's modulus are very similar to Dragon Skin 30, but unlike EcoFlex and the Dragon Skin series, it has low optical transparency, which limits its applications as a soft optoelectronic sensor. Nevertheless, its higher stiffness makes it a good option for soft

actuators, especially in soft gripper applications. Galloway et al. [210] developed an underwater two-opposing-pairs soft robotic gripper made using M4601 silicone to manipulate fragile and delicate samples on deep reefs. By applying a 310 kPa pressure, the gripper can produce a 52.9 N lift force. Mosadegh et al. [123] replaced the soft EcoFlex with a stiffer Elastosil M4601 and the actuation pressure increased 8 times for the same bending angle. Robertson et al. [211] suggested four parallel SPFAs made of M4601 to produce a higher force, around 112 N. This is 23% more than the volumetrically equivalent single SPFA. These experiments demonstrated the interest of utilizing a multiple SPFA for high-performance soft robotic applications rather than existing uniform and non-optimal SPFA designs. At room temperature, EcoFlex 00-30 (with a Shore hardness 00–30) has the shortest pot life of 45 min, while this value for Elastosil M4601 with a Shore hardness of 28A and Sylgard 184 with Shore hardness of 43A are 90 min. Wienzek et al. [212] studied the increase in long-term storage of mixed silicone liquid at low temperature for the strain-limiting top layer of a soft gripper. They tested three types of silicone samples (Elastosil M4601, EcoFlex 00–30, and Sylgard 184). They mixed and maintained the samples at -25 °C for 12 weeks. Viscosity was measured weekly to determine the curing characteristics. The results show that EcoFlex 00–30 solidified after 14 days, while the mixed sample solutions of Elastosil M4601 and Sylgard 184 were still liquid and usable for casting processes after period of 8.7 and 12 weeks, respectively. This study helps to separate the mixing and molding process and increase the fabrication options for silicones.

As listed in Table 2.3 for the production of SFAs, some approaches utilize other types of silicone, such as translucent RTV615 [213] with Shore hardness 44A and commercialized by Momentive, translucent KE-1603 with Shore hardness 28A [214], [215], blue color Mold Star 30A [216], and ExSil 100 with Shore hardness 15A. ExSil 100 was first introduced by Goff et al. [217] and later commercialized by Gelest. Although it has high elongation up to 5000%, its Young's modulus is 0.02 MPa, which makes it too soft to use as an actuator or gripper. It is normally used in diaphragms, microfluidics, vibration damping, high-performance seals, optics and electrical interconnectors [175].

As explained before, the stiffness and generated force in SFAs are dependent on the type of silicon. Considering this, some approaches combine different types of silicone materials to attain the desired stiffness. Shepherd et al. [3] developed a multigate walking robot with different silicone layers. Due to its high extensibility under low stresses,

EcoFlex 00-30 was used as the actuating layer, and Sylgard 184 was selected as a strain-limiting layer. This combination not only enables the soft robot to operate at low pressures (7 psi), but also provides the desired stiffness. In their next approach [125], these authors replaced the actuation layer of EcoFlex 00-30 by M4601 to increase to larger loads such as the weight of the robot body and components for untethered operation; inevitably, material of this hardness requires higher pressure actuation (22 psi). Hassan et al. [6] proposed a tendon-actuated soft three-finger gripper made by using three different types of soft materials: Dragon Skin 30, Smooth-Sil 950, and a third type manufactured by combining Smooth-Sil 950 with EcoFlex 00-30. The intrinsic properties of Dragon Skin 30 make it sticky compared to Sil 950. Thus, the first soft gripper made using Dragon Skin 30 shows a better performance with respect to slipping than the second one. To overcome this limitation in the second gripper, they suggested attaching silicone strips made of Smooth-Sil 950 with EcoFlex 00-30 on the surface of the third gripper to guarantee stable grasping for lateral bending. Subramaniam et al. [216] developed a multi-material SVFA gripper with an active palm for grasping applications. They used different types of silicones such as Mold Star30, Smooth Sil 940, Smooth Sil 960, and EcoFlex 00-30 to achieve the desired stiffness, Mold Star30 was selected for the skin layer because of its high deformation at low pressures.

All the silicone materials presented in the previous paragraphs use molding techniques, while in recent years additive manufacturing techniques such as 3D printing have also been employed to directly fabricate SFAs. The most successful fused deposition modeling (FDM) material for soft robotics is NinjaFlex (Shore hardness of 85A) made of thermoplastic polyurethanes (TPU), which can withstand strains above 700% with a Young's modulus of around 10 MPa. The SPFAs that are printed using this method can produce a blocking force of up to 75 N [111]. FilaFlex [218] and Agilus30 [219], [220] are the other two types of TPUs employed to print SFAs. The mechanical properties of these materials and their suppliers are listed in Table 2.3. The manufacturing methods of SFAs, and especially 3D printing technology, will be discussed in a dedicated section.

2.5.2. *Manufacturing and Fabrication of SFAs*

The classical molding method can be used to fabricate different designs of the SFA actuator [221]. Thanks to the latest developments in 3D printing technology, the design of mold parts has improved significantly, which enables the designer to make complex soft components with more accuracy. Normally, catalyzed silicone rubber consists of two

parts that should be mixed homogeneously with the specified ratio according to the manufacturer's instructions. In most cases vacuum degassing for 4-5 minutes is suggested to avoid air entrapment. An alternative and more effective way is putting the mixed silicone into a centrifuge machine. Cure time is variable and differs from 30 min to 1 day at room temperature, depending on the silicone viscosity. This time can be reduced to less than an hour by putting the mixed liquid in an oven at a temperature of around 70 °C [222]. Molding complex structures, especially with undercuts and internal architectures, is very difficult [223]. To overcome this problem, additive manufacturing (AM) methods have also been proposed [224].

SFAs can be printed directly using 3D printers. The fused deposition molding (FDM) method is one of the most widely-used techniques for material fabrication using 3D printers, at low cost and eliminating any supporting molding material, easing changes in the material, and also reducing the fabrication time. The working principle is based on a heating filament and horizontally depositing molten materials via extrusion nozzle onto a surface, layer by layer. NinjaFlex is the most common material used in the 3D printing of SFAs, due to its high strain and force-producing ability when used as an actuator [111], [225]. Peele et al. [226] used the stereolithography (SL) technique to produce a SPFA layer by layer from an elastomeric precursor material. The proposed DMP-SL printing process is a promising way to fabricate a monolithic actuator in one single process. In the SL approach, the solidification of liquid resin is controlled by photo-polymerization by a laser beam or a digital light projector. In SL, unlike FDM, one resin can be printed at one time, and this is the major potential challenge of using this technique. For more information about 3D printing methods, the reader is referred to the review articles [227], [228], [229].

2.6. Modeling

Based on previous research, SFA models can be classified into three main groups: analytical methods, numerical methods, and model-free methods. In this section, we present the latest advances and potential challenges in each category.

2.6.1. *Analytical Methods*

The earliest analytical model for SPFAs is Euler-Bernoulli’s beam theory. In this theory, SPFAs are assumed to be cantilever beams with a fixed support on one side and a

moment on the other side. The model is useful when SFAs have simple (particularly symmetric) structures. Several works can be found in the literature using this theory, such as bi-bellow actuators with three chambers developed by Shapiro [230], pneumatic bending joints with anisotropic rigidity [231], and soft biomimetic robotic fish [232]. This theory is not applicable for hyperelastic material with large bending deformations such as silicone, where cross-sectional planes do not remain perpendicular to the bending moment axis. Some approaches have been tried to improve the result of this method. In most of the previous works, Young's modulus is assumed to be constant, while experimental results show that the stress-strain behavior of these materials is more complex, and the relation between cross-section and curvature radius cannot be found easily [233]. The analytical method approach is more successful in continuum robot modeling, especially when the material is not hyperelastic. The backbone curve approach [234] was the first kinematic model for continuum robots. Later, the constant curvature model (CCM) [43] was suggested for the kinematics of multi-section soft robots. Trivedi et al. [235] deployed the work-energy principle to develop a geometric model for SPFA manipulators, and showed that their model is more accurate than the CCM. Panagiotis et al. [236] used analytical methods to model SPFA with fiber-reinforced bending pneumatic actuators. Wang et al. [237] presented a simplified model of a soft pneumatic gripper with simple line links connected by a set of viscoelastic joints. In conclusion, SPA analytical models come with a lot of approximations and simplification in terms of shape and material properties, which make them inaccurate and require a robust controller to compensate for this lack of accuracy.

2.6.2. *Numerical Methods*

2.6.2.1. Off-line FEM Simulation

Due to the highly nonlinear responses of silicone rubbers, modeling and analyzing SPFAs is quite challenging. The finite Element Method (FEM) has widely been considered to predict the behavior of SPFAs. Material properties, configuration cross-sections, compressibility effects of the pneumatic cavity, and actuation boundary conditions can be defined in the FEM software, and contribute to increasing simulation accuracy. Because of the powerful FEM tools available to model hyperelastic materials, various FEM solutions have been introduced in the literature. Optimal design is the other advantage of using FEM simulation to meet specific performance criteria such as

reducing the geometry dimensions [238], improving actuating speed [123], or enhancing the performance of soft actuators by maximizing the bending angle [239], [220]. Particularly in a commercial application, it is necessary to use FEM optimization once and then produce the SPFAs and prerequisites such as molding devices to reduce the production costs and time. In Table 2.4, we summarize the different FEM solvers and the material properties which are used to predict the hyperelastic characteristics of silicone. Silicone rubber is modeled as an isotropic, incompressible and hyperplastic material. The mechanical behavior of hyperelastic materials is characterized by the strain energy function U, which is then given by [240]:

$$U = \sum_{i+j=1}^{N} C_{ij}(\bar{I}_1 - 3)^i(\bar{I}_2 - 3)^j + \sum_{i=1}^{N} \frac{1}{k_i}(J_{el} - 1)^{2i} \quad (1)$$

where U is the strain energy potential per unit volume, N is the polynomial order, $\bar{I}_1$ and $\bar{I}_2$ are the deviatoric strain invariants, C_{ij} is a material-specific parameter, J_{el} is the elastic volume ratio and k_i expresses compressibility. Considering the silicone as an incompressible material, the term k_i is omitted, which simplifies the general polynomial form of the strain energy potential. (1) can be fitted by different hyperelastic models, i.e., Mooney-Rivlin, Yeoh, Ogden, or Neo-Hookean models.

-Mooney–Rivlin material model

This model was one of the first hyperelastic models used to predict the nonlinear behavior of isotropic hyperelastic materials [241]. The strain-energy function for this material model is:

$$U = \sum_{i=1}^{N=2} C_i(\bar{I}_i - 3)^i \quad (2)$$

-Ogden material model

Based on the theory of elasticity, the Ogden model was developed first time by Ogden in 1972 [242] and has the general form:

$$U = \sum_{i=1}^{N} \frac{2\mu_i}{\alpha_i^2}(\lambda_1^{\alpha_i} + \lambda_2^{\alpha_i} + \lambda_3^{\alpha_i} - 3) \quad (3)$$

where μ_i and α_i are material constants and λ, are principal stretches.

-Yeoh material model

This model was first presented in 1990 for incompressible materials [243]:

$$U = \sum_{i=1}^{3} C_i(\bar{I}_1 - 3)^i \quad (4)$$

As shown in this equation, the strain-energy function in this model relies only on the first strain invariant ($\bar{I}_1$).

-Neo–Hookean material model

It was presented by Holzapfel [4]. For the Neo-Hookean material model, the function of the strain energy is related to a linear equation for the principal strains

$$U = C_i(\bar{I}_1 - 3) \quad (5)$$

Table 2.4 summarizes the coefficients of these equations based on previous approaches in the literature. These constant parameters are calculated by stress-strain experiments. The uniaxial test is more widespread and typical than biaxial and planning tests. Selecting and designing the most appropriate test for the specimen of silicone increases the accuracy of the model parameters. Several approaches were studied to predict the nonlinear elastic behavior of silicone rubber under different loading conditions in order to understand the mechanics by finding the best least square curve fitting the potential strain energy function. Marechal et al. [244] provided a database of the best constitutive models and the values of the coefficients according to uniaxial tensile tests recommended in the ASTM D412 for elastomers. Each silicone specimen was cured at room temperature with the nominal mixing ratio recommended by the manufacturers. We deployed this database to compare different suggested constitutive models in the previous approaches listed in Table 2.4. The results for different silicone materials are shown in Figure 2.8. Abaqus is used as the framework to reproduce the curve fitting of the suggested constitutive model in each reference. Although the treatment conditions, such as degassing, natural aging or the addition of pigment may affect the mechanical properties of the hyperelastic materials in this simulation, we assumed that these models were extracted in general conditions, such as the mixing ratio recommended by the manufacturer and curing at room temperature, without considering differences in the testing process and measurement equipment. Furthermore, most of the reviewed articles do not mention which type of test data, true or engineering strain-stress, were used to predict the material models. Note that engineering stress, also known as nominal stress, is calculated by dividing the applied force by the primary cross-section area of the material, while in true stress this area is changed and calculated with respect to time. We extracted the true and engineering strain-stress data from the proposed constitutive models in these articles using ABAQUS software. These figures help to compare the models by assuming that the experimental protocol is the same and based on ASTM D412.

Table 2.4. Material modeling for various types of silicone for soft fluidic

Material	*Treatment*	*Software*	*Model*	*Coefficient (MPa)*	*Refs.*
EcoFlex 00-10	-	ABAQUS	Ogden (*N=1*)	$\mu_1 = 12.605 \times 10^{-3}, \alpha_1 = 4.32$	Sparks et al. [245]
EcoFlex 00-30	Curing at 120 °C for 60 min after vacuum degassing (EcoFlex) Strain rate: 300 mm/min	ABAQUS	Yeoh	$C_{10} = 5.072 \times 10^{-3}, C_{20} = -3.31 \times 10^{-4}, C_{30} = -1.5 \times 10^{-5}$	Elsayed et al. [187]
	ASTM D638, strain rate: 500 mm/min	ABAQUS	Yeoh	$C_{10} = 0.012662$	Polygerinos et al. [236]
	ASTM D412, curing at room temperature	ABAQUS	Ogden (*N=3*)	$\mu_1 = 0.024361, \alpha_1 = 1.7138, \mu_2 = 6.6703 \times 10^{-5}, \alpha_2 = 7.0679, \mu_3 = 4.5381 \times 10^{-4}, \alpha_3 = -3.3659$	Moseley et al. [239]
	-	ABAQUS	Ogden (*N=3*)	$\mu_1 = 1.887 \times 10^{-3}, \alpha_1 = -3.848, \mu_2 = 2.225 \times 10^{-2}, \alpha_2 = 0.6632, \mu_3 = 3.574 \times 10^{-3}, \alpha_3 = 4.225, , D_1 = 2.9259$	Agarwal et al. [246]
	Curing at 60 °C for 15 min after vacuum degassing	ABAQUS	Arruda-Boyce	$\mu = 0.03, \lambda = 3.9$	Martinez et al.[247]
	Curing at 55 °C for 20 min after vacuum degassing	ABAQUS	Yeoh	$C_{10} = 7.61 \times 10^{-3}, C_{20} = 2.42 \times 10^{-4}, C_{30} = -6.2 \times 10^{-7}$	Sareh et al. [248]
	ISO 527-3	ABAQUS	Ogden (*N=3*)	$\mu_1 = 2.2 \times 10^{-2}, \alpha_1 = 1.3, \mu_2 = 4 \times 10^{-4}, \alpha_2 = 5, \mu_3 = -2 \times 10^{-3}, \alpha_3 = -2$	Steck et al. [249]
		ABAQUS	Yeoh	$C_{10} = 1.7 \times 10^{-2}, C_{20} = -2 \times 10^{-4}, C_{30} = 2.3 \times 10^{-5}$	
	-	ABAQUS	Neo-Hookean	$C_{10} = 0.01$	Subramaniam et al. [216]
	ASTM D412, the strain rate of 450 mm/min, curing at room temperature with vacuum degassing	Developed Python code	Ogden (*N=3*)	$\mu_1 = -0.322, \alpha_1 = 3.31, \mu_2 = 0.19, \alpha_2 = 3.115, \mu_3 = 0.145, \alpha_3 = 3.468$	Marechal et al. [244]
EcoFlex 00-50	Curing at 120 °C for 60 min after vacuum degassing (EcoFlex)	ABAQUS	Ogden (*N=3*)	$\mu_1 = 107.9 \times 10^{-3}, \alpha_1 = 1.55, \mu_2 = 21.47 \times 10^{-6}, \alpha_2 = 7.86, \mu_3 = -87.1 \times 10^{-3}, \alpha_3 = -1.91$	Elsayed et al. [187]
	-	ABAQUS	Yeoh	$C_{10} = 1.9 \times 10^{-2}, C_{20} = 9 \times 10^{-4}, C_{30} = -4.75 \times 10^{-6}$	Runge et al. [250]
	-	ANSYS	Hookean	-	Nasab et al. [251]
	Strain rate: 0.2 mm/s	-	Mooney-Rivlin	$C_1 = 10.401 \times 10^{-3}, C_2 = 21.362 \times 10^{-3}$	Pineda et al.[252], Lee et al.[253]
	ASTM D412, the strain rate of 450 mm/min, curing at room temperature with vacuum degassing	Developed Python code	Ogden (*N=3*)	$\mu_1 = 1.97, \alpha_1 = 2.911, \mu_2 = -3.671, \alpha_2 = 3.008, \mu_3 = 1.740, \alpha_3 = 3.096$	Marechal et al. [244]
Dragonskin 10	-	ABAQUS	Yeoh	$C_{10} = 36 \times 10^{-3}, C_{20} = 2.58 \times 10^{-5}, C_{30} = -5.6 \times 10^{-7}$	Sareh et al. [248]
	ISO 37, strain rate: 450 mm/min, curing at room temperature with vacuum degassing	ABAQUS	Ogden (*N=3*)	$\mu_1 = -1.8261, \alpha_1 = 1.613, \mu_2 = 1.12, \alpha_2 = 2.0184, \mu_3 = 0.7951, \alpha_3 = 0.9386$	Byrne et al. [254]
	-	ANSYS	Mooney–Rivlin	$C_{10} = 0.04, C_{01} = -0.033, C_{11} = 1.2 \times 10^{-3}$	Basturen et al. [255]
	ASTM D412, Strain rate of 500 mm/min	-	Yeoh	$C_{10} = 7.61 \times 10^{-3}, C_{20} = 2.42 \times 10^{-4}, C_{30} = -6.2 \times 10^{-7}$	Low et al. [256]
	ASTM D412, the strain rate of 450 mm/min, curing at room temperature with vacuum degassing	Developed Python code	Ogden (*N=3*)	$\mu_1 = 1.971 \times 10^{-19}, \alpha_1 = 18.341, \mu_2 = 1.03, \alpha_2 = 2.729, \mu_3 = -1.059, \alpha_3 = 2.649$	Marechal et al. [244]

Dragon Skin 30	Strain rate: 300 mm/min	ABAQUS	Yeoh	$C_{10} = 1.19 \times 10^{-3}, C_{20} = 2.3 \times 10^{-2}$	Elsayed et al. [187]
	-	ANSYS	Ogden (*N=1*)	$\mu_1 = 75.449 \times 10^{-3}, \alpha_1 = 5.836$	Heung et al. [257]
	-	ANSYS	Ogden (*N=1*)	$\mu_1 = 0.1581, \alpha_1 = 2.7172$	Al-Rubaiai et al. [258]
	ASTM D412, the strain rate of 450 mm/min, curing at room temperature with vacuum degassing	Developed Python code	Mooney–Rivlin	$C_{10} = 0.247, C_{01} = -0.33, C_{20} = 2.09 \times 10^{-4}$	Marechal et al. [244]
Elastosil M4601	ASTM D638, strain rate: 500 mm/min	ABAQUS	Yeoh	$C_{10} = 0.11\,, C_{20} = 0.02$	Polygerinos et al. [236], Zhang et al. [259]
	-	ABAQUS	Hookean	$E = 0.54\ MPa$	Yang et al. [260]
	ASTM D638	ABAQUS	Yeoh	$C_{10} = 0.125, C_{20} = 0.0075$	Wang et al. [261]
	Curing at 70 °C for 20 min	ANSYS	Hookean	$E = 0.387$	Hu et al. [262]
	ASTM D638	-	Mooney-Rivlin	$C_1 = 10.401 \times 10^{-9}, C_2 = 21.362 \times 10^{-9}$	Ogura et. al. [215]
Silica gel	-	ABAQUS	Yeoh	$C_{10} = 0.036\,, C_{20} = 0.007$	Zhang et al. [263]
Agilus30		ABAQUS	Mooney-Rivlin	$C_{10} = -0.4889, C_{01} = 0.7147, C_{11} = -0.2704, C_{20} = 0.07929\,, C_{02} = 0.4709, D_1 = 0.4574, D_2 = 0$	Pasquier et al. [219], Chen et al. [220]
SmoothSil 960	Curing at room temperature for 24 hours	ABAQUS	Neo-Hookean	$C_{10} = 0.17$	Subramaniam et al. [216]
SmoothSil 940	-	ABAQUS	Neo-Hookean	$C_{10} = 0.12$	Subramaniam et al. [216]
MoldStar 30	-	ABAQUS	Neo-Hookean	$C_{10} = 0.055$	Subramaniam et al. [216]
Elastomeric Precursor	-	ANSYS	Hookean	-	Peele et al. [226]
RTV-KE1603	Curing at room temperature after vacuum degassing	MSC Marc	Mooney–Rivlin	$C_{10} = 8.635 \times 10^{-2}, C_{01} = 6.213 \times 10^{-2}, C_{11} = -1.2896 \times 10^{-2}, C_{20} = 3.425 \times 10^{-3}, C_{02} = -6.577 \times 10^{-1}$	Wakimoto et al. [214], Ogura et al. [215]
NinjaFlex	Printing temperature: 245°C	ABAQUS	Ogden (*N=3*)	$\mu_1 = -30.921, \alpha_1 = 0.508, \mu_2 = 10.342, \alpha_2 = 1.375, \mu_3 = 26.791\,, \alpha_3 = -0.482$	Yap et al. [111]
	ISO 37, strain rate: 100 mm/s, printing Temperature 240 °C	ANSYS	Mooney–Rivlin	$C_{10} = -2.33 \times 10^{-1}, C_{01} = 2.562, C_{11} = -0.561, C_{20} = 0.9$	Tawk et al. [264], [265]
FilaFlex	Printing temperature: 235°C	ANSYS	Mooney–Rivlin	$C_{10} = 1.594, C_{01} = 0.44, C_{11} = -4.4 \times 10^{-3}$	Hu et al. [218]

We take Marechal's test data as the reference and compare it with the other models for each type of silicone, by true and engineering stress versus strain results, as presented in Figure 2.8. This figure shows the experimental data compared with the best-fitting FE models results for the various silicone rubbers. As shown in (Figure 2.8a, b), for EcoFlex 00-30 in a small stress-strain range, most of the models are fitted with acceptable divergence. The Yeoh model suggested by Sareh et al. [248] fits the experimental data with few differences. In the EcoFlex 00-50 graphs (Figure 2.8c, d) the variation between the proposed models and raw experimental data is obvious even for small stress-strain values. The Yeoh model by Low et al. [256] (Figure 2.8e, f) and the first-order Ogden

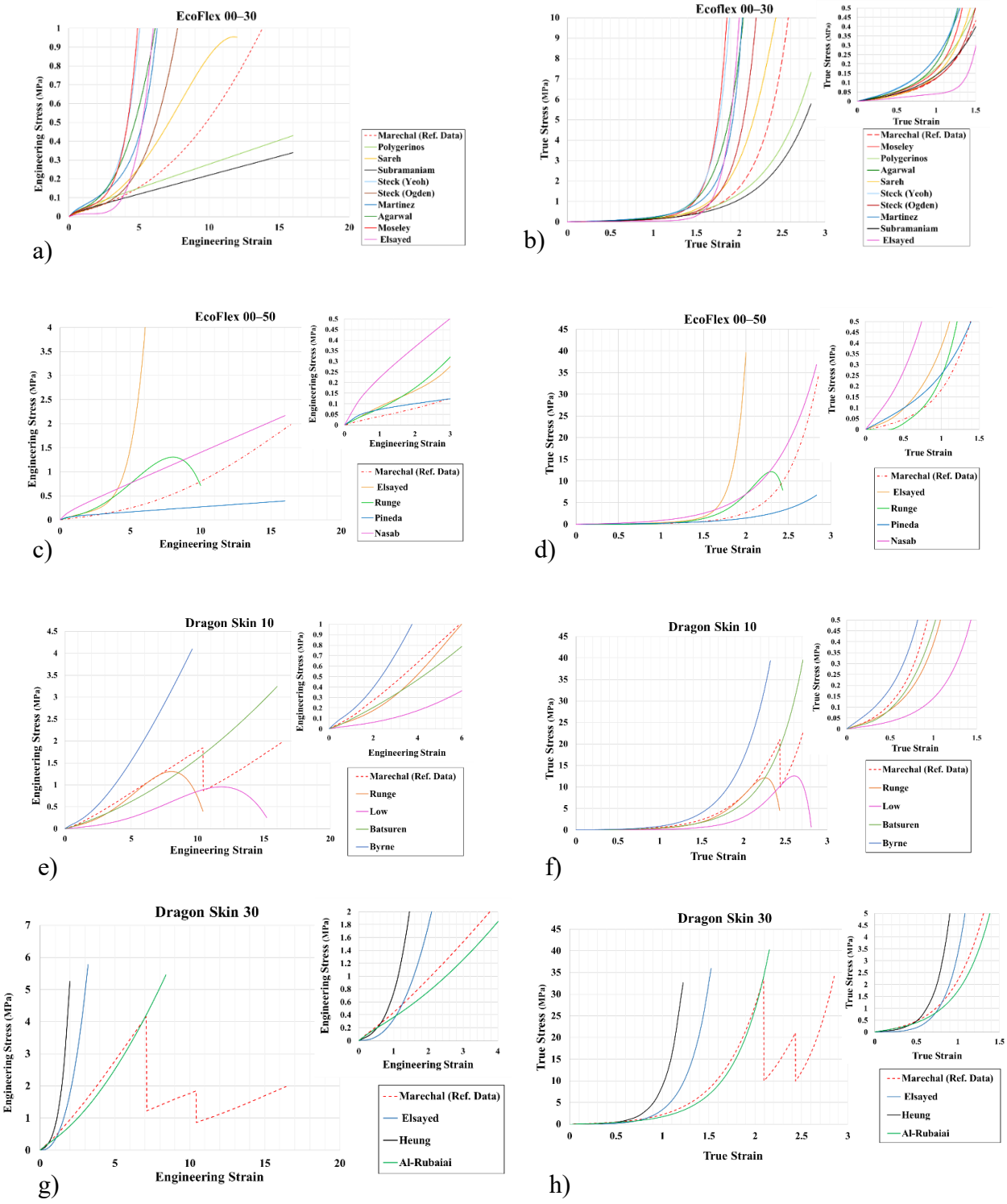

Figure 2.8. Comparison of the responses of proposed constitutive models for silicone materials in different references with uniaxial experimental standard test data from Marechal et al. [244]: a) Engineering stress-strain comparison of EcoFlex 00-30, b) True stress-strain comparison of EcoFlex 00-30, c) Engineering stress-strain comparison of EcoFlex 00-50, d) True stress-strain comparison of EcoFlex 00-50, e) Engineering stress-strain comparison of Dragon Skin 10, f) True stress-strain comparison of Dragon Skin 10, g) Engineering stress-strain comparison of Dragon Skin 30, h) True stress-strain comparison of Dragon Skin

model by Al-Rubaiai et al. [258] (Figure 2.8g, h) predict the behavior of Dragon skin 10 and 00-30 respectively with minimum divergence, even in large stress values.

2.6.2.2. Real-Time FEM Simulation

Although FEM software applications such as Abaqus and Ansys can generate precise calculations of SFPA, their slow simulation speed restricts their usage in real-time problems. To speed up the simulation, real-time software has been developed in recent years. One of the real-time simulation engines that provide several iterative algorithms and mechanical models for users is SOFA. It was first released in 2007 [266]. Due to its open-source availability, it has steadily evolved and different libraries such as a soft robot plugin have been added by users. SOFA uses general layers such as an internal model with independent DOFs, mass and material constitutive laws, a collision model, and a visual framework for modeling an object [267]. Dynamic control of SFPA is another advantage of using SOFA for simulation/control co-design procedures [268]-[269]. SOFA can interact with other software to co-design the controller; in this case, SOFA is a real-time FEM simulator and Matlab/Scilab are the control designer simulation engine [270]. However, real-time constraints make the method possible only for relatively coarse meshes and simple material constitutive laws. Furthermore, anisotropic material models are not available in SOFA and must be integrated with additional simulator codebases [193].

Vega-FEM is a free and open-source middleware C/C++ library for simulating 3-D deformable objects based on physics rules. In Vega, various linear and nonlinear material models can be implemented, including linear and co-rotational FEM elasticity, Saint-Venant Kirchhoff FEM model, invertible FEM models, and mass-spring systems [272]. It can efficiently predict the behavior of deformable materials such as silicone, and provides the base infrastructure to implement additional force models [273]. The potential challenge in Vega is it cannot correctly implement collision detection or contact points, so its application in contact approaches is limited [271]. Like SOFA, Voxelyze is another multi-material Open Dynamics Engine (ODE) for general static and dynamic analysis suggested by Hiller et al. [274]. It works based on the lattice of voxels of discrete points connected by spring-like beam elements including translational and rotational stiffness to simulate very large deformations and heterogeneous properties under an applied force. Although some applications of Voxelyze have been reported on soft robots [275], [276], it has some limitations which hinder its wide expansion. For instance, a precise

approximation of some geometrical shapes requires an increase in the number of voxels, which increases computation time. Moreover, beam theory in Voxelyze is used for the mechanical modeling of the object, which is different from the realistic deformation behavior of continuous material.

2.6.2.3. Model-free Methods

The obstacles we have discussed to developing analytical and numerical models have led to research attempts being made to control soft robots using nonparametric methods based on learning or vision. These aim to be a more efficient alternative. Lee et al. [277] proposed a nonparametric local learning technique to learn the inverse kinematics and control of SFAs. The model is able to predict the end-effector position of the robot accurately in the presence of an external dynamic disturbance. They utilized FEM to generate a sample of kinematic data to pre-train the initial control. A neural network was applied in [278] to control a 1-DOF SPFA, with a vision-based motion capture system acquiring unknown soft actuator parameters. A feedforward neural network to learn the 3D nonlinear inverse kinematic model of a soft octopus-arm was implemented and tested in [279]. The potential challenges of this method are the accuracy of the training-based kinematic computation, dependent on properly selected datasets. Several works can be found in the literature concerning the visual servoing of soft actuators. Li et al. [280] proposed an adaptive Kalman filter for continuum robot path tracking. They used pressures and tip position as input data. Then they estimated the robot's Jacobian of deformation by gathering the required data from the vision system. Zhang et al. [281] used real-time FEM simulation using SOFA to predict the Jacobian matrix of the robot. The correct position of the tipping point was modified in the feedback control law using a visual servoing system. Although the vision-based methods are efficient to reduce the number of sensors required to provide the state-space variables of the robots, the hardware requirements and the complex calibration process are the main remaining challenges to using this method in soft robot control scenarios [282], [283].

To summarize this section, Figure 2.9 shows the steps of the SFA fabrication procedure considering all the design parameters, including geometry, materials, constitutive law, and pressure which affect each other during the analysis and manufacturing of soft actuators. It should be noted that selecting the proper material for soft actuators depends on the different factors calculated during analysis.

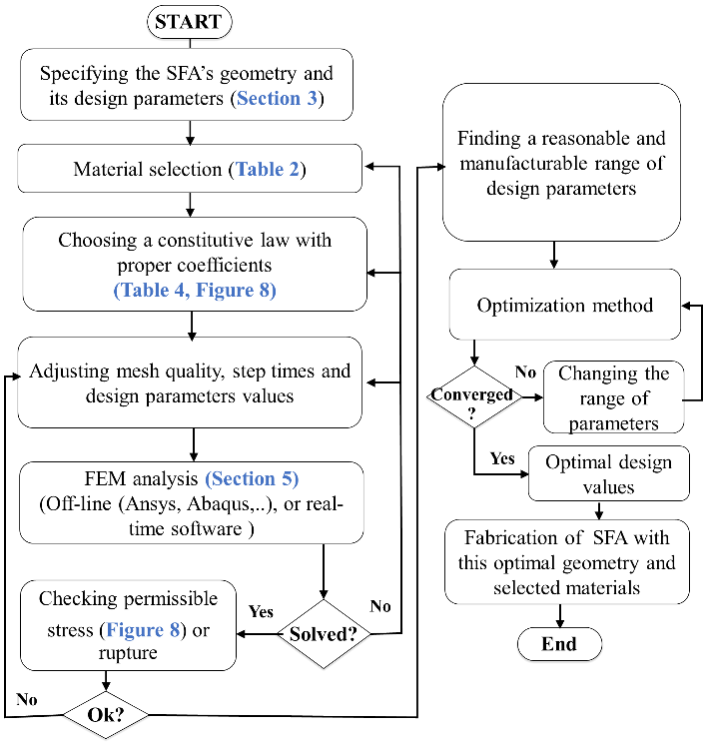

Figure 2.9. A flowchart of the fabrication procedure of SFA step by step from choosing material to build a prototype.

2.7. Sensing Technology in SFAs

As discussed in the previous section, the modeling and control of SFAs, because of their nonlinear behavior, are generally difficult, and in most cases come with a lot of simplified assumptions. Sensing technology is integrated into SFAs to detect the strain, curvature, contact point, and applied force to facilitate the control process of these kinds of actuators. However, to be integrated into soft actuators, these kinds of sensors must incorporate some special capabilities, such as high stretchability and stiffness, similar to those of the actuator, to prevent any motion restriction. Resistive or capacitive sensors are very popular in force, curvature, or tactile sensing applications. Most of them consist of conductive particles of carbon black (CB) [284],[285], graphene [286], [287], metal nanowires, carbon or nano-tubes (CNT) [288], [289]. McCoul et al. reviewed other types of electrode materials that are used in stretchable sensors [290]. The main functional difference between the resistive strain and capacitive sensor is that the resistive sensor works by strain changes that alter the conductivity, while the capacitive sensors are dependent on the geometry changes of the area between two electrodes. Yang et al. [291] printed resistive and capacitive sensors on a paper which was embedded in the SFAs (Figure 2.10a).

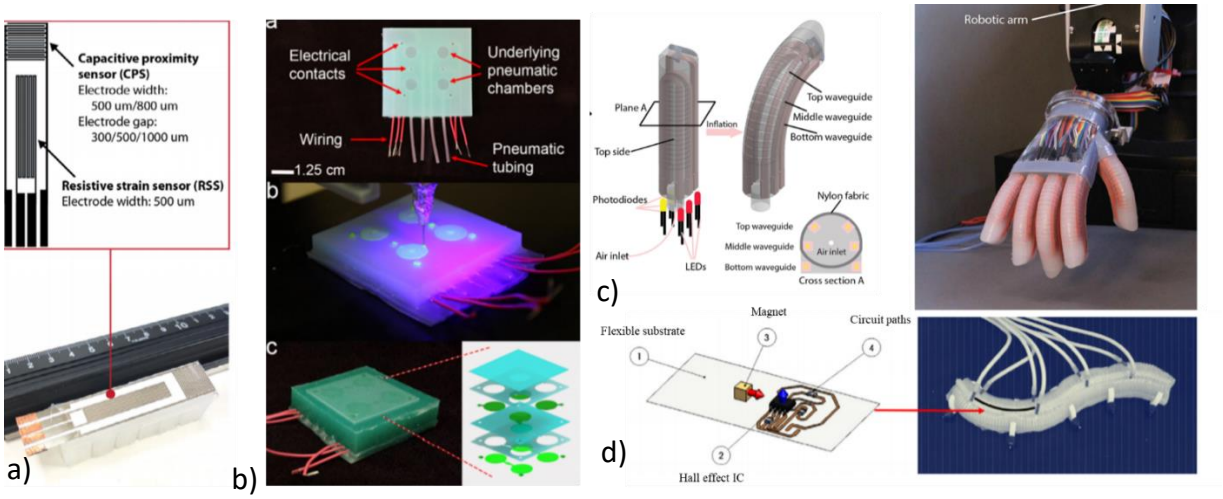

Figure 2.10. Soft fluidic actuators with integrated sensors: a) Combining resistive and capacitive sensors [291], b) Using a 3D printer to integrate hydrogel electrodes into silicone as a tactile sensor [292], c) Employing the optoelectronic sensor method as a tactile sensor with SFAs to detect curvature and bending angle [293], d) Embedded magnetic curvature sensor in SFA [294].

As they suggested, paper is cheap and can be used as a strain-limiting layer. In some approaches, they integrated commercial flex sensors in the SFAs to measure the bending angle [40], [295]. Kim et al. [296] compared the performance of two commercial products, Bend Sensor® and Flex Sensor®, to study the bending angle of the finger in hand posture estimation applications. These flex sensors only work in one direction and the results are not accurate when the sensor bends in a different direction. Robinson et al. [292] demonstrated a highly extensible capacitive sensor that was integrated into SFAs. They use 3D printing to integrate hydrogel electrodes into the silicone. This can also be used as a tactile-kinesthetic sensor (Figure 2.10b). An optoelectronic sensing method was integrated into SFAs by Zhao et al. [293]. Its principal functions are based on measuring Lossy waveguides by using a photodetector to specify its deformation, and it just requires a transparent material to transmit the light. As shown in Figure 2.10c, compared to resistive and capacitive sensors, there is no need to embed conductive materials, and consequently no modification to the stiffness of the actuator. Jung et al. [297] deployed this kind of sensor to estimate the configuration and shape control of SFAs. To increase optical resolution, the surface of the chamber is coated with a reflective metal layer. The use of a magnetic sensor has recently been reported to indicate SFA curvature [298], [299], [300]. The generated output voltage based on the Hall effect is changed due to the position and orientation of the magnet of the Hall element on a flexible circuit. Figure 2.10d shows the developed embedded magnetic curvature sensor in a SFA by Ozel et al. [294]. Although a magnetic sensor, unlike capacitive and resistive sensors, detects SFA

curvature accurately without requiring the application of external forces, adding the magnet and the Hall element affect the stiffness and performance of the actuator. Sensors play a significant role in detecting the behavior of soft actuators, so developments in this area will have promising effects on soft robot actuator applications.

2.8. Summary and Outlook

SFAs were the principal focus of this review study, due to their advantages, including minimal assembly, cost-effectiveness, large deformations, and high generated forces. These capabilities make them suitable for various applications such as gripping, mobility, robotic manipulation, medical tasks, rehabilitation and assistive purposes. We proposed a new general classification of soft pneumatic actuators by considering positive and negative pressure as a power source. We then categorized SFAs based on their design and mechanism into seven classes: Mckibben, continuum robot, PneuNets, universal gripper, origami soft structure, VAMPs, and HASEL design. This study provides various information on these well-known approaches, as well as other related works which have been inspired by these effective mechanisms. This classification helps the researcher to present the general kinematic or dynamic modeling or control strategies of each class. In the Hybrid section, the combination of SFAs with other actuating mechanisms is illustrated. This hybrid strategy improves the performance of SFAs with respect to shape configuration, control ability, variable stiffness, and operation range. In SFAs, material selection plays an important role and seems very challenging. Considering this fact, we studied and compared the mechanical properties of the various silicones which are reported in the previous studies. After explaining the different types of modeling and simulation of SFAs, the constitutive materials modeling reported in different articles was reviewed. Toward a better understanding of the differences between the constitutive equations, ABAQUS software was utilized to regenerate the strain-stress data of each article and depicted it in two different graphs, representing engineering strain-stress and true strain-stress for the most popular silicone rubbers. To be more realistic, we selected the Marechal et al. [244] database as a reference strain-stress database because of its standard procedure of extracting uniaxial tensile stress-strain data. Recent advances in sensor technology in the field of SFAs are illustrated in the sensor section. Finally, two different strategies for SFA fabrication are briefly explained at the end of this study.

Ongoing potential challenges of SFAs in future works can be addressed by improving the controllability of SFAs by embedding distributed sensors. These sensors should measure multi-contact points and simultaneously gather a wide range of object information including surface texture and mass while being stretchable and not increasing the actuators' stiffness. The other critical challenges of SFAs are their portability limitation due to requiring an external source of compressed air, especially for biomimicry applications. Several suggested solutions can be found in the literature but have not been commercialized as of yet. In addition, 3D printing of soft actuators reduces the molding cost and assembly's difficulties of current fabrication methods of SFAs.

Based on this chapter, due to the huge potential of SFAs including easy fabrication, low-cost elastomer materials, fast actuation speed, and high force generation, we choose this technology to study and improve the functionality of in-hand manipulation in the next chapters of this thesis.

II

Chapter 3: Paper #2

Design and Optimization of a Robotic Finger with a Sliding, Rotating, and Soft-Bending Mechanism

DOI:

10.1109/MRA.2020.3024283

Published in:

IEEE Robotics & Automation Magazine (Volume: 27, Issue: 4, Dec. 2020)

3.1. Abstract

In this article, a new soft finger with a pneumatic-actuated movable joint is introduced, optimized and characterized in terms of degrees of freedom, workspace and fingertip force. The finger consists of one soft link as the body and the bending pneumatic joint as the actuator. Due to the additional translation and rotation movement capabilities of the joint carried out by two stepper motors, the finger can bend in any direction while having different lengths, thanks to a configurable bending point. This results in more dexterity of the finger dealing with a target inside its 3D workspace by increasing the number of configurations in which the finger can reach the target and exert force. The finite element method (FEM) and NSGA-II algorithm are applied to optimize the joint geometry to maximize the bending angle and minimize the joint dimensions. Furthermore, the variations of each design parameter and the consequent effects on the optimization objectives are analyzed. The optimal geometrical parameters are used to fabricate a prototype with silicone rubber. Tests on bending angle and tip force variability are conducted on the prototype to validate the numerical modeling. The experimental results show that the finger exerts force up to 650 mN with a response time of less than three seconds. The stiffness of the finger can be changed by applying the pneumatic pressure in the hollow space inside the link. This consequently varies the amount of applied force at the tipping point of the finger up to two times.

3.2. FEAs Actuators

Introduced as a novel technology in recent years, soft robotics broadens new horizons in the field of robotics thanks to promising characteristics such as adaptability, lightweight, less assembly, and low cost [12]. The intrinsic deformable structure of soft robots encourages scientists to engage different technologies for their dynamization. One of the most widely used actuating technologies for soft robotics is Fluidic Elastomer Actuation (FEA), powered by a pressurized fluid (gas or liquid) [1]. Due to many advantages of FEAs including easy fabrication, producing high forces, large strokes, and low-cost elastomer materials [2], they have been used in numerous configurations for various purposes such as locomotion [3], manipulation [4], medical applications [108], and wearable devices [6]. These actuators can generate distributed forces which are proportional to the operating pressure of the fluid and the surface area on which the

pressure is applied [111]. Even though there is a large diversity of applications for FEAs, many challenges remain in this field including stiffness control and shape configuration. Researches have increased the performance of these kinds of actuators by integrating them with other types of actuation methods that help FEAs in terms of shape control and variable stiffness. These lateral technologies are mainly based on using variable stiffness materials, including shape memory polymers (SMPs) [93], combinations of SMPs with thermoplastic polyurethane (TPU) [167], and low melting point alloys (LMPAs) [156]. The main drawbacks of SMPs are a high hysteresis and a low actuation speed differs from 5 to 60 seconds regarding to the size of the actuator [2]. Using LMPAs is another suggested method for changing bending point and shape configuration in FEAs. Applying an electric current to the alloy and heating, the structure phase changes locally from rigid to soft and thus, variable stiffness can be achieved [110]. Like SMPs, the transition time is the main issue in LMPAs. Depending on size and geometry, the melting time for LMPAs differs from 1 to 30 seconds, while cooling takes over 60 seconds [301].

In this article, we introduce a novel type of soft finger based on bending point control and variable stiffness. The proposed finger is more flexible than previous solutions in terms of the attainable 3D space and applicable contact forces at the fingertip by changing the position of its joint, and thus, the bending point. The design consists of one elastomer tube as the soft link and one movable soft joint as the actuator. Applying the air pressure to the joint, the joint and the link will bend concurrently. Two stepper motors are responsible for moving the joint longitudinally along the link as well as rotating that around its axis. The joint can thus change the effective length of the finger and the bending direction. Unlike the previously proposed integrating methods with FEAs, based on SMPs or LMPAs, the position of the bending point is movable along the length of the link, which makes the finger more dexterous and reconfigurable.

Due to the nonlinear behavior of FEAs, their performance strongly depends on the geometry and dimensions of the actuator. Elsayed et al. [302] showed the effects of the position and shape configuration of the chamber on bending direction and angle value; they deployed a Finite Element Method (FEM) to study and optimize these design parameters. Decroly et al. [238] conducted an optimization study using a numerical model to miniaturize FEAs to be applicable in minimally invasive surgery. In our work, developing an optimization procedure is also essential for the achievement of our operating objectives: reconfigurability and variable stiffness. The NSGA-II algorithm is chosen as the optimization method due to its fast non-dominated sorting approach, fast

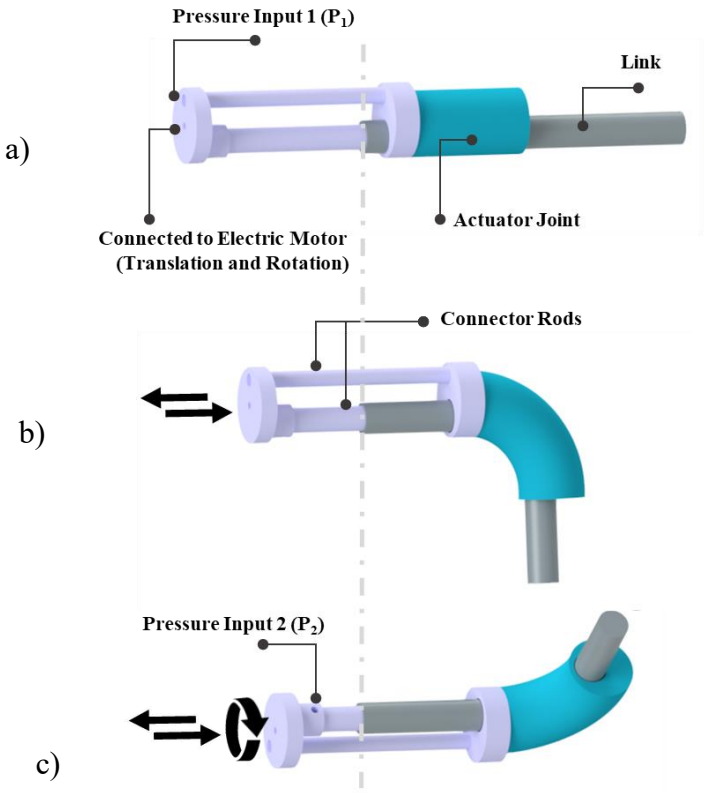

Figure 3.1. a) Schematic view of the proposed finger. b) sliding the joint along the link will change the bending point and the effective length of the finger. c) rotation of the joint along with its axis results in changing the bending direction in 3D space.

crowded distance estimation procedure and simple crowded comparison operator [303]. We use these capabilities for maximizing the bending angle up to 90 degrees and simultaneously minimizing the length and diameter of the joint while dealing with a variety of design parameters. Moreover, we investigate the sensitivity of each design parameter to reduce the computational cost and thus increase the convergence speed of the design procedure.

In the following section, we discuss the conceptual design of the proposed finger, followed by the description of the optimization process. The design parameters are optimized to guarantee a correct bending operation and reduce the joint dimensions. Permissible stress and required pressure are also taken into account. Numerical validation and experimental results are presented in the results and discussions section. The workspace of the optimized finger is determined to evaluate its dexterity compared to a conventional finger. Experiments are then conducted to validate the reconfigurability function and to verify the possibility of obtaining different shape configurations with various exerted forces at the same target position. The article ends with conclusions and discussions over future works.

3.3. Operating Principles and Design

The schematic of the proposed soft finger is illustrated in Figure 3.1. The finger is composed of a pneumatically actuated joint (blue cylinder) and a soft link (gray cylinder). A longitudinal channel is embedded inside the joint which inflates by supplying the air pressure (P_1) and leads to the bending of the joint and consequently, the link (Figure 3.1a). The bending location can be longitudinally changed by sliding the joint along the link (Figure 3.1b). The joint can also rotate around its main axis while the link remains steady due to its fixed connection to the base. This causes the finger to bend in any direction in 3D space (Figure 3.1c).

In Figure 3a, a conventional FEA finger (on the right) and the proposed finger (on the left) are compared in terms of dexterity and the strategies to reach a particular point in the workspace. Due to the uniform structure of the conventional FEA fingers and their limited degree of freedom, it is not possible for them to attain each point in their workspace with various configurations. On the contrary, the design of the proposed finger suggests an array of possible configurations in which the finger can reach each point. This not only results in more flexibility of the finger in dealing with obstacles that limit the workspace but also enhances the possible configurations in which the finger can exert a

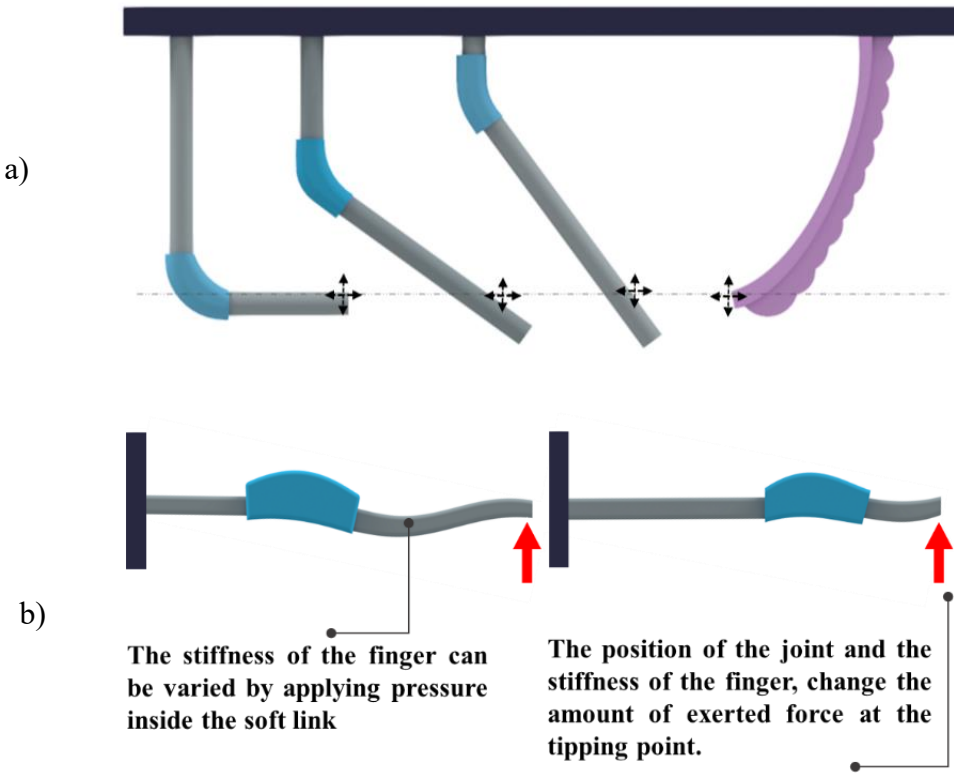

Figure 3.2. Comparison between the configurations of the proposed finger (left) and a conventional FEA-based finger (right) a) reaching a particular point. b) exerting a different amount of force to a tipping point.

different amount of force to a particular point (Figure 3.2b). The workspaces of these two fingers will be compared in the results and discussion section.

The mechanism used for changing the bending point of the finger mainly consists of two stepper motors connected to the joint (Figure 3.3). The first stepper motor is linked directly to the joint and is responsible for its rotational displacement. The connection includes two rigid rods; one for transmitting the rotational movement of the motor to the joint and the other with a tubular shape passing through the center of the link, for enhancing the stiffness of its region between the vertical support and the joint, which facilitates its deformation downstream and improves its controllability. As for the linear longitudinal movement of the joint, the assembly of the joint and the first motor are entirely displaced by the second stepper motor using a ball screw mechanism. We chose using a stepper motor solution for the movable joint due to its position accuracy and fast reactivity. Two air streams with different pressures are supplied to the finger; P_1 which deforms the joint and P_2 regulates the stiffness of the link. These two air streams are applied to the joint and the link via the two aforementioned rods between the joint and the stepper motor for rotation.

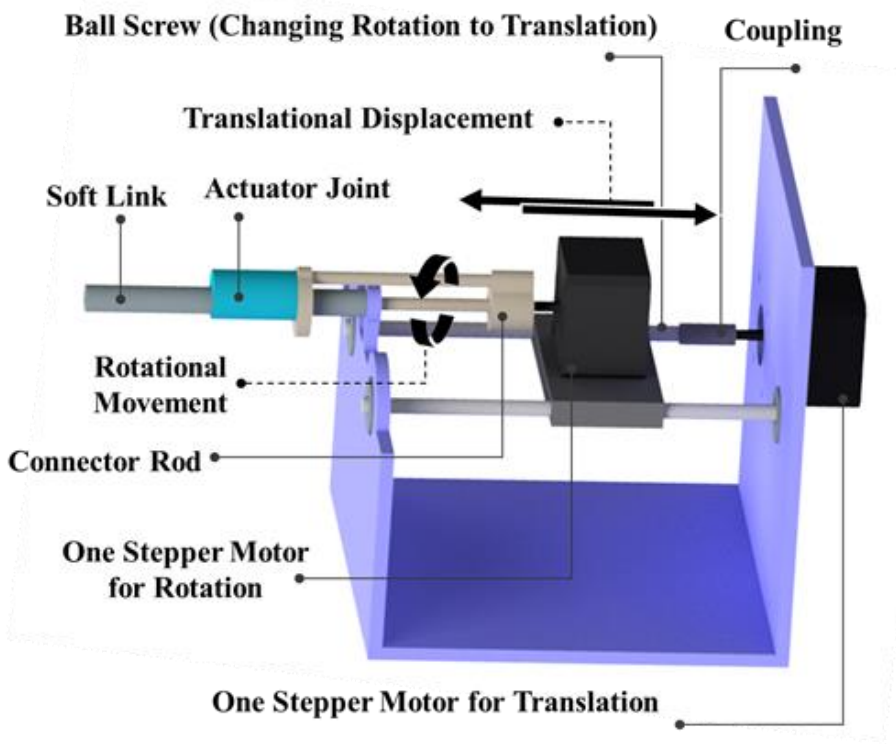

Figure 3.3. Assembly structure of the proposed finger and the motors.

3.4. Design Optimization

3.4.1. *Finite Element Modeling*

In this section, the optimization procedure is described for a finger with the approximate dimensions of the human finger (diameter=10 mm and length=150 mm). The objective of the optimization is to find the best values of the design parameters to meet the design objectives; i.e., maximizing the bending angle of the finger (θ) and minimizing the joint dimensions (length and diameter) under an approximate value of applied pressure to the joint (P_1). The amount of this pressure is numerically determined based on the 80% of the pressure that causes the joint to burst with 1 mm thickness of the chamber wall (H_1) which is equal to 14 kPa. Figure 3.4 summarizes the design parameters under investigation, including the main geometrical parameters of the joint. The range of variation for each design parameter is tabulated in Table 3.1. The lower and the upper bounds are specified based on the fabrication considerations and also the dimensions of the finger which are expected to be equivalent to the human finger. The pressure inside the link (P_2) is taken into account as another design parameter and the range of variation is selected in a way that a sensible variation can be observed in the stiffness of the finger. FEM is employed to solve the relevant equations for flexible materials numerically in the aim to evaluate the candidates within the design search space. ANSYS Workbench with the option of large nonlinear deformation for hyperelastic materials is used as the framework for solving these numerical equations and performing optimizations. As for selecting the materials, two variations of platinum-catalyzed silicones are nominated to

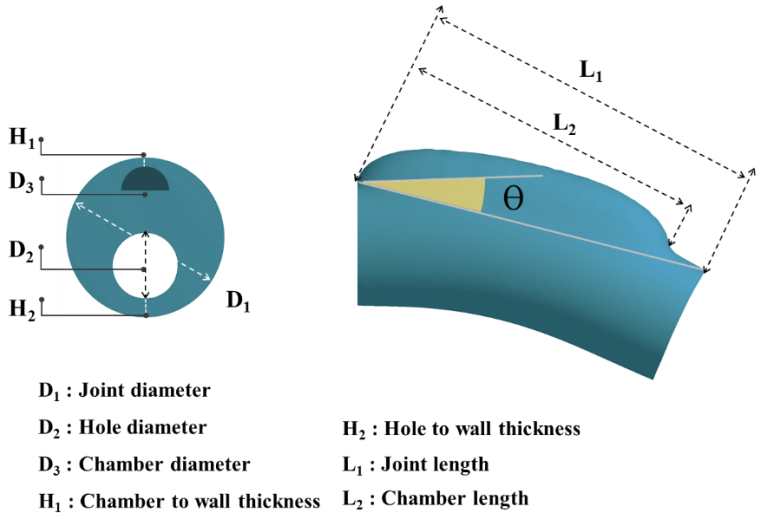

Figure 3.4. The geometrical optimization parameters.

fabricate the actuator module: Ecoflex 00-30 and 00-50, the code numbers referring to the material's shore hardness. As studied by Elsayed et al. [187], both the silicones exhibited the same bending behavior; however, lower pressure is required to deform the joint made of Ecoflex 00-30; accordingly, in this work, this material is selected to fabricate the joint. As for the link, Dragonskin 00-30 is selected. This is due to the direct interaction of the link with objects and consequently, the need for higher stiffness. Simulating the behaviors of these materials, silicone rubber is presumed as an isotropic and hyperplastic material. According to [249], for the Ecoflex 00-30, the third-order Ogden model (N=3) for the strain energy potential is expressed with μ and α as the empirical parameters (1). The parameters values $\mu_1 = 22$ kPa, $\alpha_1 = 1.3$, $\mu_2 = 0.4$ kPa, $\alpha_2 = 5$, $\mu_3 = -2$ kPa, and $\alpha_3 = -2$ show the best curve fit with the experimental stress-strain data of the mechanical tests:

$$U = \sum_{i=1}^{N} \frac{2\mu_i}{\alpha_i^2}(\lambda_1^{\alpha_i} + \lambda_2^{\alpha_i} + \lambda_3^{\alpha_i} - 3) \quad (1)$$

As for Dragon skin 00-30, the second-order Yeoh model is chosen due to the promising fitting with the stress-strain data of the mechanical tests with the parameter values of $N = 2$, $C_{10} = 1.190$ kPa, and $C_{20} = 23.028$ kPa [187]. This model can be presented for incompressible materials as in (2).

$$U = C_{10}(\bar{I}_1 - 3) + C_{20}(\bar{I}_1 - 3)^2 \quad (2)$$

Due to the large deformations in the joint structure, SOLID187 elements are used to mesh the model. These elements with quadratic displacement behavior are defined by ten nodes having three degrees of freedom at each node. This characteristic along with capabilities such as plasticity, hyperelasticity, creep, stress stiffening, large deflection, and large strain make them well suited to irregular model meshes (such as those produced in

Table 3.1. Ranges for design optimization parameters

Design Parameters	***Lower Bound***	***Upper Bound***
Joint length - L_1 (mm)	40	60
Chamber length - L_2 (mm)	30	50
Joint diameter - D_1 (mm)	20	40
Chamber diameter - D_3 (mm)	6	10
Chamber to wall thickness - H_1 (mm)	1	2
Hole to wall thickness - H_2 (mm)	1	5
Pressure inside the link - P_2 (kPa)	110	150

this analysis). Fixed support boundary conditions are applied to the beginning of both the link and the joint while the tips are set free to move. As for simulating the pressures in the joint and the link chambers (P_1 & P_2), constant normal pressure boundary conditions are considered with relevant values. Figure 3.5a illustrates the results of the bending simulation of a sample up to 90 degrees under the actuation pressure of 14 kPa.

3.4.2. *Sensitivity Analysis*

Before optimization, local sensitivity analysis helps to find the positive or negative effect of each design parameter on the objective output. This analysis is useful when a large number of variables exist and need to figure out the most critical design parameters to reduce the computational cost of the optimization [304]. The local sensitivity is calculated according to the (3),

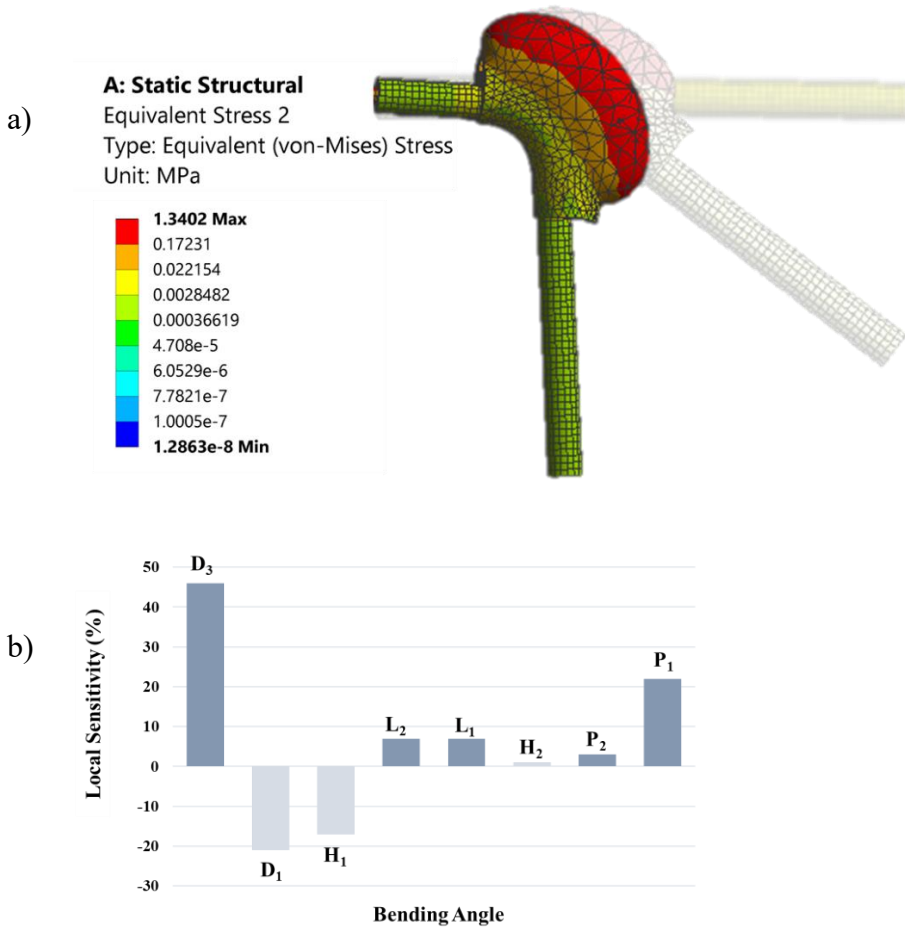

Figure 3.5. a) FEA simulation of a finger up to 90 degrees under the actuation pressure of 14 kPa. b) local sensitivity of the optimized result to each design parameter.

$$Local\,Sensivity(\%) = \pm \frac{(output_{\max} - output_{\min})_{local}}{(output_{\max} - output_{\min})_{global}} \times 100 \quad (3)$$

Where $(output_{\max} - output_{\min})_{local}$ is calculated when one input value varies and other values are assumed to be constant in particular geometry and $(output_{\max} - output_{\min})_{global}$ is calculated when all the inputs vary. Figure 3.5b presents the local sensitivity analysis of each design parameter in percent, as it can be observed, the chamber diameter (D_3) and the actuation pressure (P_1) are estimated to be the most important elements with direct relation to the bending angle; in other words, compared to other variables, increasing these two elements results in more intense positive changes in the final bending angle. The joint diameter (D_1) and the chamber to wall distance (H_1) stand in the next ranks of the most influential parameters, but in reverse relation with the main objective which means that the reduction in the values of these parameters causes the final bending angle to increase. On the other hand, the variations of the hole to wall distance (H_2) and the pressure inside the link (P_2) are estimated to be almost ineffective to the main objectives of the optimization and hence

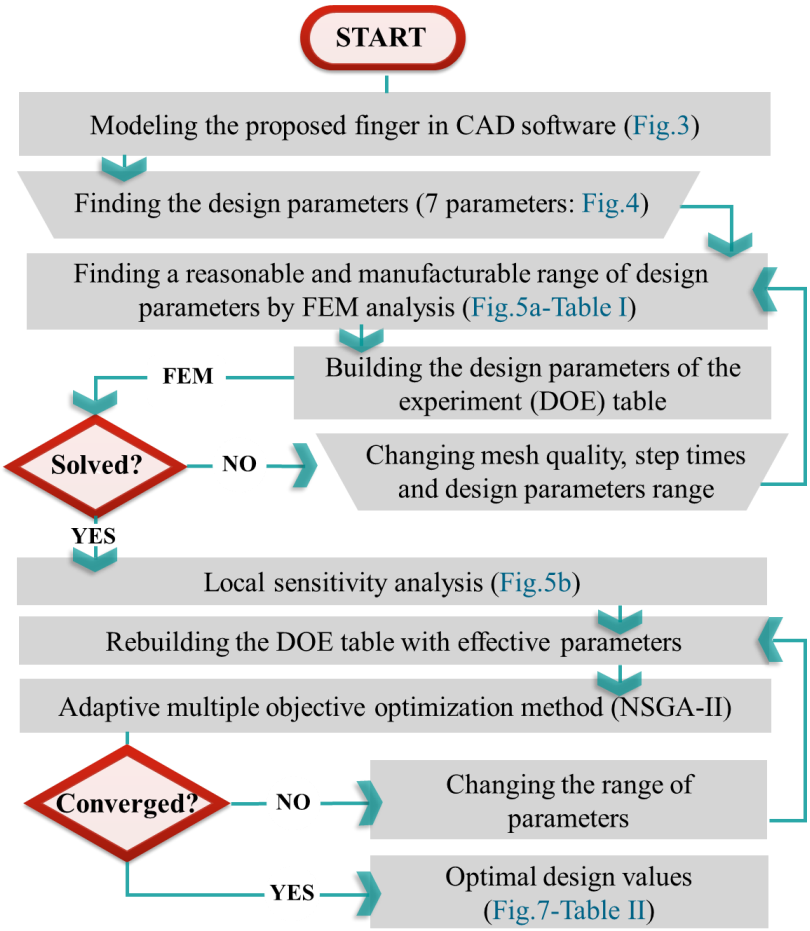

Figure 3.6. Flowchart of the proposed optimization methodology. The trapezoid shapes represent a manual operation and the other rectangular shapes are the automated process.

a)

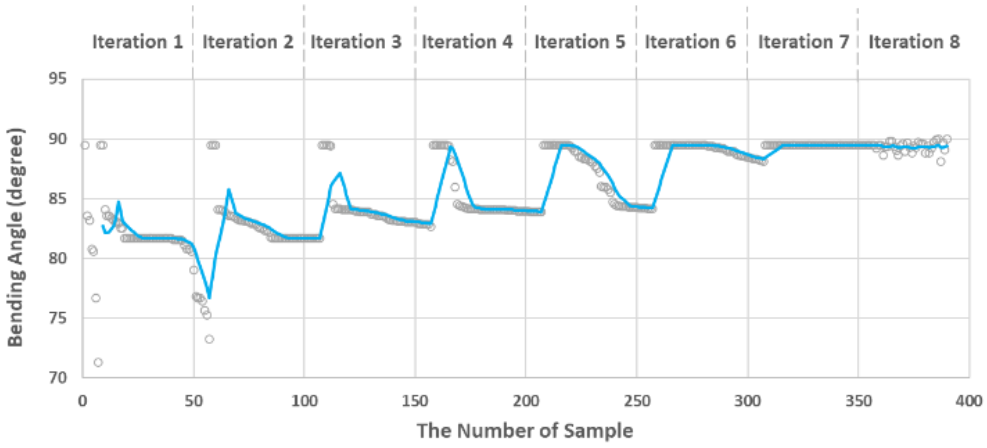
Iteration 1
Iteration 2
Iteration 3
Iteration 4
Iteration 5
Iteration 6
Iteration 7
Iteration 8
Bending Angle (degree)
95
90
85
80
75
70
0
50
100
150
200
250
300
350
400
The Number of Sample

b)

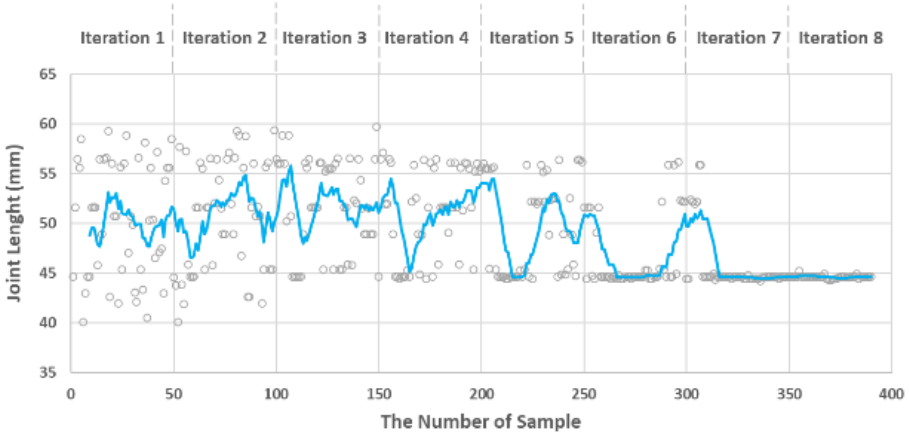
Iteration 1
Iteration 2
Iteration 3
Iteration 4
Iteration 5
Iteration 6
Iteration 7
Iteration 8
Joint Lenght (mm)
65
60
55
50
45
40
35
0
50
100
150
200
250
300
350
400
The Number of Sample

c)

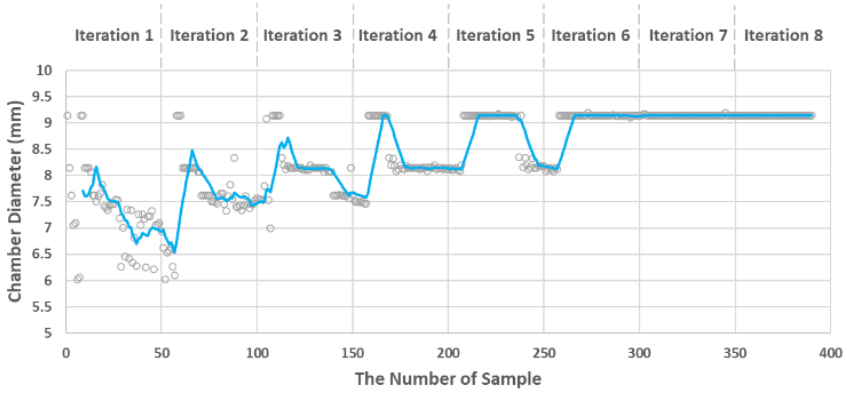
Iteration 1
Iteration 2
Iteration 3
Iteration 4
Iteration 5
Iteration 6
Iteration 7
Iteration 8
Chamber Diameter (mm)
10
9.5
9
8.5
8
7.5
7
6.5
6
5.5
5
0
50
100
150
200
250
300
350
400
The Number of Sample

d)

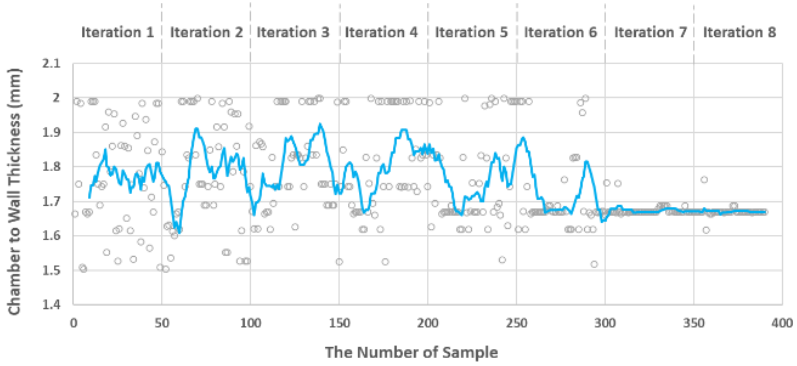
Iteration 1
Iteration 2
Iteration 3
Iteration 4
Iteration 5
Iteration 6
Iteration 7
Iteration 8
Chamber to Wall Thickness (mm)
2.1
2
1.9
1.8
1.7
1.6
1.5
1.4
0
50
100
150
200
250
300
350
400
The Number of Sample

e)

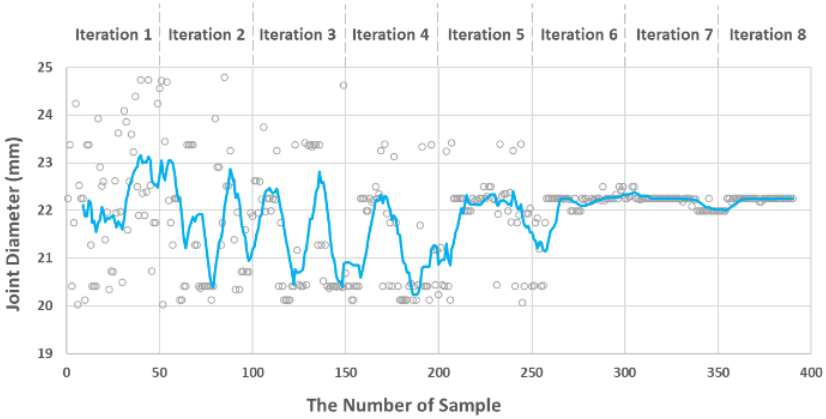

Figure 3.7. a-e) Optimization of the proposed soft finger: convergence of the design parameters to the final optimized values (blue lines show the moving average of each design parameter).

Table 3.2. FEM optimized parameters

Design Parameters	***Optimized value***
Joint length - L_1 (mm)	44.6
Chamber length - L_2 (mm)	42.5
Joint diameter - D_1 (mm)	22.3
Chamber diameter - D_3 (mm)	9.1
Chamber to wall thickness - H_1 (mm)	1.7

can be neglected; nevertheless, it should be noted that P_2 is an important parameter for changing the finger stiffness and thus the applied fingertip force. The effect of this parameter will be discussed in the following of this paper. As for H_2, the value is determined according to manufacturing considerations and is set to 2 mm. The low value of this parameter would result in aligning the surfaces of the joint and the link in the bending direction. This eventually leads to a uniform smooth surface in that area which can be beneficial in future possible grasping applications.

3.4.3. *Optimization Process*

After identifying the influential design parameters with local sensitivity analysis, an optimization analysis must be conducted. The goal is to maximize the bending angle up to 90 degrees and simultaneously minimizing the length and diameter of the joint (miniaturizing the dimension of the finger to be more like a human finger) under the

applied pressure to the joint (P_1) around 14 kPa. The optimization process and perquisites are shown in the flowchart in Figure 3.6. Due to the multiple numbers of design parameters, objectives and constraints, the Adaptive Multiple-Objective optimization method is selected to find the global optimum parameters. This method is a type of the Non-dominated Sorted Genetic Algorithm (NSGA-II) which is based on controlled elitism concepts [303]. This average value is selected through trial and error so that the finger with the specified ranges of geometrical dimensions can bend up to 90 degrees and not burst. The calculation converged by generating 400 samples with 50 samples per iteration and finding the best candidate in 8 iterations. Furthermore, during the process, if the FEM simulation of a sample fails (e.g. bursting), it will be eliminated and replaced by a new sample. Totally, 146 new samples have been generated and replaced the failed ones. The optimization charts are shown in Figures 3.7a-3.7e. In these figures, empty circles show the samples and the blue lines illustrate the moving average which is the best-fitted line that represents the convergence trend of the samples to the optimized values. Table 3.2 summarizes the eventual optimized values. These dimensions will be used to manufacture the prototype of the finger. The molds are printed with the Ultimaker3 3D printer. Thanks to recent advances in 3D printing technology, the fabrication process of soft components has been facilitated significantly which leads to producing more complex parts with higher precision. For each silicone, two liquid parts

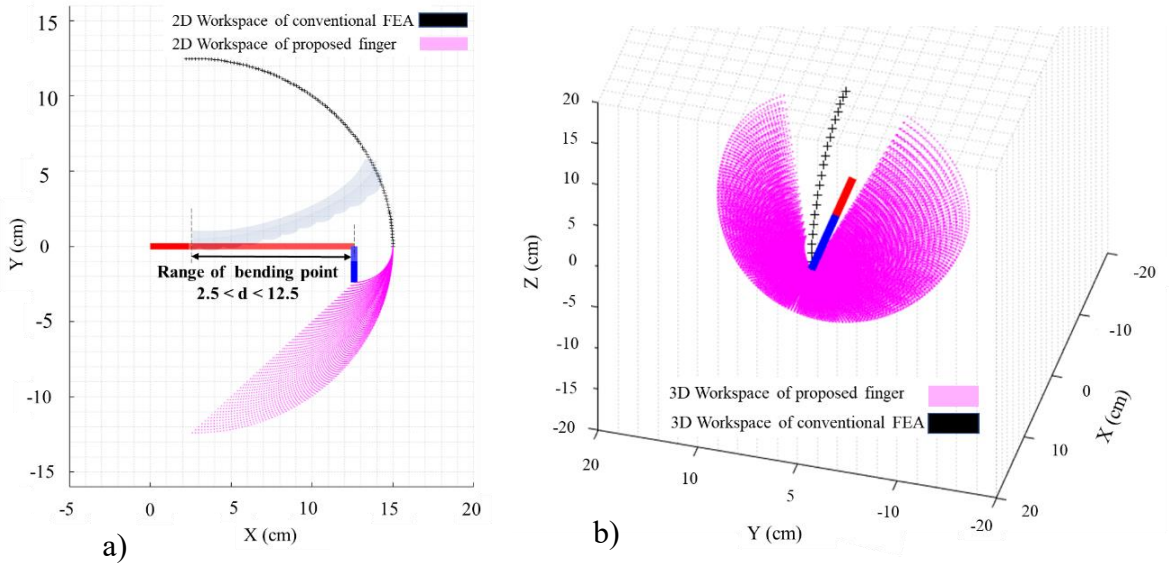

Figure 3.8. Workspace evaluation of proposed finger compared to conventional FEAs with 12.5 cm length a) in 2D space. b) in 3D space (the finger can rotate around its axis of about 300°)

should be mixed with the same ratio followed by 2-3 minutes vacuum degassing eliminate any entrapped air bubbles. This will be done by placing the molds in a vacuum chamber.

3.5. Results and Discussions

3.5.1. *Workspace Analysis*

Towards a better understanding of the finger mechanism, the workspace analysis is evaluated (Figure 3.8). The kinematic model of the finger is considered as one joint and two links. The first link (red) is fixed and the second one (blue) can bend up to 90 degrees in the XY plane. The whole finger can rotate around the X-axis about 300 degrees. By changing the position of the joint, the bending point and consequently lengths of the two links are changed. From an earlier section, the length of the finger and joint were presumed as the range of 15 and 4.46 cm. The bending point (center of joint) can be moved along the X-axis from 2.5 to 12.5 cm, the resulting workspace of every point touched by a fingertip in 2D (Figure 3.8a) and 3D (Figure 3.8b) is calculated. The 2D workspace comparison between the proposed finger and a traditional design shows that changing the position of bending increases the number of accessible points while the tipping point workspace of previous traditional FEAs is assumed to be a constant arc [236].

3.5.2. *Experimental Results*

Validating the numerical model introduced in the previous sections, the fabricated finger undergoes two sets of experiments, i.e., bending and force tests. Figure 3.9a shows the prototype assembled to conduct the experimental tests. Controlling the whole process including reading sensors, switches, and electric motors are performed by an Arduino Uno board which is connected to the computer via a USB wire. A 12 V 350 kPa air pump is used for supplying the pressurized air for the system. Regulating the pressures P_1 and P_2 independently, one solenoid valve and one silicon piezoresistive pressure sensor are embedded in each air stream. The feedback signals transfer from each pressure sensor to the Arduino are used to switch on and off the air pump and the relevant solenoid valve. Two test benches are developed to characterize the bending angle as well as the blocking force of the fingertip. The bending angle of the finger is checked using a printed protractor placed at the joint's center of bending (Figure 3.9b). As for measuring the force

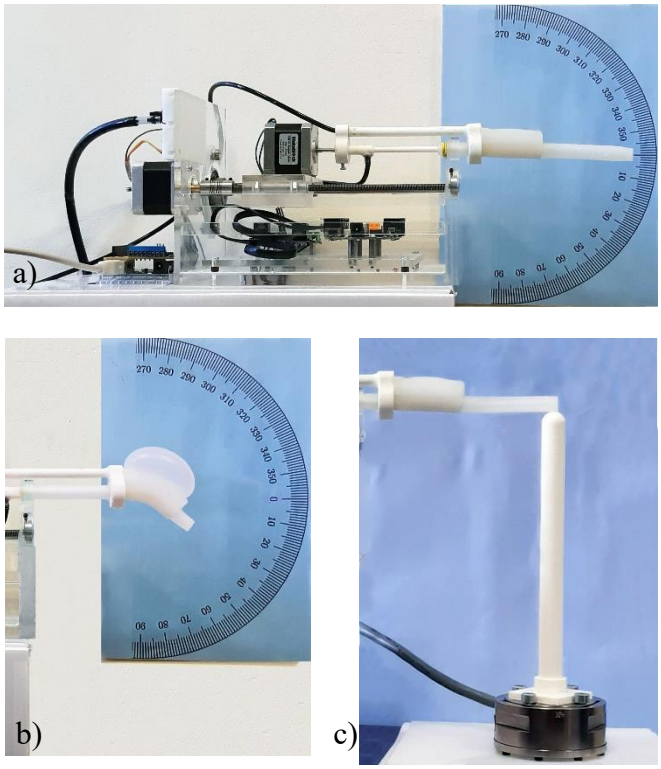

Figure 3.9. a) The overall view of the assembled prototype. b) test bench for measuring the joint angle. c) test bench for measuring the fingertip force.

applied by the fingertip, a force sensor is situated below the tipping point of the finger and directly transfers the force data to the computer (Figure 3.9c). Due to the weight of the link, at the initial state, a deflection of 10 degrees at the tipping point of the finger can be observed which will be resolved by applying the pressure P_2 inside the link. Different pressures P_1 are applied to the joint and the consequent bending angles are measured. These angles are compared with the numerical results in Figure 3.10a. It can be noticed that there is an acceptable agreement between the experimental and numerical data which can be taken as the validity of the model and thus the optimization results. As the second test with the assembled prototype, the force at the tipping point of the finger is measured as a function of different parameters including the longitudinal position of the joint and the stiffening pressure (P_2). All the tests are conducted under the actuation pressure of $P_1 = 14$ kPa. The results are presented in Figure 3.10b. As illustrated, by changing the position of the joint toward the tip of the finger, the applied force increases by almost three times. Furthermore, applying the pressurized air into the link results in higher stiffness and thus a higher amount of force up to 650 mN which is twice the initial value.

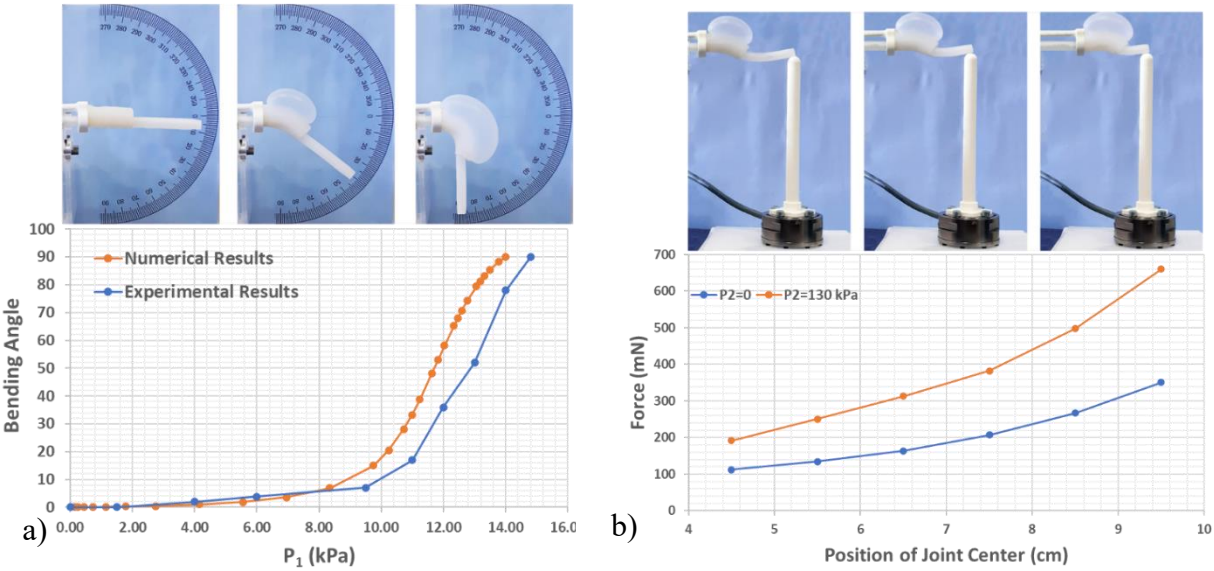

Figure 3.10. a) Bending angles of the finger under different applied pressures, comparison between ANSYS FEM numerical simulation and experimental results, b) fingertip force test results as a function of stiffening pressure (P_2) and joint longitudinal position.

3.6. Conclusions

In this paper, an innovative variable stiffness soft finger with a fluid-actuated movable joint was introduced and optimized in terms of its main characteristics. The finger mainly consists of one soft sliding and rotating joint as the bending actuator and a soft link as the body. Applying pressurized air into the joint's chamber, the joint and consequently, the link bends in a specific direction. The location and the direction of the bending can be changed by sliding the joint longitudinally along the link and rotating it around its main axis using two electric motors. The variable length of the finger with the capability of bending in different directions results in a large diversity of configurations. The workspace analysis exhibited the advantage of this reconfigurability by extending the available workspace of the fingertip in contrast to conventional FEAs. Local sensitivity of the design parameters involved in the problem was analyzed. Optimization over the important parameters was performed to minimize the joint dimensions and maximize the bending angle of the finger. The model included a large number of design parameters with nonlinear relations which made the prediction of the deformation difficult, i.e., small changes in each one can lead to large deviations in the final results. Hence, implementing the optimizing process is necessary to investigate the acceptable and manufacturable

range of these parameters. The optimal geometrical parameters were used for fabricating a prototype that validates the numerical model. Another experiment was designed to study the amount of force applied by the fingertip. It was shown that the longitudinal location of the joint and also the pressure inside the link (P_2) were highly effective to this force. The wide range of force applied to the fingertip as well as the diversity of possible configurations to reach a given target leads to a variety of strategies to deal with situations such as the variable amount of force required or presence of any obstacles in the workspace. Besides, optimizing the dimension of the finger allowed us to reduce the volume of the required air and consequently the response time. The experiments showed that the joint can bend up to 90 degrees in less than three seconds, in contrast with previous approaches (i.e. SMPs or LMPAs).

In this chapter, we proposed a soft reconfigurable finger with a movable joint for controlling the shape and bending position. In the next chapter, this reconfigurability design will be used for introducing a soft three-fingered gripper with increased dexterity for in-hand manipulation applications.

Chapter 4: Paper #3

A Soft Robotic Gripper with an Active Palm and Reconfigurable Fingers for Fully Dexterous In-Hand Manipulation

DOI:

10.1109/LRA.2021.3098803

Published in:

IEEE Robotics and Automation Letters (Volume: 6, Issue: 4, Oct. 2021)

4.1. Abstract

This study is focused on developing a new dexterous soft robotic gripper with three fingers and an active palm capable of performing in-hand manipulation purposes. This innovative design meets all the dexterous manipulation requirements without any increase in mechanical complexity. In each finger, the bending position can be modified and controlled by moving a stiff rod inserted inside the center hole of the finger. In this way, the effective length of the manipulation can be changed. As a result, these reconfigurable fingers provide a more accessible workspace than conventional soft grippers. Besides, a large diversity of the finger's shape configurations results in more dexterity and in-hand manipulation capability. Workspace analysis is accomplished to characterize the advantages of the proposed design. The effectiveness of this soft robotic gripper is validated by different in-hand manipulation experimental tests, including rotation, regrasping, and rolling. The results suggest a promising solution to bridge the design gap between hard and soft robots for dexterous manipulation tasks. The hybrid design carries advantages of these two classes, such as reconfigurability, position, and shape control from hard robots, with large degrees of freedom (DOFs), complex deformations, and lightweight from soft robots. Like human manipulation, the palm plays a major role in stable grasping, especially for enhancing the in-hand manipulation capability. Therefore, we also investigate two types of vacuum palms (suction cup and granular particles) to guarantee a wide range of object manipulation tasks that cannot be completely performed by previously suggested soft grippers.

Index Terms: Soft robotics, in-hand manipulation, dexterous gripper, shape adaptation, active palm.

4.2. Introduction

The soft fluidic actuator (SFA) is one of the most widely used actuation mechanisms in soft robotics. SFA has several advantages such as simple assembly, cost-effective materials, large deformation, and high generated force [1]. The positive or negative pressure exerted inside the chamber can cause the soft actuator to bend, extend, twist, or contract (depending on the type of surface on which the pressure is applied) [111]. These unique characteristics make them promising candidates for various applications, such as

gripping [2], mobility [3], robotic manipulation [4], as well as medical applications [108], and rehabilitation or assistive robotics [6]. Recent advances in soft grippers have been reviewed by Shintake et al. [2]. They found that SFA grippers can grasp a wide variety of objects of different sizes and shapes. They can mimic the behavior of human hand manipulation with more compatibility. They can securely handle objects with different shapes and dimensions without needing exact knowledge of their properties. Human hands can either move or translate an object using the fingers and the palm. In-hand manipulation is defined as the ability to hold and reposition an object within one hand and translate or rotate it between the fingers and the palm. It is referred to as one of the fundamental tasks for investigating the dexterity of robotic hands. This kind of manipulation has several advantages over full-arm manipulation, including its better performance in the presence of obstacles or joint singularities. Different manipulation approaches have been proposed in recent years. Ma et al. [305] categorized various within-hand manipulation strategies of hard robots into six groups: grasping [306], finger gaiting [307], in-grasp manipulation [308], finger pivoting/tracking [309], rolling [310], and sliding [311]. Shadow Hand is considered as one of the most dexterous robotic hands, including five fingers with a total of 24 DOFs [312]. Andrychowicz et al. [313] developed a reinforcement learning (RL) framework for the Shadow Hand to perform in-hand manipulation strategies such as pivoting and finger gaiting. Due to complex contact interaction between the hand and the object, these kinds of rigid dexterous hands require accurate planning and control strategies (e.g., machine learning) based on models of the object and fingers. The design and manufacturing of soft robots are more straightforward and more cost-effective than a dexterous hard robot that needs a lot of joints and motors for achieving dexterity. Consequently, soft robots can be an appropriate alternative for dexterous grippers. The use of soft robots as anthropomorphic robotic hands has emerged quickly in the last decades [314]-[134]. For instance, Batsuren et al. [255] proposed a soft robotics gripper with three fingers. Each finger includes three independent chambers, which can be actuated pneumatically to provide distinct types of motions. This gripper can rotate a lamp at around 35°. Shih et al. [315] integrated a similar design with a flexible sensor and identified an object's shape. This soft gripper could rotate an object at around 30°. Abondance et al. [106] suggested four soft robot grippers for finger gaiting and translation of objects. The anthropomorphic and dexterous soft hand proposed by Zhou et al. [316] consists of three fingers and a thumb with 13 DOFs, which enables the hand to carry out different types of in-hand manipulation tasks such as sliding, rolling,

and translation. They revealed that in-hand manipulation capability is empowered by increasing the common workspace area of the fingers.

The purpose of this paper is to develop a new type of soft gripper with three reconfigurable fingers and an active palm. Like human manipulation, the palm plays a substantial role in grasping, especially enhancing in-hand manipulation capabilities. For instance, this active palm can not only improve the stability of an object's grasping but also provides different in-hand manipulation tasks such as fingers and palm's regrasping, full rotation, and in-grasp manipulating that cannot be completely performed by the previously suggested soft grippers [315][21]. Each finger includes three chambers and a movable stiffed rod as a backbone in the center. The bending point and the effective length of the finger can simultaneously be changed by moving the stiff rod inserted inside the finger. This reconfigurable design results in enhancing the shape control of the finger, while the shape adaptability of the finger to the object is achieved by more possible grasping configurations. Furthermore, moving the bending points along with the fingers increases their workspace with a larger and more complex intersection area. The rest of the paper is organized as follows. The next section presents the conceptual and structural design for the proposed gripper. Section III discusses the workspace area of the proposed reconfigurable soft fingers. The manufacturing procedure is introduced in section IV. In section V, experimental in-hand manipulations are performed for five different tasks. Finally, a conclusion and future work are reported.

4.3. Operating Principles and Design

Figure 3.1 shows the model of the proposed soft gripper. The three symmetric fingers are radially located around a central axis passing through the palm of the gripper. Each finger is made of silicone elastomer and composed of three pneumatic chambers, which can be inflated independently (plus one central hole for reconfigurability). A wide range of workspace is achieved by activating combinations of two or three chambers. We previously demonstrated that the bending angle depends on several elements: the cross-section shape of the chamber, the finger diameter, as well as the applied pressure, and the distance between chambers and fingers [160]. Then, a sensitivity analysis was utilized to investigate the positive or negative effects of these parameters. Consequently, an optimization algorithm was deployed to find the best geometry for a maximum bending angle. In the present study, these optimized parameters are considered for designing the

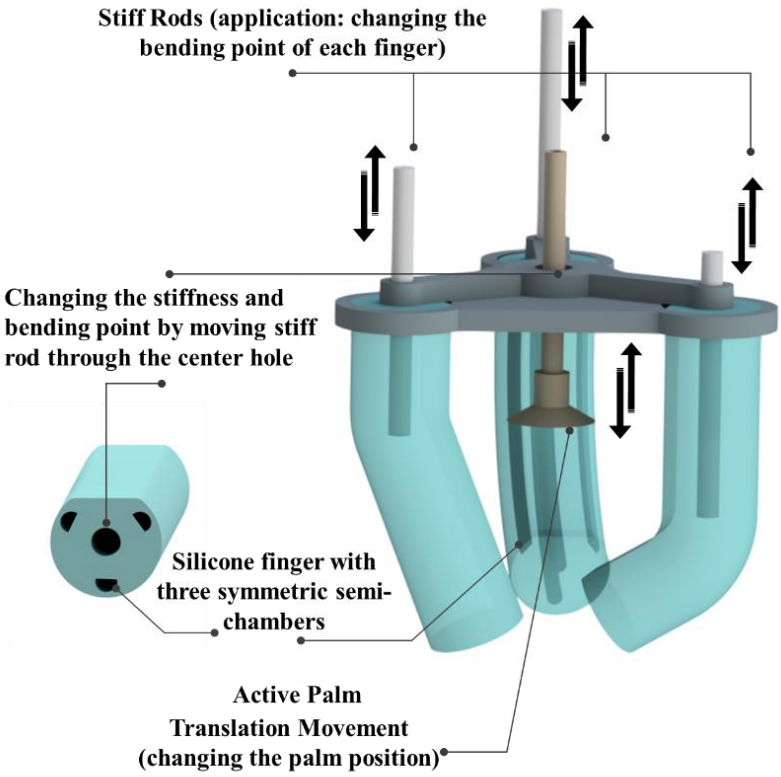

Figure 4.1. Schematic view of the proposed gripper

dimensions of the fingers and chambers. A semi-circular cross-section design is considered to reduce the ballooning effect of the chambers (in Elsayed et al. [187] and our previous work [160]). The other innovative part of our design is related to the addition of the stiff rod, which plays a principal role in grasping and in-hand manipulation tasks. As shown in Figure 4.1, the location of the bending point is modified by sliding the stiff rod. This process is carried out through the hollow center of the finger. This mechanism not only helps to control the shape of the soft finger effectively but also provides stable grasping of a wide range of objects with irregular shapes. The comparison of grasping between a conventional soft gripper and the proposed gripper is shown in Figure 4.2a. The curvature control of a conventional soft finger with one section is difficult. Therefore, the gripper made of this finger cannot adapt itself to the shape of the object. Consequently, proper contact and stable grasping remain incomplete. On the contrary, the movable joint reshapes the soft finger's bending curvature according to the object's contour, and thus more contact points are provided between the gripper and object. This adaptability guarantees a stable and reliable grasping. Besides, this design creates various

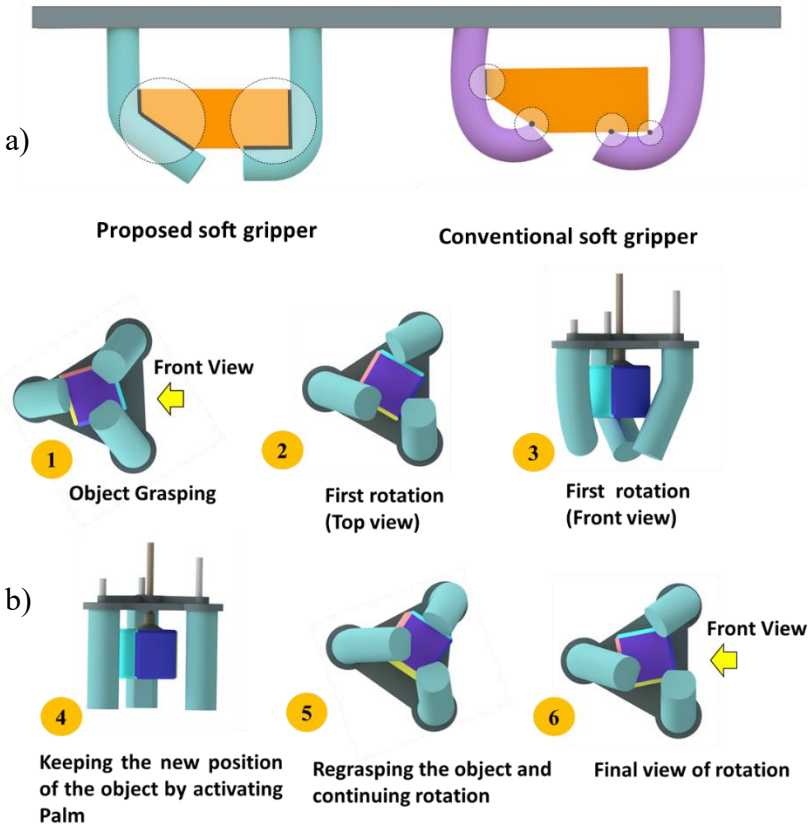

Figure 4.2. a) Performance comparison of the proposed finger and a conventional SFA, b) In-hand manipulation ability of the proposed soft gripper with active palm

possible configurations to access each point. It increases finger dexterity to encounter objects under unrecognized conditions or uncertainties. Human's hands can grasp an object by using the fingers and translate it from finger to palm or vice versa. The palm significantly contributes to supporting objects by providing an adequate and stable grasp. An active palm is attached to the center of the fingers for improving the capability of the proposed gripper. The distance between the palm and finger tipping point can be set based on the size of objects. Figure 4.2b shows how the inclusion of a palm in our design improves in-grasp manipulation. An active palm enables us to complete the in-hand manipulation task without taking advantage of the ground or gravity to fix or support the object when the palm is above the object, which is more like human in-hand manipulation. Besides the palm provide a reliable grasping approach of the wider range of object's weights. At the same time, applying air pressure to the lateral chamber in each finger leads to the rotation of an object around the principal axis of the gripper, while the palm is not active and acts as a fixture to keep the position of an object. After first-round rotation, the suction palm is activated to hold the object position, and then fingers will be

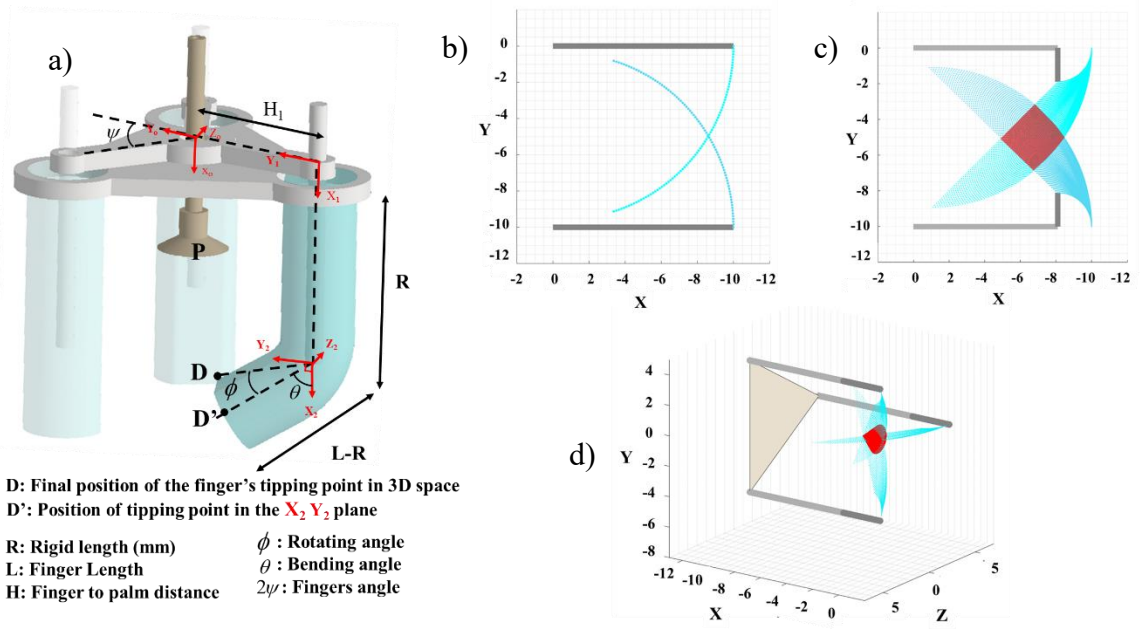

Figure 4.3. a) Kinematic modeling of the soft finger with a movable rod, b, c, d): 2D Workspace analysis and common reachable area of two fingers of 10 cm length: b) Conventional SFA compared with c) Proposed movable joint design, d) Common workspace area of the proposed soft gripper in 3D space.

inactivated and repositioned. Thereafter, it is actuated again to make a second rotation after inactivating the palm. This design provides stable and full rotation of the object (i.e., 360 degrees), using the necessary number of repetitions, with only three fingers and a palm. Other types of in-hand manipulation like rolling would also be possible by using the palm of the gripper. Three stepper motors with through-type lead screws are responsible for changing the bending position in each finger. This mechanism reduces the number of connection parts between the motor and finger. Also, it increases the position accuracy for the bending point with fast reactivity. Small solenoid valves control two types of airstreams: the positive one in the chambers (to deform the finger) and the negative one in the suction cup. Furthermore, the position of the palm is changed by another stepper motor connected to the suction cup in the center of the gripper's base. This mechanism changes the position of the palm based on the size of the object and the effective length of the finger. This functionality is especially useful during manipulations. This issue is discussed in the in-hand manipulation and dexterity validation section. The proposed gripper has a lower design, modeling, and fabrication complexities than the other dexterous rigid hands like Shadow Hand (24 joints) [312], Pisa/II (19 joints) [317], DLR Hand II (20 joints) [318], or even some dexterous soft hand like BCL-13 (13 chambers) [316] and BCL-26 (26 chambers) [314]. Moving the rod inside the finger changes the

bending point and the effective length of the finger results in different finger shape configurations with more dexterity. While in the previously cited approaches, the dexterity and in-hand manipulation capability are improved by increasing the number of joints and links.

4.4. Workspace Analysis of the Proposed Gripper

This section is focused on the workspace analysis and evaluating the mechanical design, manipulation range, and dexterity of the fingers. The finger kinematic model is configured as a movable joint and a soft link. By moving the stiff rod inside the finger, the position and the length of each part will consecutively be changed. The bending point divides the link into two separate parts: the rigid link (first part) and the soft link (second part). By applying pressure to the inside of a chamber which is located head-on the object, the finger starts to bend in the XY plane from the bending point. Actuating the other side chamber rotates the tipping point of the finger in a 3D space. The transformation matrix of the tipping point for each finger can be calculated by these steps (Figure 4.3a):

1) Rotation D point to D' by ϕ angle about x_2 axis

2) Rotation by $-\theta$ angle about z_2 axis

3) Translation by R along x_1 axis

4) Translation by H along y_0 axis

The final transformation matrix can be defined as in (1)

$$A = \left(R_{\phi}^{X_2}\right)\left(R_{-\theta}^{Z_2}\right)\left(H_{R}^{X_1}\right)\left(H_{H}^{Y_0}\right) \tag{1}$$

The final transformation matrixes for each finger after simplification can be written as (2)

$$A = \begin{pmatrix} cos(\theta) & sin(\theta) & 0 & R\,cos(\theta) + H\,cos(\theta) \\ -cos(\phi)sin(\theta) & cos(\phi)cos(\theta) & -sin(\phi) & cos(\phi)*(H*cos(\theta) - R*sin(\theta)) \\ -sin(\phi)sin(\theta) & cos(\theta)sin(\phi) & cos(\phi) & sin(\phi)*(H*cos(\theta) - R*sin(\theta)) \\ 0 & 0 & 0 & 1 \end{pmatrix}. \tag{2}$$

Monte Carlo numerical algorithm is employed to calculate the resulting workspace for every point touched by a fingertip. The outcomes are depicted in Figure 4.3b, c, d. It is assumed that the length of the finger is 10 cm, and the bending point (the center of the joint) can move along with the link axis from 2 to 8 cm. The first link is fixed and the second one can be bent up to 90 degrees in the XY plane. By actuating the side chambers,

the finger can rotate from -120 to 120 degrees. It is presumed that the projected distance between two fingers in the XY plane is 10 cm. In Figure 4.3b, a comparison is made between the conventional soft finger with one section and the proposed finger for evaluating the accessible area in a 2D space. It shows that if the tipping point workspace of the previous traditional soft pneumatic actuator with one section is assumed to be a constant arc [236], the capability of changing the bending point enhances not only the reaching areas of the tipping point but also increases the common workspace between the fingers. The results of the references [316] and [319] revealed that the accessible area of each finger and the common workspace area are taken into account as two critical metric factors for measuring dexterity and in-hand manipulation capability. The larger reachable area with more shared intersection workspace results in more in-hand manipulation capability. The intersection area for two fingers is highlighted in Figure 4.3c by red color, and it is around 6.125 cm^2. For three fingers in a 3D space (Figure 4.3d), the total intersection volume is about 11.22 cm^3.

4.5. Manufacturing and Fabrication Process

One of the promising advantages of a soft robot in comparison with a hard robot is its low manufacturing cost. Soft pneumatic actuators are usually made of silicone rubber to support large elongation. Besides, silicone is not expensive, and its manufacturing process is fast. In this study, EcoFlex was chosen with shore hardness 00-30. It is selected due to its low viscosity, which provides the ability to bend the finger up to 90 degrees by using small pumps and applying a pressure of less than 0.1 bar. The recent advances in 3D printing technology significantly facilitate the fabrication process for soft components by producing more complex parts with higher precision. In this study, the printer's resolution is set at around 20 microns, and thus the printing process of all the molds lasts for about 14 hours. For each silicone, two liquid parts must be mixed with the same ratio followed by 2-3 minutes of vacuum degassing to eliminate any entrapped air bubbles. It is performed by placing the molds in a vacuum chamber. The standard cure time of Eco-Flex 00-30 is around four hours at ambient temperature. This time can be reduced to less than an hour by putting it in an oven at 100 °C.

4.6. In-hand Manipulation and Dexterity Validation

To validate the performance of the proposed movable joint, a workspace test was

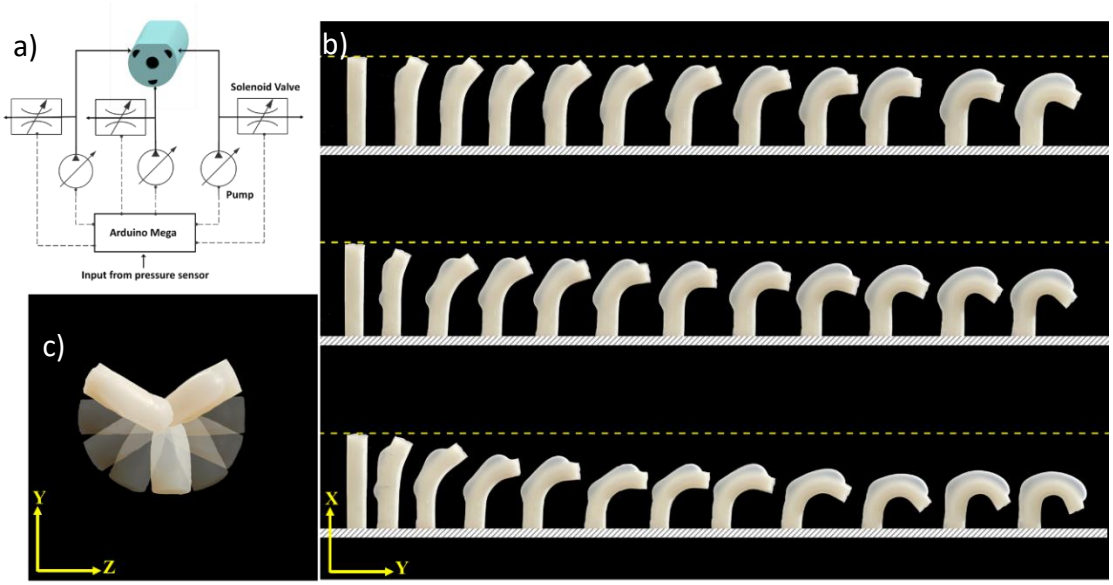

Figure 4.4. a) Electro-pneumatic control system of one soft finger, b) and c) Time-lapse of the soft finger with a movable joint workspace test in b) XY plane and c) YZ plane.

performed using camera recording positions. The pressure of each chamber is supplied by one micropump, and it is controlled by one solenoid valve and a piezoresistive pressure sensor. The microcontroller (Arduino Mega 2560) is used to control two different elements: (I) the switching of the micropumps and solenoid valves and (II) the handling of the electric motors following the feedback signals of the pressure sensors (Figure 4.4a). The test bench has been developed for one finger to characterize the performance of the movable joint. Figure 4.4b illustrates the time-lapse for different configurations of the finger in three positions of the bending points. It shows that a wide range of areas can be reached by a continuous movement of the bending point along with the finger. While the

Table 4.1. Device parameters: dimension and ranges

Finger length (mm):	$L_1=L_2=L_3=130$
Finger diameter (mm):	30
Rod diameter (mm):	8
Chamber length, diameter (mm):	125, 9.4
Palm translation range (mm):	$40 < X_p < 250$
Distance between fingers and palm (mm):	$30 < H < 95$
Bending point range (mm):	$40 < R < 125$

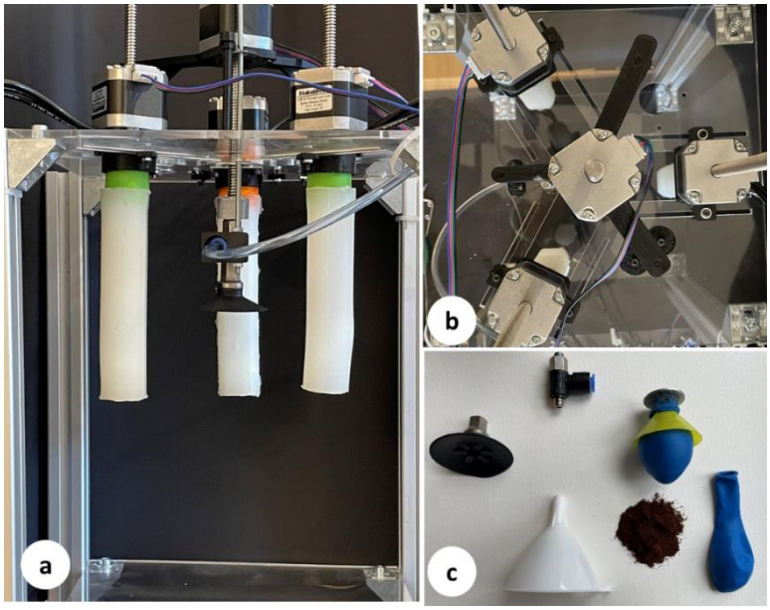

Figure 4.5. Schematic view of the proposed set-up assembly: a) The three soft fingers with variable lengths, b) The stiffed rod assemblies with their through-type stepper motors, c) Two easily interchangeable palms (suction cup and granular one).

main chamber is responsible for bending in the XY plane, activating the side chambers leads to the rotation of the tipping point of the finger from -120 to 120 degrees in the YZ plane (Figure 4.4c). The dimensions and ranges of variation for device parameters are tabulated in Table 4.1. The time-lapse of the one finger in the XY plane is conducted to show different possible shape configurations with a larger reachable area by changing the bending point.

As mentioned previously, the in-hand manipulation technique is generally categorized into three main classes: translation, rotation of the object, and relocation of the fingers. In this section, different tasks are defined based on these three categories to demonstrate the in-hand manipulation capability for the proposed gripper. Figure 4.5 shows the prototype setup for the proposed gripper to conduct the experimental tests. Three stepper motors are connected directly to the fingers for controlling the bending position (Figure 4.5a), while the fourth motor is located in the center of the gripper, and it is responsible for moving the palm (Figure 4.5b). In this study, two palm designs (i.e., suction cup and granular matter) are suggested to maintain the grasping of a wide variety of objects' shapes. These two designs are similar and work with the same actuation mechanism and control units. As shown in Figure 4.5c, they can easily be inverted. The connection part is utilized to convert these palms very easily and quickly.

Task 1- Stable grasping: Like the human hand, the palm significantly contributes to

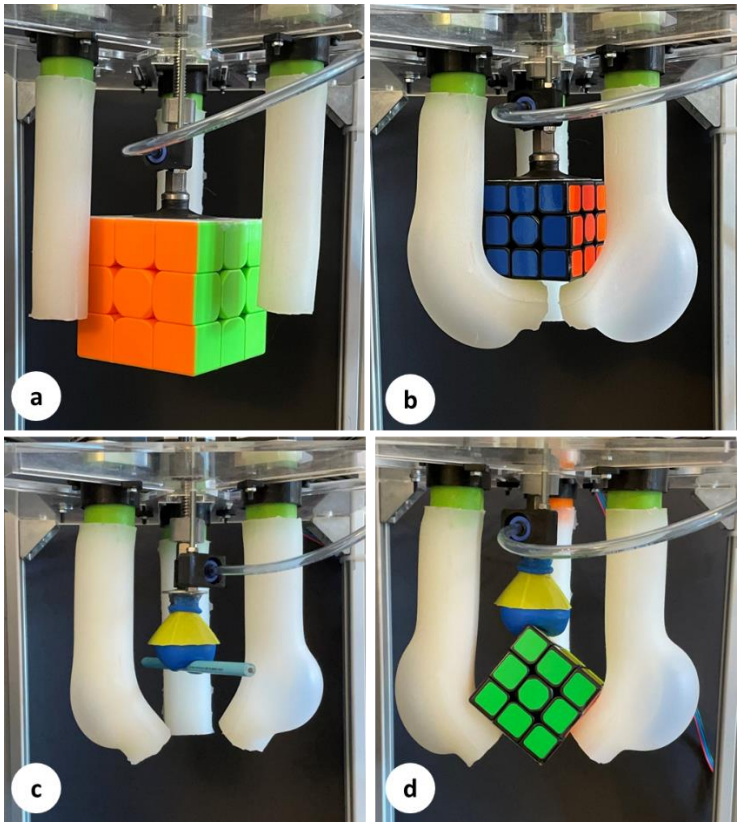

Figure 4.6. Different types of grasping with the proposed gripper: a) Large cube by the suction cup, b) Suction cup and soft fingers for stable grasping, c) Granular palm for a non-flat object like a pencil, d) Shape adaptability of the fingers with the object (see Figure 4.2a).

supporting objects manipulated by hand. In the proposed gripper, an active palm has been designed to improve manipulation performance. The position of the palm can be changed along with the principal axis of the palm to ensure that there is proper contact between the fingers and an object in terms of the size and shape of objects. Two different types of palms are considered: (I) simple suction cup and (II) membrane palm with granular particles (Figure 4.5c). A suction cup is an appropriate choice for a flat and deformable object (Figure 4.6a, b), whereas the granular palm is useful for an object with an edge or non-smooth surface like a pencil (Figure 4.6c). The other aspect of this task is grasping and holding the object by the palm and fingers with adjusted bending points for reliable grasping strategies (Figure 4.6d).

Task 2- Full rotation of the object by regrasping between the palm and the fingers: This task is principally concerned with the issue that the object should be able to translate from palm-to-finger and finger-to-palm and change the contact points. This capability is validated using the 3×3×3 Rubik's Cube with a dimension of 5.6 cm to make a full

rotation around its principal axis. In the proposed gripper, the active palm helps to make a full rotation of objects. In this regard, the first step is dealt with activating the palm to

Table 4.2. Task 2, Full rotation procedure

1- The bending point for three fingers is set to R=70 mm
2- Fingers are actuated to grasp the cube ($\theta_1 = \theta_2 = \theta_3 \simeq 70°$)
3- Palm is inactive and fingers hold the cube (X_P =80 mm)
4- Side chambers are activated to rotate the cube ($\phi_1 = \phi_2 = \phi_3 \simeq 35°$)
5- Palm moves close to the cube and grasps the cube (X_P =85 mm)
6- Fingers are inactivated and ready for the second rotation

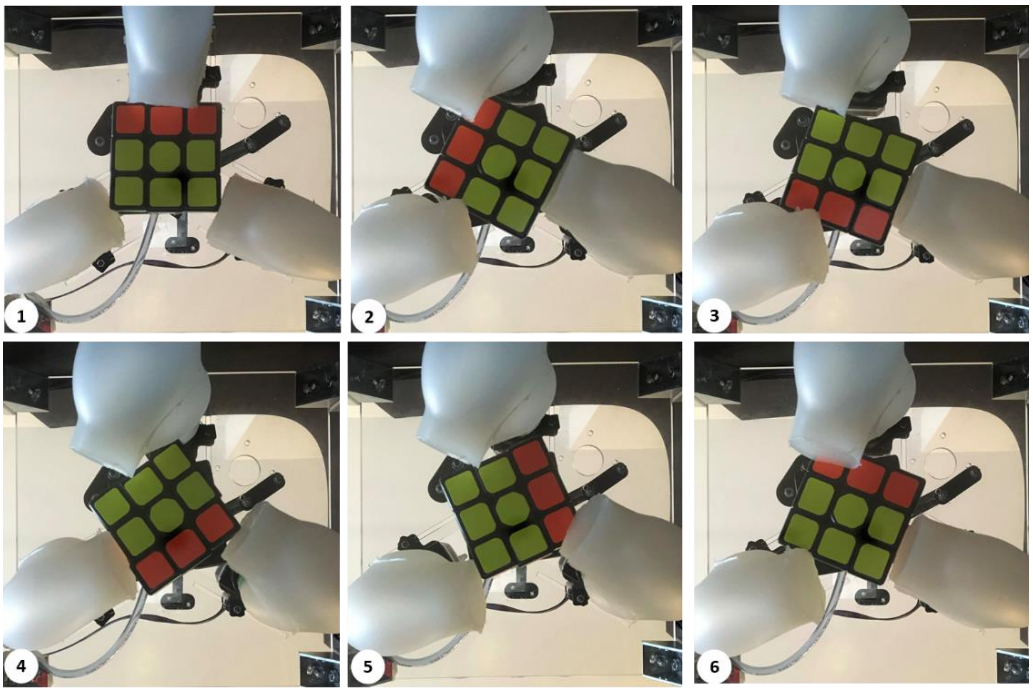

Figure 4.7. In-hand manipulation task 2: full rotation of Rubik's Cube around its axis including rotation.

hold the object. Then, the main chamber of each finger is activated, and the fingers are bent to contact the cube and subsequently, hold it. Afterward, the palm is inactivated, and the fingers hold the cube. The palm acts as a fixture to guarantee the proper rotation of the cube (Table 4.2). As illustrated in Figure 4.7, the right or left side chambers in each finger are actuated based on the direction of rotation. The fingers are released, and the palm is activated at the same time. Thus, the current position of the cube is preserved. Thereafter, the finger bends again and grasps the cube at the new contact points. The cube is now ready for the second rotation. This process continues until the desired angle is reached.

Task 3- Finger gaiting: A cube similar to the one used in the previous task is employed to show the capability of the proposed gripper in terms of a full rotation of the

Table 4.3. Task 3: Finger gaiting procedure

1- The bending point for three fingers is set to R=100 mm
2- Palm is activated to hold the Rubik's cube (X_p=80 mm)
3- Fingers are bent to contact the last section of the cube ($\theta_1 = \theta_2 = \theta_3 \simeq 90°$)
4- Side chambers are activated to rotate the cube ($\phi_1 = \phi_2 = \phi_3 \simeq 45°$)
5- Fingers are non-actuated and get released.
6- This process is repeated to reach the desired angle

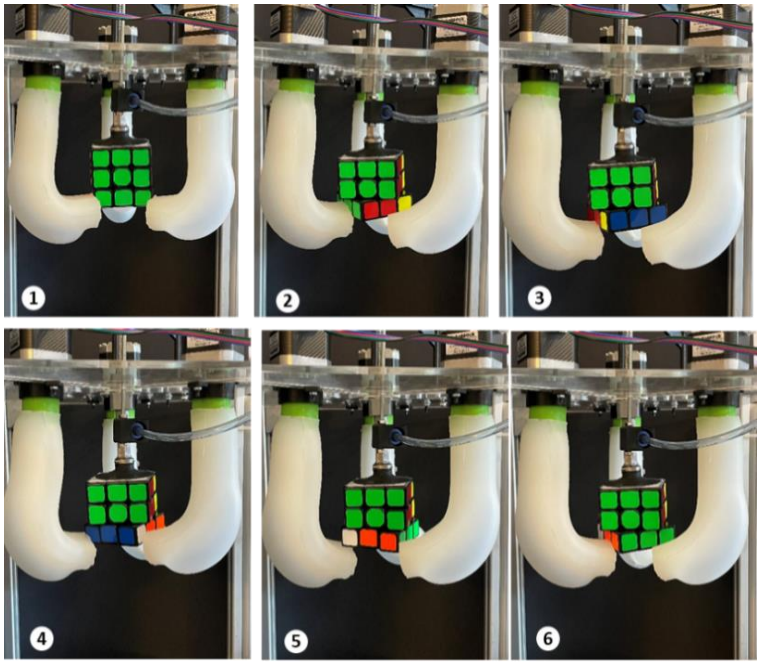

Figure 4.8. In-hand manipulation task 3: rotate one section of rubric cube to the desired angle by controlling the bending shape of the finger and active palm.

last section of the cube around its axis. This process is a kind of finger gaiting task by replacing the grasping fingers with the active palm. As observed previously, the active palm enables not only the proposed gripper to grasp an object with irregular shapes or considerable weight but also to hold the object and simultaneously allows the fingers to change their contact points with the object. The palm is activated during the experimental test to hold the position (Table 4.3). Then, the main chamber of each finger is actuated to grab the object. In the next step, the left side chambers of each finger are simultaneously actuated to produce a clockwise rotation of the last section of the cube (Figure 4.8). The

ultimate angle for each rotation is around 45 degrees. The fingers are released and activated again for the second rotation. This process sticks out to reach the desired angle.

Table 4.4. Task 4: In-grasp manipulation procedure

1- The bending point for three fingers is set to R= 90 mm
2-Two fingers are responsible for grasping the cup ($\theta_1 = \theta_2 \simeq 55°, \theta_3 \simeq 30°$)
3- Palm is inactive but acts as a fixture to keep the position of the cup (X_p=100 mm)
4- By pressurizing another finger, the water begins to pour from the cup $\theta_3 \simeq 95°$

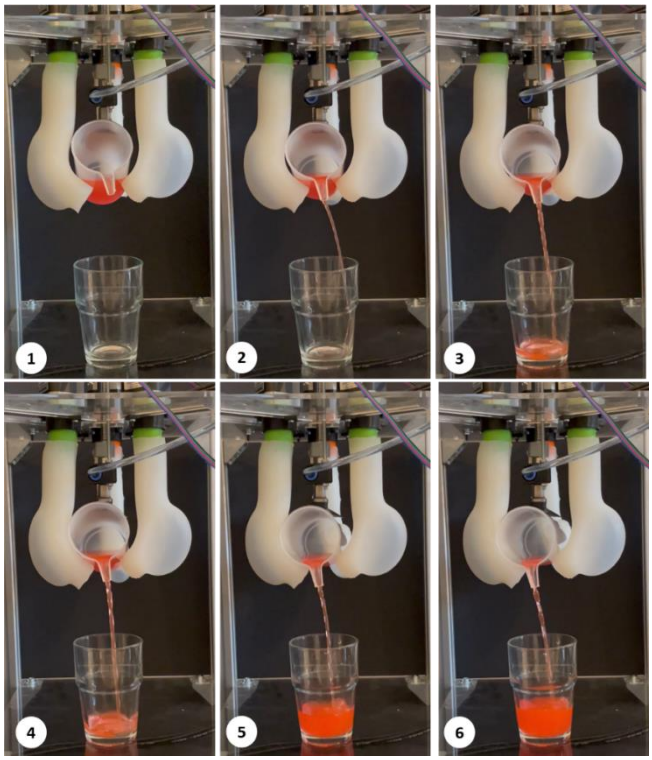

Figure 4.9. In-hand manipulation task 4: pouring colored water from a glass.

Task 4- In-grasp manipulation: This task is involved in handlining the object through the fingers and applying small changes in its position and orientation while fingertip contact is preserved (i.e., no contact break while there are small rolling motions around the contact point). The palm and the fingers with the capability of changing the bending point enable the gripper to manipulate the objects with different shapes (Table 4.4). As illustrated in Figure 4.9, the three fingers are actuated to grasp a glass with colored water. In this task, the palm is not active and only acts as a support to enable stable grasping. An increase in pressure inside the rear finger results in pouring some water from a cup.

Task 5- Rolling: The proposed movable bending and stiff rod design enable the gripper to perform different types of movements. Driving the stiff rod towards the end of two of three fingers increase the stiffness of fingers and can be used as a rigid surface for rolling movement. The other finger with the movable joint is responsible for rolling a pencil with 8 mm in diameter and 20 mm in height. As shown in Figure 4.10, the marker circle paper is attached to the pencil to facilitate the rotation tracking process. The pencil can reach a maximum rotation angle of around 160 degrees. These experimental results realize the in-hand manipulation capability of the proposed three soft fingers with the movable bending point. The active palm improves the grasping ability and the handling of various shapes of objects (Table 4.5). The Supplementary Video provides a full sequence of these tasks.

Table 4.5. Task 5: Rolling procedure

1- Stiffness of two fingers is increased by moving the stiff rode inside each finger R_1= R_2=125 mm, R_3=80 mm
2- These two fingers act as a support and help the rolling
3- By actuating the third finger, the pencil starts to bend up to around 160°

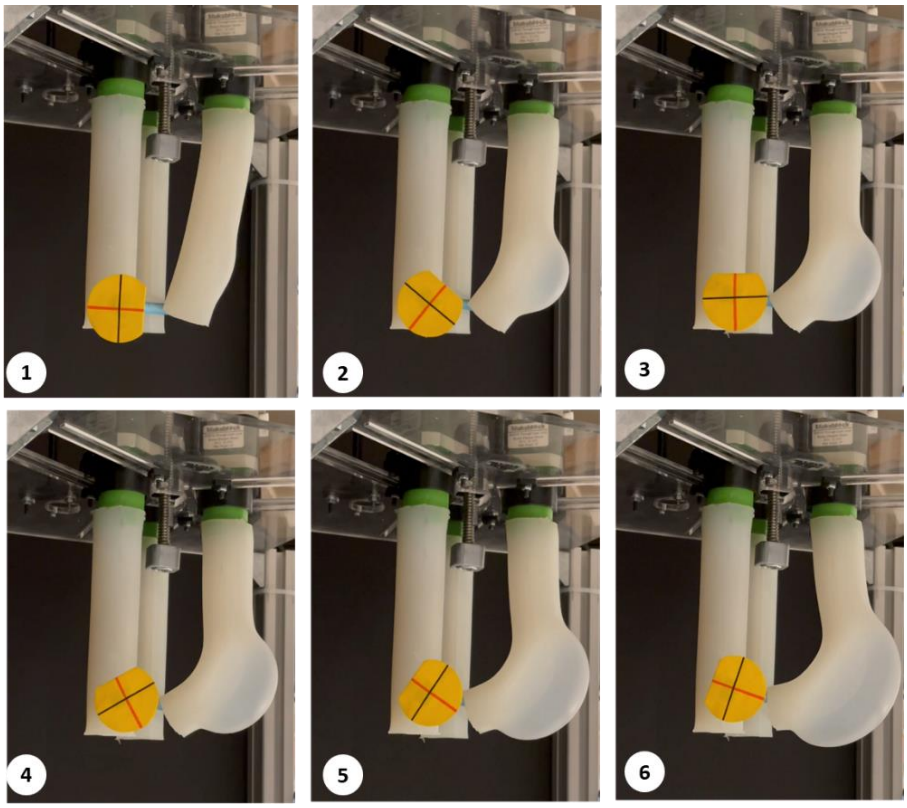

Figure 4.10. In-hand manipulation task 5: rolling the pencil.

4.7. Conclusion

In this paper, an innovative soft gripper with three fingers and a palm has been described. Each finger consists of three inflatable chambers and a movable stiff rod, which controls the position of the bending, and subsequently the shape of the finger. The stiff rod can longitudinally slide along with the principal axis of the finger using an electric stepper motor. The effective variable length of the fingers with the bending capability at different points increases the hand's dexterity considering a large diversity of configurations. The workspace analysis is performed to highlight the advantages of this reconfigurability. This approach extends the available workspace of the fingertips in comparison with the SFAs. Besides, this design increases the dexterous grasping capability of the soft gripper, especially for in-hand applications. Two types of easily interchangeable palms (suction cup and granular particles) are added to improve the in-hand manipulation tasks such as full rotation by regrasping a cube between the palm and the fingers, finger gaiting, and finally pouring some water from a cup. Five popular in-hand manipulation tasks [305] are designed to investigate the performance of the movable bending points and active palm. The experimental results reveal that the proposed soft gripper can successfully carry out these in-hand manipulation functionalities. The proposed design represents a promising solution for a dexterous anthropomorphic gripper, which can potentially interact with humans. In this study, an optimized semi-circular geometry has been employed for chambers to reduce the ballooning effect. This balloon is produced, especially when the bending angle is large (around 90 degrees). Adding fiber reinforcement [236], [320] or sleeve [321] could reduce the ballooning effect but at the price of increasing the required bending pressure and the local stiffness. Also, it requires more powerful equipment (bigger pumps and solenoid valves) with drivers to be connected to the control board. Ultimately, it makes the gripper design more complex and expensive. Furthermore, the balloon does not affect the in-hand manipulation performances or decrease the capability of the proposed grippers which is the main contribution of this paper.

In this chapter, a soft dexterous gripper for grasping and manipulating a wide variety of objects is proposed. The control system is not yet intended to measure the applied force or contact point as feedback. So, in the next chapter, we will introduce the design of a large area capacitive sensor for soft robot applications to precise the grasping and manipulation capability of this gripper.

IV

Chapter 5: Paper #4

Large-Area and Low-Cost Force/Tactile Capacitive Sensor for Soft Robotic Applications

5.1. Abstract

This paper presented the novel design and development of a low-cost and multi-touch sensor based on capacitive variations. This new sensor is very flexible and easy-use which makes it an appropriate choice for soft robot applications. Materials (conductive ink, silicone, control board) used in this sensor are inexpensive and can be found easily in the market. The proposed sensor is made by a wafer of different layers, silicone layers with electrically conductive ink, and a pressure-sensitive conductive paper sheet. Previous approaches like E-skin can measure the contact point or pressure of conductive objects like the human body or finger, while the proposed design enables the sensor to detect the contact point of the object and also the applied force without considering the material conductivity of the object. The sensor can detect five multi-touch points at the same time. Neural network architecture is used to calibrate the applied force with acceptable accuracy with the presence of noise, variation in gains, and non-linearity. The force measured by the ATI sensor in real-time is mapped with the produced voltage made by changing the capacitance of the layer between two electrode layers. Finally, the soft robot gripper embedding the suggested tactile sensor is utilized for grasping an object with position and force feedback signals.

5.2. Introduction

Inspired by nature, scientists have tried to build a new field of robotics similar to human body interactions called soft robotics. Thanks to recent advances in smart and soft materials, the new types of soft actuators can perform different complex tasks. These include several advantages like infinite degree of freedom (DOFs) and lightweight, easy and cost-effective fabrication. Unlike conventional robots, soft robots utilize various types of actuation, such as pressurized fluids, electric or magnetic fields, temperature, chemical reaction, etc. [10], which increase the variety of soft robot applications in different areas, including manipulation [4], grasping [2], locomotion [3], and medical applications [108]. Although their deformable features enable them to perform in uncontrolled environments without requiring complex protection or stability control algorithms like hard robots, their morphological structures restrict utilizing traditional sensors like encoders, metal or semiconductor strain gauges, or inertial measurement units (IMUs) [13]. While in a magnetic sensor, the magnet and the Hall element affect the stiffness of the actuator

[294], and also optoelectronic sensors need a transparent material to transmit the light [293], resistive or capacitive sensors are the most commonly used method due to the fewer limitations for measuring force, curvature, or tactile sensing. Elastomer sensors allow for minimal impact on the actuation of the robot [19].

On the other hand, sensing design for soft robots should be at least flexible or ideally stretchable. Besides, the integrated sensors should not increase the stiffness of the soft actuator. Recent advances and applications of the embedded sensor in soft actuators are reviewed in [20]-[322]-[323]. Li et al. reviewed the last developed sensing technologies in soft robotic systems, including resistive, capacitive, optoelectronic, and magnetic sensors [324]. So flexible and curvature sensors are still interesting subjects for observing and closed-loop controls of soft actuators. In a resistive sensor, applying mechanical pressure changes the strain and, consequently, the conductivity. In a capacitive sensor, the conductivity is dependent on the geometry area of the dielectric materials between two electrodes [325]. Koivikko et al. integrated resistive sensors in a soft gripper to detect the curvature [326]. Yang et al. [291] used a thin layer of paper printed with resistive and capacitive nano-silver ink as electrodes. The proposed sensor was able to detect the bending angle and the object's proximity. Most of the electrode materials which have been embedded in soft grippers as capacitive sensors consist of conductive particles of carbon black (CB) [284], conductive ink [327], graphene [286], and carbon nanotubes [328]. Other types of materials that can be operated as electrodes in flexible sensors are reviewed in [290]. Gafford et al. used a rapid prototyping method, shape deposition manufacturing (SDM), for fabricating a surgical three fingers gripper with an embedded microelectromechanical pressure sensor on its fingertips [329]. Cheng et al. [330] implemented a large-area highly-twistable artificial skin by winding the copper wires around an elastic nylon line. The applied force and tactile sensing can be detected through electrical resistance and pressure, respectively. Ho et al. [331] developed elastomer fingers with a multi-layer fabric capacitive sensor to detect proximity and contact feedback information and grasp delicate objects. A highly stretchable tactile capacitive sensor for a soft pneumatic actuator is proposed in [292]. The 3D printing method is employed to integrate hydrogel electrodes into the silicone.

Due to better performance and easier implementation and calibration than resistive soft sensors, capacitive sensors are widely used in tactile sensors. Besides, they can also detect multi-touch gestures and allow one to infer pressure information. Regarding these advantages, capacitive sensing is selected in this study for soft robot applications.

Recently, artificial neural networks (ANN) have been used for modeling non-linear systems. They can solve highly complex problems by mathematical calculation or other classical procedures without needing to define the model structure explicitly [332]. It reduced the modeling process to network training, useful especially for non-linear sensor calibrations when sensor arrays signals are used for calculating the parameters [333]. Sensor calibration includes a non-linear process. In literature, ANN-based soft sensors are usually employed to find the relation between inputs and outputs by minimizing the mean square error. After calibrating the sensors, the trained model can predict the output whenever required. One drawback of ANNs is that the training time for training the network usually is a long procedure. Almassri et al. [334] proposed the Levenberg Marquardt Back Propagation Artificial Neural Network (LMBP-ANN) model for self-calibrating of a pressure sensor for reliable grasping by wearable robotic hand gloves. The model successfully predicts the pressure in the presence of hysteresis, creep, and nonlinearity. Back-Propagation (BP) neural network is suggested by Ye et al. [335] for self-calibration of non-array tactile sensor's structure. This design doesn't require arrays of electrodes is much easier for fabrication, and also it covers a large area of force detection.

In this work, we propose a new multi-touch large-area capacitive sensor. Our proposed sensor exhibits several advantages such as stretchability, fast response, and low-cost materials for measuring the contact point and also applied force for soft robot grippers. Compared to conventional grippers, soft grippers can grasp an object with a larger contact area which consequently requires covering a wide range of sensing regions with high spatial resolution. The previous sensing approaches cover a small area of the tipping point without specifying other contact points. Moreover, most of the capacitive sensors like e-skin are just sensitive to conductive objects (e.g., human body), while our proposed sensor is independent of the material of the object. A neural network was used to calibrate the applied forces to achieve higher accuracy. Then, the calibrated sensor is embedded into a soft finger to validate the grasping of an object by sending out the contact position and related force as a feedback signal. The rest of this paper is organized as follows. The following section presents the conceptual and operating principles of the proposed sensor. Then we discussed the manufacturing procedure and tactile performance of the sensor. After that, an application of the suggested sensor in soft robot application is introduced. Finally, a conclusion and future work are reported.

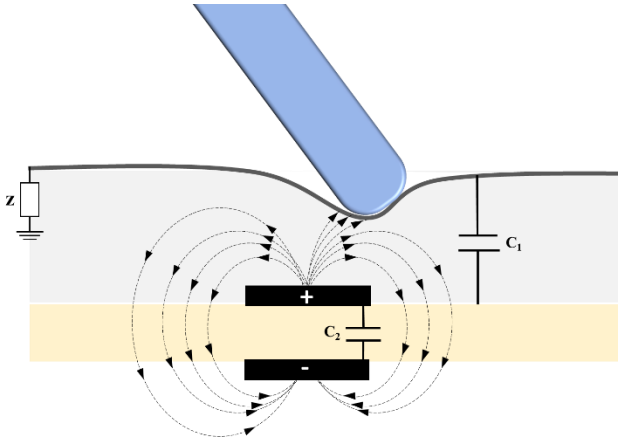

Figure 5.1. Schematic view of the working principles of the proposed sensor

5.3. Operating Principles and Design

Capacitance sensors mainly consist of two conductive layers separated by a dielectric elastomer layer. When the object moves nearer to the electrodes, the capacitance changes. This also changes the local electric field. In the most recent approaches, the object should be conductive or semiconductive with great impedance for having the observable changes in the electric field. However, some approaches depend on the sensitivity material of electrodes, such as elastic carbon nanotube (CNT). In this case, the capacitance is altered for non-conductive material [328]. The purpose of this work is to develop a new type of

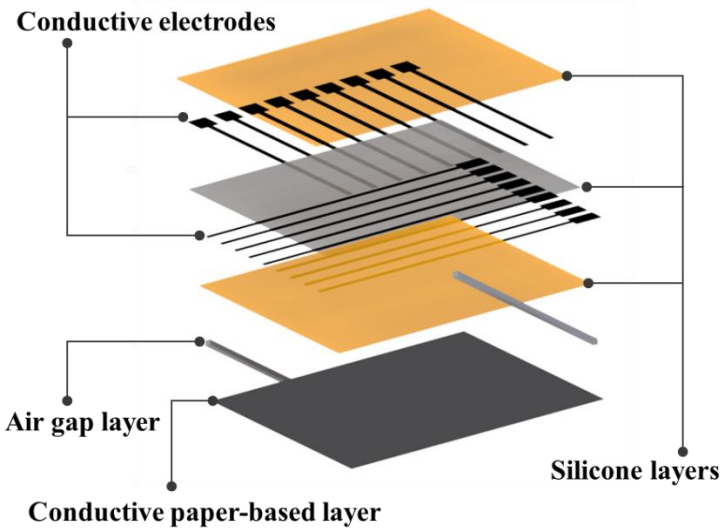

Figure 5.2. Schematic illustration of Internal layers of the proposed sensor

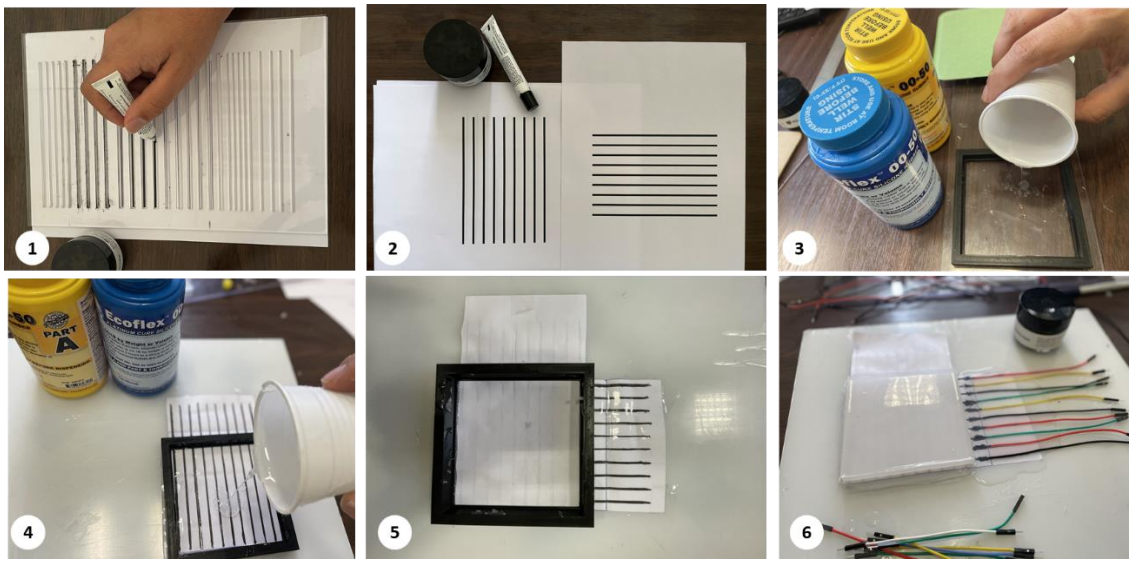

Figure 5.3. The manufacturing procedure of the proposed sensor

capacitance-type sensor which can measure contact points and also applied pressure without considering the material conductivity range of objects. Figure 5.1 shows the working principles of the proposed sensor schematically. It consists of two orthogonal arrays of electrodes: vertical line (T_x) for sending and horizontal lines (R_x) for receiving. A small voltage is applied to T_x to build an electrical field between the electrodes. The displacement current resulting from changing electric field is measured at R_x. A conductive flexible substrate with a ground connection is designed at the top of the layers, as described in Figure 5.2. Getting close to the object to the surface drains a certain amount of field lines between T_x and R_x which can be observed by and specify the touchpoints. Furthermore, the other complementary effect of this kind of design is pressure sensitive. By applying an external force, the electrode distance changes. The amount of force can be measured from the produced displacement current. The capacitance for a parallel plate can be described as calculated by equation (1),

$$C_{sensor} = \varepsilon \frac{A}{d} = k\,\varepsilon_0 \frac{A}{d} \tag{1}$$

where A represents electrode area, d represents dielectric thickness, ε_0 is the permittivity of vacuum, k is called the dielectric constant of the layer between two plates. The capacitance can be varied by changing the thickness of the dielectric layer between two plates. Our sensor is composed of two capacitors that are connected in parallel. its capacitance is

$$C_T = C_1 + C_2 \tag{2}$$

with

$$C_1 = k_1 \varepsilon_0 \frac{A_1}{d_1}, C_2 = k_2 \varepsilon_0 \frac{A_2}{d_2} \quad (3)$$

we obtain

$$C_T = \varepsilon_0 (k_1 \frac{A_1}{d_1} + k_2 \frac{A_2}{d_2}) \quad (4)$$

where ε_0 equals to $8.854 \times 10^{-12}\ F/m$ and k_1 for air is considered as $1\ F/m$. While for EcoFlex 00-50 this constant is around $k_2 = 2.65\ F/m$ [336].

5.4. Fabrication of a Flexible Capacitive Sensor

Figure 5.3 presents the fabrication steps of our flexible capacitive sensor. The sensor architecture has been developed with a top layer of silicone, two conductive layers for horizontal and vertical tracks, layers of silicone elastomer, and a conductive shield as a bottom layer, which should be fabricated layer by layer. The fabrication process starts by pouring EcoFlex 00-50 silicone (Figure 5.3a) with 2 mm as the base substrate. After curing the top layer consisting of silicone EcoFlex 00-50 with thickness 3 mm, the painted paper, including 9 horizontal electrodes with 2 mm thickness, is placed on the top layer. The distance between these electrodes is set as 10 mm (Figure 5.3b). Then these electrodes are covered by a very thin layer of silicone which affects the measured range of pressures. For achieving the maximum sensitivity, the thickness of this layer should not exceed 0.5 mm. In the next step, the second layer of electrodes is laid down vertically compared to the previous electrode layer to build a 10 × 10 matrix grid form of the electrodes. Finally, the conductive paper shield covered by silicone is attached to the electrodes layer with an air gap. The optimal air gap between the electrode layer and conductive shield is between 3 and 4 mm to have maximum sensitivity. To easily make the prototype samples, the water-based, non-toxic bare conductive electric paint [337] was chosen for electrodes and the conductive shield. The electric paint dries at room temperature. The electrodes are then connected to the hardware sensing platform by Mucca breakout. This data acquisition system was presented by Tesseyer et al. [338]. The FT5316DME controller in this breakout provides 33 connectors (maximum 12 sensing electrodes and 21 transmitting electrodes). It can detect 5 multi-touch coordinates and send them out via i2C to the Arduino Uno. This controller can detect 5 multi-touch coordinates and send them out via i2C to the Arduino Uno. A serial communication transforms then the data from Arduino

to a PC. The position of the external touch can be calculated by reading the row and column data separately, which present the X and Y coordinates, respectively. MATLAB software is utilized for communicating with the microcontroller board for receiving, logging, visualizing, and analyzing the external contacts in real-time. The measurement results with the 10*10 mm soft rectangular pad and mutual-capacitive readout are represented in Figure 5.4. When the object is touching the surface of the pad, the x, y coordinates and magnitude of contact points are calculated and depicted in real-time. Two types of experiment, non-conductive object (plastic pen Figure 5.4a) and conductive object (human finger), are tested to show the performance of the sensor. As shown in Figure 5.4b, the sensor can detect three touchpoints with different pressure amounts at the same time. The radius of the circle shows changes with the capacitance from touching the pad. By increasing the pressure, the size of the circle will be increased. For instance, we applied more pressure with our thumb finger. To reduce the background noises, small changes in capacitance (less than 5%) are filtered and have not been presented in these figures.

5.5. Calibrating Proposed Sensor for Soft Robot Applications

In our previous work, we developed a soft robotic finger with a movable joint for enhancing the shape control of soft actuators [160]. Later we proposed a soft robot

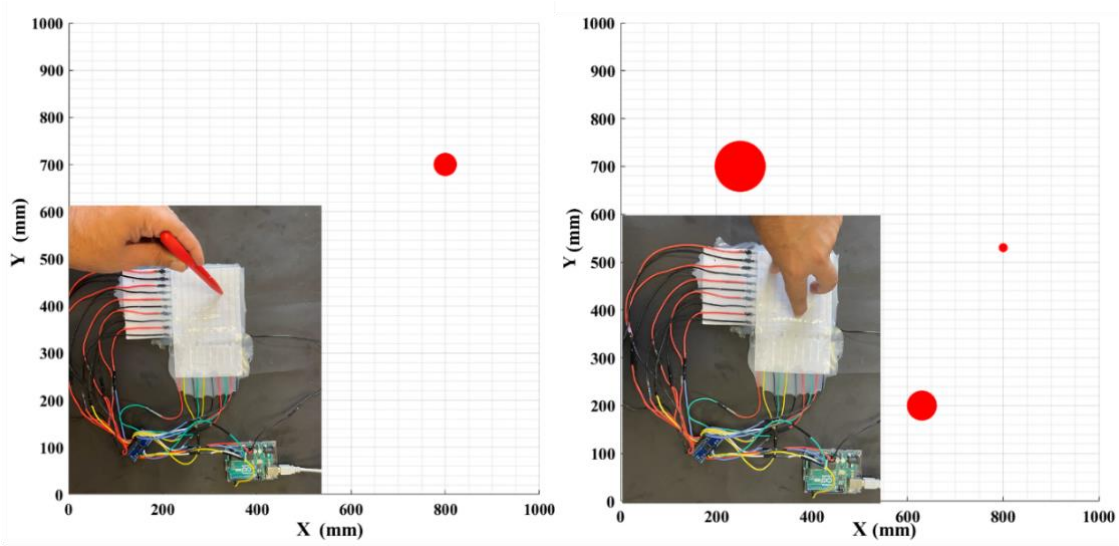

Figure 5.4. Multi-touch force/tactile capacitive 10*10 soft rectangular pad a) non-conductive object (plastique pen) b) conductive object (human finger) with applying different pressures

gripper with three fingers for in-hand manipulation application [339]. An open-loop control law has been used to control the pressure. The feedback data from the tactile sensor attached to the soft finger is used to increase the grasping quality. The fabrication of the sensor is here composed of 5 horizontal lines and 2 vertical lines (5*2) to gather the sensing data similarly to the previous section regarding the surface dimension of the finger (50*25mm). As shown in Figure 5.5, the sensor can be attached easily to the finger by pouring a very thin layer of silicone between the sensor and the soft finger. After curing the silicone, the sensor and finger are being unified. The finger was used to push on the ATI FT14000 Sensor and the produced voltage corresponding to the applied force is measured by the ATI sensor. The maximum force that the finger can apply is measured by the ATI sensor and is around 4 N. For producing this force range, a small pump with a working pressure of around 14 kPa was used. Due to the background crosstalk, finding the proper equation between the force and voltage is very difficult. Artificial neural networks offer an alternative way to address unknown systems and are applied in different

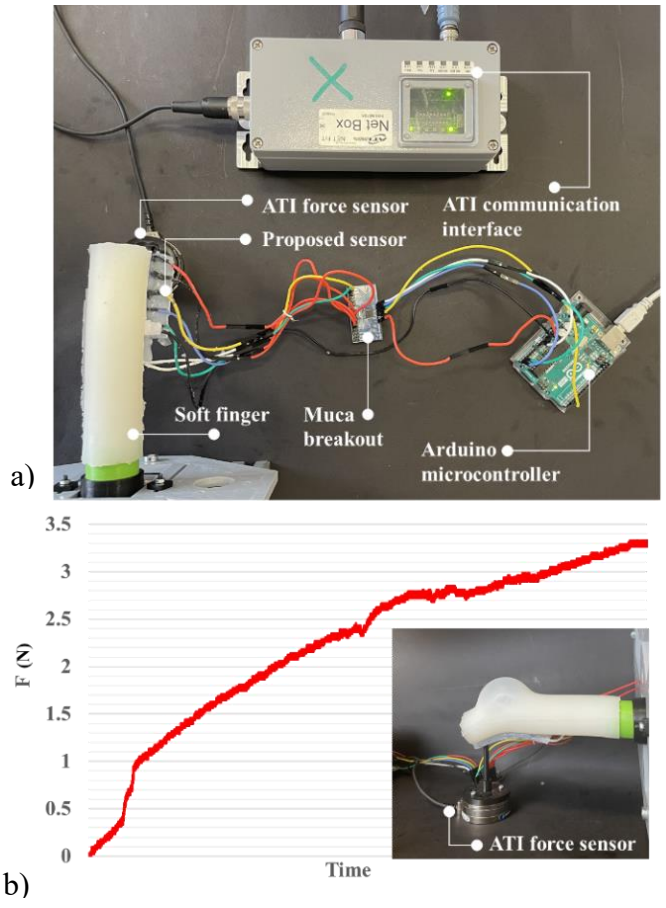

Figure 5.5. a) Calibration set-up assembly, b) testbench for measuring the finger

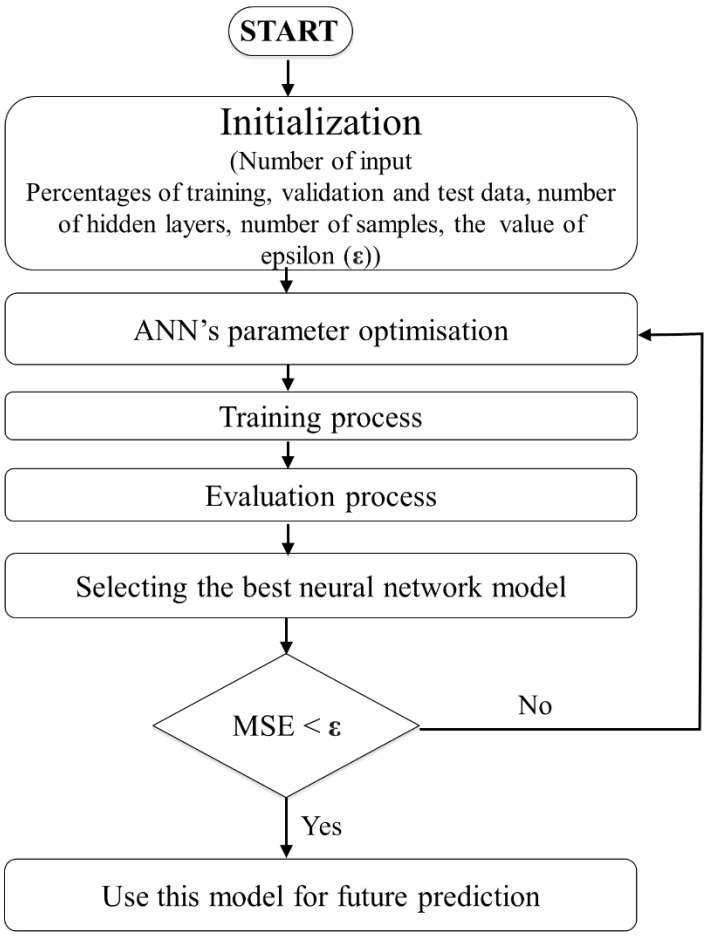

Figure 5.6. Artificial Neural Network flowchart for calibrating the proposed sensor

applications like control, robotic, manufacturing, optimization, etc. Several studies have been conducted on the application of ANNs to model and forecast for various applications because of the ANN's ability to model complex relationships between inputs and outputs or find patterns in data. ANN can be described as a group of simple processing elements called neurons. Neuron tries to provide a mapping between input space (input layer) and the desired space (output layer) by recognizing the inherent relationship between data. Each hidden layer is responsible for transforming the propagated data to the next layer. The learning process continues for several iterations until the average mean square error (MSE) attains an asymptotic. Figure 5.6 represents the flowchart of the ANN development. The process used for training the network is called a learning algorithm, it is designed to change the junction weights of the network to obtain the desired objectives. The ANN in this study consists of a two-layer feed-forward network with a tangent sigmoid transfer function (tansig) between input and hidden layer, a linear transfer function (purelin) between hidden and output layer, and Levenberg-Marquardt back-propagation method due to its fast convergence compared to

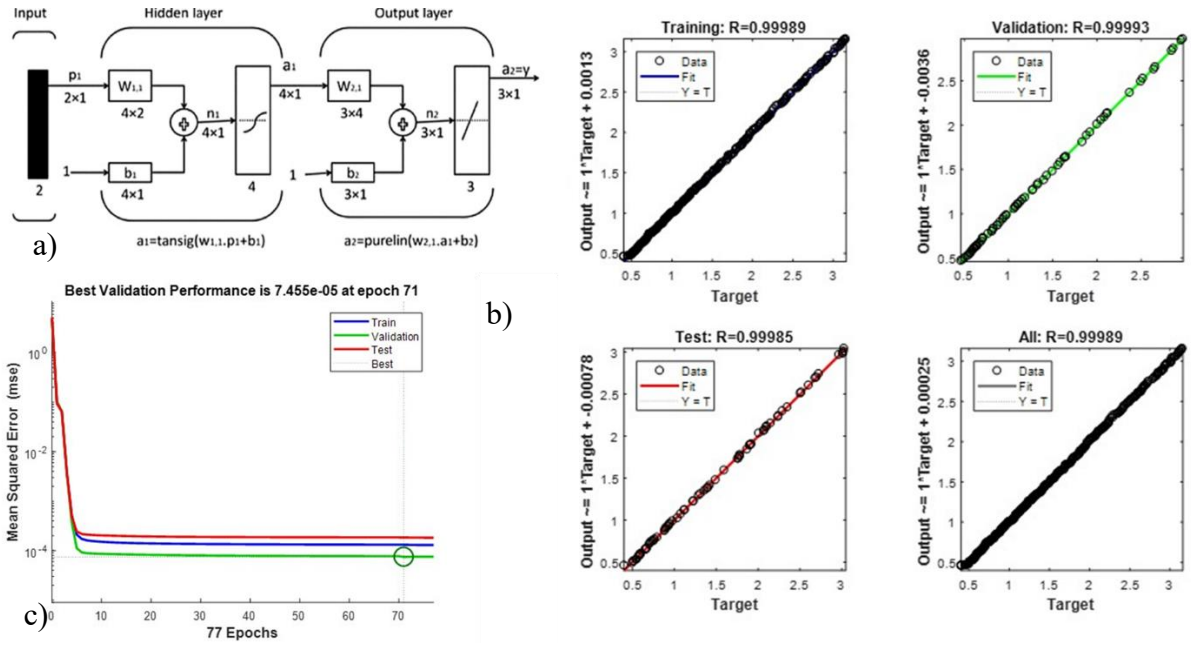

Figure 5.7. a) A two-layer feed-forward network, b) Approximation capability of the trained neural network, c) Mean Squared Error of finger force

alternative backpropagation methods. A sample of a two-layer feed-forward network is illustrated in Figure 5.6a. These networks include input, hidden, and output layers, where the number of the hidden layer neurons is determined by experimental design and analysis method. 500 experiments are executed. The data are randomly divided into three training, validation, and testing groups to avoid any bias (70 % for training, 15 % for validation, and 15 % for testing). Therefore, 350, 75, and 75 samples were used for training, validation, and testing subsets, respectively. There is a variety of methods for determining the number of neurons of the hidden layer. For example, the number of neurons of the hidden layer is in the range of the input layer and the output layer. For this reason, a variety of methods have been developed. Hecht-Nielsen [340] provided one of the best predictions for the number of neurons of the hidden layer:

$$m = 2n + 1 \tag{4}$$

where m is the number of hidden layer neurons and n is the number of input neurons. Considering that there is one input, the number of hidden layer neurons is 3. To compare the optimization algorithms, first, it is necessary to design ANN and then evaluate the performance of ANN in predicting the objective function value. It is important to measure

how well the ANN adapts to the training data. If the ANN generalizes well, it has captured the characteristics of the system well. There are some different performance measures used through the training to evaluate ANN architectures. In this study, the mean square error (MSE) and correlation coefficient (R^2) is considered as the performance function. The mean square error (Eq. 5) is used to determine how well the ANN output fits the desired output presented in the training data, and the correlation coefficient (Eq. 6) is related to the difference between the network output and the desired output [341].

$$MSE = \frac{1}{N}\sum_{i=1}^{N}(y_{prd,i} - y_{exp,i})^2 \tag{5}$$

$$R^2 = 1 - \frac{\sum_{i=1}^{N}(|y_{prd,i} - y_{exp,i}|)}{\sum_{i=1}^{N}(y_{prd,i} - y_m)} \tag{6}$$

Where $y_{prd,i}$ is the predicted value using the ANN model, $y_{exp,i}$ the experimental value, N the number of data, and y_m the average of the experimental value. Figure 5.7b shows the values of the ANN model plotted versus the corresponding experimental values to visualize the modeling capabilities of the ANN models. The R^2 for the training,

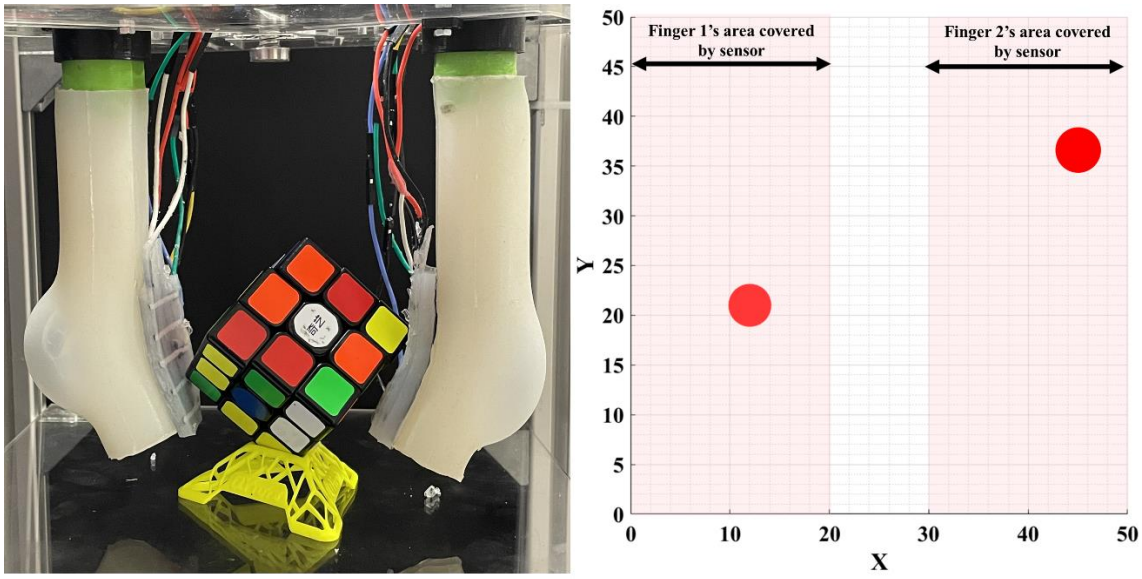

Figure 5.8. Calibrated capacitive/tactile sensor used for soft robot application. The sensor is able to measure the contact point and applied force (2.5 N) with an acceptable accuracy

validation, and testing datasets are 0.99989, 0.999933, and 0.99985, respectively. The high values of R^2 show that the proposed ANN model captured the relationships between the provided input and output data with high performance. Therefore, the efficiency of the designed neural network is satisfactory, and it could be used for predicting the values of the response variable. The ANN converged very fast to the desired accuracy. Figure 5.7c reports the average Mean Square Error for 77 runs. At 71 epochs the value of MSE is $7.455*10^{-5}$, which is the best performance. To evaluate the applicability of the proposed sensor, some experiments with the calibrated sensors assembled with a soft gripper have been carried out. The soft gripper consists of two fingers to grasp the object. As shown in Figure 5.8, the applied force contact points can be detected with good approximation. The captured data have been smoothed with calculating moving average over ten frames of sensing data. The measured force limit can be increased by changing the softness and the thickness of the silicone layer between two electrodes. As shown in Figure 5.7, the cube's contact points and the applied force of two fingers can be detected with a good approximation. The separated ANN real-time calibration models for each attached sensor are used to measure the applied forces of the finger to the object. Equal pressure with small pumps and solenoid valves is applied in two fingers simultaneously. Figure 5.7b shows the calculated forces with 10 kPa pressure in each calibrated sensor as the radius of the circle. The two sensors show approximately the same force of 2.5N. The potential challenge of this sensor is when the bending angle is large and affects the sensor's performance. Dividing the sensor into separated parts and designing some spacers between each part could solve this problem. However, this will require a very precise fabricating and molding procedure.

5.6. Conclusion

This work presents a wide area covered tactile sensor for soft robot applications. The lower layer was made of silicone films embedded with paper covered with conductive ink. It helps to measure the changes of the electric field even for non-conductive objects. Closing the object near the surface changes the electricity and increasing the mutual capacitance. The spatial sensitivity of the sensor with simultaneous sensing of multi-touch points and various amounts of forces has been measured. Then, a calibration technique by neural networks has been proposed to find the best model of calibration. The ATI force sensor has been used as a reference for measuring the applied force. A MATLAB

program was used to execute the LMBP-ANN training process and output calculation based on the proposed method. The training process of the proposed network model updated the weight values in the connection between neurons until to reach the highest performance by achieving the minimum MSE. After calibration, the derived models have been tested onboard by exploiting a soft gripper to grasp the Rubik's cube when the soft sensor is pushed against this object. The experiment shows that the sensor has measured the applied force and contact points with a good approximation. The proposed sensor has been covered a large surface area of the gripper, which is very useful for soft robot grippers to detect several contact points while in rigid grippers only the tipping point is important as a contact. Future works will be primarily needed to improve the long-time stability and resolution of the sensor. These may include efforts to print the electrodes by conductive ink and use resin-coated papers to reduce the resistance and increase the sensitivity.

5.7. Acknowledgment

This work has been received funding from the French government research program "Investissements d'Avenir" through the IDEX-ISITE initiative 16-IDEX-0001 (CAP20-25), the European Union's Horizon 2020 research and innovation program under grant agreement nº 869855 (Project SoftManBot), and the ANR agency (Project MANIMAT ANR-20-CE33-0005).

V

Chapter 6: Conclusion and Perspectives

6.1. Conclusion

Recently, the development of soft robots has been growing fast to work out numerous problems in the field of robotics and can be considered an appropriate supplement of the rigid robotic system. This Ph.D. thesis aimed to explore the design of a soft pneumatic robotic gripper fabricated with innovative materials, with the capability of accomplishing complex actuation tasks such as grasping, in-hand manipulation, rehabilitation, and medical purposes. Before addressing the main ideas of our study, different types of soft pneumatic actuators and their application have been highlighted. A hybrid class which is the combination of SFAs with other actuating mechanisms has been then categorized. The corresponding mechanisms improve the performance of SFAs by means of shape configuration, control ability, variable stiffness, and operation range. We used a hybrid structural design to enhance the performance of our proposed soft gripper. Selecting proper material in a soft robotic system is very challenging and determinative in the functionality of the soft actuators. A general review of the constitutive materials modeling reported in different articles has been done with ABAQUS to find the differences between the constitutive equations. The best-fitting FE models of engineering strain-stress and true strain-stress for the most popular silicone rubbers have been calculated and depicted. Comparing data with Marechal's database as a reference based on ASTM D412 for elastomers shows that most of the models can predict the behavior of the model with acceptable divergence in a small stress-strain range. A variable stiffness soft finger with a fluid-actuated movable joint has been designed. The movable joint design provides not only variability of the finger's length but also increases the capability of bending in different directions with different configurations. FEM analyses have been deployed to investigate the non-linear behavior of design parameters and find their sensitivity in actuation and deformation performance. Then the optimized parameters have been used for fabricating a prototype that validates the numerical model. This finger can bend up to 90 degrees and exert force up to 650 mN in less than three seconds, in contrast with previous approaches such as SMPs or LMPAs. Besides, regulating pressure inside the link can change the finger's stiffness and increase the fingertip's applied force up to two times. Furthermore, the optimized design parameters have been used in chapter 3 to design and manufacture the soft robotic gripper. This gripper consists of three soft fingers and an active palm. Each finger consists of three inflatable chambers and a movable stiff rod, which varies the effective length of the fingers and subsequently the

shape of the finger. Two types of easily interchangeable palms, suction cup and granular particles, have been integrated allowing the gripper to work as a manipulator. This design increases the dexterous grasping capability of the soft gripper, especially for in-hand manipulation. The functionality of the proposed gripper has been explored by different in-hand manipulation tasks. The experimental results show that the proposed soft gripper with active palm fully accomplishes these in-hand manipulation functionalities. Finally, in chapter 4, a large area and low-cost capacitive sensor is attached to the soft fingers to read the force and contact data. The fabrication of the sensor is straightforward and can detect the contact points with high accuracy. Besides, it is made of silicone which can be attached easily to the soft finger. Artificial neural networks have been utilized to calibrate the force output of the sensor by considering the related voltage. Considering the type and cost of the materials fabricated by the sensor, the force and contact points can be detected with acceptable accuracy.

Dexterous rigid hands such as Shadow Hand (24 joints) [312], Pisa/II (19 joints) [317], and DLR Hand II (20 joints) [318] require a lot of joints and motors in the fingers and in their connections with the palm to reach large DOFs; this increases the complexity of the kinematic model, fabrication, and control of this kind of robot. Thanks to the reconfigurable structure of the fingers in our proposed gripper, the rod can move along the finger and change the bending point only by a few additional DOFs. On the other hand, the kinematic modeling of our gripper is more straightforward by reducing the number of joints and their limits. Furthermore, the proposed gripper has simpler modeling, fabrication, and control strategy than the other soft dexterous hands such as BCL-26 (26 chambers). While our prosed dexterous gripper includes nine chambers, three movable joints, and an active palm (14 DOFs) which enable it to pick up and hold a wide variety of object sizes (up to 900 mm) with different weights (up to 400 g thanks to the active palm). It can be useful in creating mechanisms that:

1- can contact and manipulate objects (e.g., fruits, vegetables, tissues) without damaging them (useful for making assembly line robot, automated packaging robot, fruit-picking robot, etc.),

2- work safely and collaboratively with humans (useful for in-hand rehabilitation and assistance and other workplaces which involve collaboration between machines and humans).

6.2. Perspectives

Some possible directions for the future have been presented in each chapter of this thesis. Here are several additional suggestions mainly intended to improve the design, the knowledge of the theory, and the performance of the gripper.

Offline FEM analyses like Abaqus and ANSYS software were used in this research to simulate a pneumatic actuation. Although they succeed in predicting precisely the behavior of SFAs, their slow simulation speed restricts their usage in real-time problems. To speed up the simulation, real-time software such as SOFA would be an interesting strategy along the lines of controlling in real-time the soft gripper. Due to its open-source availability, it has steadily evolved and users have added different libraries such as a soft robot plugin.

In Chapter 2, an optimized semi-circular geometry has been employed for chambers to reduce the ballooning effect. This balloon is produced, especially when the bending angle is large (around 90 degrees). Soft fiber reinforcement [342], sleeve [321] or origami structure [343] could be used to reduce the ballooning effect but at the price of increasing the required bending pressure and the local stiffness.

The gripper design can be improved in size, weight, and cost reduction. For instance, in this study, we suggested a stiffed rod with a stepper motor to change the bending point and the stiffness of the soft fingers. Electrorheological fluid (ER) and magnetorheological fluids (MR) could be interesting materials to replace the stiffed rod providing variable stiffness and controlling the bending points. The viscosity of these fluids increases with the presence of electric or magnetic fields respectively and leads to a mechanical stiffness change of the entire structure. Their response time is fast and around 10 ms [24]. Their relative stiffness can increase up to ten times [344], and generally, magnetic fluids have shown greater changes than ER fluids [345]. However, the potential challenges of these fluids result in high energy consumption and heating. The palm plays an essential role in grasping, especially when using it for in-hand manipulation tasks. Further analysis to better understand the relationship between the palm and finger could be useful for dexterous applications. Besides, further analysis about the effect of granular size on the grasping load and object ranges could be helpful. A very interesting test could be investigating the effect of various grain sizes on the performance of the applied force.

Bibliography

[1] A. D. Marchese and D. Rus, “Design, kinematics, and control of a soft spatial fluidic elastomer manipulator,” *Int. J. Robot. Res.*, vol. 35, no. 7, pp. 840–869, 2016.

[2] J. Shintake, V. Cacucciolo, D. Floreano, and H. Shea, “Soft Robotic Grippers,” *Adv. Mater.*, p. 1707035, 2018.

[3] R. F. Shepherd *et al.*, “Multigait soft robot,” *Proc. Natl. Acad. Sci.*, vol. 108, no. 51, pp. 20400–20403, 2011.

[4] W. McMahan *et al.*, “Field trials and testing of the OctArm continuum manipulator,” in *Proceedings 2006 IEEE International Conference on Robotics and Automation, 2006. ICRA 2006.*, 2006, pp. 2336–2341.

[5] A. B. Dawood, J. Fras, F. Aljabr, Y. Mintz, A. Arezzo,H. Godaba, and K. Althoefer, “Fusing Dexterity and Perception for Soft Robot-Assisted Minimally Invasive Surgery: What We Learnt from STIFF-FLOP,” *Appl. Sci.*, vol. 11, no. 14, p. 6586, 2021.

[6] P. Polygerinos, Z. Wang, K. C. Galloway, R. J. Wood, and C. J. Walsh, “Soft robotic glove for combined assistance and at-home rehabilitation,” *Robot. Auton. Syst.*, vol. 73, pp. 135–143, 2015.

[7] P. Polygerinos *et al.*, “Soft robotics: Review of fluid-driven intrinsically soft devices; manufacturing, sensing, control, and applications in human-robot interaction,” *Adv. Eng. Mater.*, vol. 19, no. 12, p. 1700016, 2017.

[8] A. Zolfagharian, A. Z. Kouzani, S. Y. Khoo, A. A. A. Moghadam, I. Gibson, and A. Kaynak, “Evolution of 3D printed soft actuators,” *Sens. Actuators Phys.*, vol. 250, pp. 258–272, 2016.

[9] C. Majidi, “Soft robotics: a perspective—current trends and prospects for the future,” *Soft Robot.*, vol. 1, no. 1, pp. 5–11, 2014.

[10] P. Boyraz, G. Runge, and A. Raatz, “An overview of novel actuators for soft robotics,” in *Actuators*, 2018, vol. 7, no. 3, p. 48.

[11] H. Fischer, M. Vulliez, P. Laguillaumie, P. Vulliez, and J.-P. Gazeau, “RTRobMultiAxisControl: a framework for real-time multiaxis and multirobot control,” *IEEE Trans. Autom. Sci. Eng.*, vol. 16, no. 3, pp. 1205–1217, 2019.

[12] D. Trivedi, C. D. Rahn, W. M. Kier, and I. D. Walker, “Soft robotics: Biological inspiration, state of the art, and future research,” *Appl. Bionics Biomech.*, vol. 5, no. 3, pp. 99–117, 2008.

[13] D. Rus and M. T. Tolley, “Design, fabrication and control of soft robots,” *Nature*, vol. 521, no. 7553, p. 467, 2015.

[14] S. I. Rich, R. J. Wood, and C. Majidi, “Untethered soft robotics,” *Nat. Electron.*, vol. 1, no. 2, p. 102, 2018.

[15] S. Kim, C. Laschi, and B. Trimmer, “Soft robotics: a bioinspired evolution in robotics,” *Trends Biotechnol.*, vol. 31, no. 5, pp. 287–294, 2013.

[16] C. Laschi, B. Mazzolai, and M. Cianchetti, “Soft robotics: Technologies and systems pushing the boundaries of robot abilities,” *Sci. Robot.*, vol. 1, no. 1, p. eaah3690, 2016.

[17] J. Hughes, U. Culha, F. Giardina, F. Guenther, A. Rosendo, and F. Iida, “Soft manipulators and grippers: a review,” *Front. Robot. AI*, vol. 3, p. 69, 2016.

[18] N. El-Atab *et al.*, “Soft Actuators for Soft Robotic Applications: A Review,” *Adv. Intell. Syst.*, vol. 2, no. 10, p. 2000128, 2020.

[19] B. Gorissen, D. Reynaerts, S. Konishi, K. Yoshida, J.-W. Kim, and M. De Volder, "Elastic Inflatable Actuators for Soft Robotic Applications," *Adv. Mater.*, vol. 29, no. 43, p. 1604977, 2017.
[20] J. Walker *et al.*, "Soft Robotics: A Review of Recent Developments of Pneumatic Soft Actuators," in *Actuators*, 2020, vol. 9, no. 1, p. 3.
[21] W. Hu, G. Z. Lum, M. Mastrangeli, and M. Sitti, "Small-scale soft-bodied robot with multimodal locomotion," *Nature*, vol. 554, no. 7690, pp. 81–85, 2018.
[22] P. Glick, S. A. Suresh, D. Ruffatto, M. Cutkosky, M. T. Tolley, and A. Parness, "A Soft Robotic Gripper With Gecko-Inspired Adhesive," *IEEE Robot. Autom. Lett.*, vol. 3, no. 2, pp. 903–910, 2018.
[23] C. S. Haines *et al.*, "Artificial muscles from fishing line and sewing thread," *science*, vol. 343, no. 6173, pp. 868–872, 2014.
[24] P. Sheng and W. Wen, "Electrorheological fluids: mechanisms, dynamics, and microfluidics applications," *Annu. Rev. Fluid Mech.*, vol. 44, pp. 143–174, 2012.
[25] J. Cramer, M. Cramer, E. Demeester, and K. Kellens, "Exploring the potential of magnetorheology in robotic grippers," *Procedia Cirp*, vol. 76, pp. 127–132, 2018.
[26] P. K. Singh and C. M. Krishna, "Continuum arm robotic manipulator: A review," *Univers. J. Mech. Eng.*, vol. 2, no. 6, pp. 193–198, 2014.
[27] G. S. Chirikjian, "Conformational modeling of continuum structures in robotics and structural biology: A review," *Adv. Robot.*, vol. 29, no. 13, pp. 817–829, 2015.
[28] V. Vikas, E. Cohen, R. Grassi, C. Sözer, and B. Trimmer, "Design and locomotion control of a soft robot using friction manipulation and motor–tendon actuation," *IEEE Trans. Robot.*, vol. 32, no. 4, pp. 949–959, 2016.
[29] M. Dehghani and S. A. A. Moosavian, "Dynamics modeling of a continuum robotic arm with a contact point in planar grasp," *J. Robot.*, vol. 2014, 2014.
[30] H. Shigemune *et al.*, "Dielectric elastomer actuators with carbon nanotube electrodes painted with a soft brush," in *Actuators*, 2018, vol. 7, no. 3, p. 51.
[31] J. Wang, Y. Wang, Z. Zhu, J. Wang, Q. He, and M. Luo, "The effects of dimensions on the deformation sensing performance of ionic polymer-metal composites," *Sensors*, vol. 19, no. 9, p. 2104, 2019.
[32] J. M. Jani, M. Leary, A. Subic, and M. A. Gibson, "A review of shape memory alloy research, applications and opportunities," *Mater. Des. 1980-2015*, vol. 56, pp. 1078–1113, 2014.
[33] M. Behl and A. Lendlein, "Shape-memory polymers," *Kirk-Othmer Encycl. Chem. Technol.*, pp. 1–16, 2000.
[34] M. Fatahillah, N. Oh, and H. Rodrigue, "A Novel Soft Bending Actuator Using Combined Positive and Negative Pressures," *Front. Bioeng. Biotechnol.*, vol. 8, p. 472, 2020.
[35] B. Ouyang, Y. Liu, and D. Sun, "Design of a three-segment continuum robot for minimally invasive surgery," *Robot. Biomim.*, vol. 3, no. 1, pp. 1–4, 2016.
[36] K.-R. Heng, A. S. Ahmed, M. Shrestha, and G.-K. Lau, "Strong dielectric-elastomer grippers with tension arch flexures," in *Electroactive Polymer Actuators and Devices (EAPAD) 2017*, 2017, vol. 10163, p. 101631Z.
[37] H. A. Kashmery, "Polyvinylidene fluoride/sulfonated graphene oxide blend membrane coated with polypyrrole/platinum electrode for ionic polymer metal composite actuator applications," *Sci. Rep.*, vol. 9, no. 1, pp. 1–11, 2019.
[38] M. Cianchetti, A. Licofonte, M. Follador, F. Rogai, and C. Laschi, "Bioinspired soft actuation system using shape memory alloys," in *Actuators*, 2014, vol. 3, no. 3, pp. 226–244.

[39] Q. Ge, A. H. Sakhaei, H. Lee, C. K. Dunn, N. X. Fang, and M. L. Dunn, "Multimaterial 4D printing with tailorable shape memory polymers," *Sci. Rep.*, vol. 6, p. 31110, 2016.
[40] K. Elgeneidy, N. Lohse, and M. Jackson, "Bending angle prediction and control of soft pneumatic actuators with embedded flex sensors–a data-driven approach," *Mechatronics*, vol. 50, pp. 234–247, 2018.
[41] G. S. Chirikjian and J. W. Burdick, "Kinematically optimal hyper-redundant manipulator configurations," *IEEE Trans. Robot. Autom.*, vol. 11, no. 6, pp. 794–806, 1995.
[42] M. W. Hannan and I. D. Walker, "Kinematics and the implementation of an elephant's trunk manipulator and other continuum style robots," *J. Robot. Syst.*, vol. 20, no. 2, pp. 45–63, 2003.
[43] B. A. Jones and I. D. Walker, "Kinematics for multisection continuum robots," *IEEE Trans. Robot.*, vol. 22, no. 1, pp. 43–55, 2006.
[44] N. Simaan, "Snake-like units using flexible backbones and actuation redundancy for enhanced miniaturization," in *Proceedings of the 2005 IEEE International Conference on Robotics and Automation*, 2005, pp. 3012–3017.
[45] K. Xu and N. Simaan, "Actuation compensation for flexible surgical snake-like robots with redundant remote actuation," in *Proceedings 2006 IEEE International Conference on Robotics and Automation, 2006. ICRA 2006.*, 2006, pp. 4148–4154.
[46] R. J. Webster III and B. A. Jones, "Design and kinematic modeling of constant curvature continuum robots: A review," *Int. J. Robot. Res.*, vol. 29, no. 13, pp. 1661–1683, 2010.
[47] I. D. Walker, "Continuous backbone 'continuum' robot manipulators," *Int. Sch. Res. Not.*, vol. 2013, 2013.
[48] L. J. Romasanta, M. A. López-Manchado, and R. Verdejo, "Increasing the performance of dielectric elastomer actuators: A review from the materials perspective," *Prog. Polym. Sci.*, vol. 51, pp. 188–211, 2015.
[49] P. Brochu and Q. Pei, "Dielectric elastomers for actuators and artificial muscles," in *Electroactivity in Polymeric Materials*, Springer, 2012, pp. 1–56.
[50] M. Shahinpoor, K. J. Kim, and D. J. Leo, "Ionic polymer-metal composites as multifunctional materials," *Polym. Compos.*, vol. 24, no. 1, pp. 24–33, 2003.
[51] W.-B. Li, W.-M. Zhang, H.-X. Zou, Z.-K. Peng, and G. Meng, "A fast rolling soft robot driven by dielectric elastomer," *IEEEASME Trans. Mechatron.*, vol. 23, no. 4, pp. 1630–1640, 2018.
[52] K. J. Kim and S. Tadokoro, "Electroactive polymers for robotic applications," *Artif. Muscles Sens.*, vol. 23, p. 291, 2007.
[53] R. Pelrine *et al.*, "Dielectric elastomers: generator mode fundamentals and applications," in *Smart Structures and Materials 2001: Electroactive Polymer Actuators and Devices*, 2001, vol. 4329, pp. 148–156.
[54] C. Keplinger, T. Li, R. Baumgartner, Z. Suo, and S. Bauer, "Harnessing snap-through instability in soft dielectrics to achieve giant voltage-triggered deformation," *Soft Matter*, vol. 8, no. 2, pp. 285–288, 2012.
[55] L. Maffli, S. Rosset, M. Ghilardi, F. Carpi, and H. Shea, "Ultrafast All-Polymer Electrically Tunable Silicone Lenses," *Adv. Funct. Mater.*, vol. 25, no. 11, pp. 1656–1665, 2015.
[56] K. Jung, J. C. Koo, Y. K. Lee, and H. R. Choi, "Artificial annelid robot driven by soft actuators," *Bioinspir. Biomim.*, vol. 2, no. 2, p. S42, 2007.

[57] C. Rendl *et al.*, "FlexSense: a transparent self-sensing deformable surface," in *Proceedings of the 27th annual ACM symposium on User interface software and technology*, 2014, pp. 129–138.
[58] G. Rizzello, D. Naso, A. York, and S. Seelecke, "Closed loop control of dielectric elastomer actuators based on self-sensing displacement feedback," *Smart Mater. Struct.*, vol. 25, no. 3, p. 035034, 2016.
[59] U. Gupta, L. Qin, Y. Wang, H. Godaba, and J. Zhu, "Soft robots based on dielectric elastomer actuators: a review," *Smart Mater. Struct.*, vol. 28, no. 10, p. 103002, 2019.
[60] C. Lee *et al.*, "Soft robot review," *Int. J. Control Autom. Syst.*, vol. 15, no. 1, pp. 3–15, 2017.
[61] I. A. Anderson, T. A. Gisby, T. G. McKay, B. M. O'Brien, and E. P. Calius, "Multi-functional dielectric elastomer artificial muscles for soft and smart machines," *J. Appl. Phys.*, vol. 112, no. 4, p. 041101, 2012.
[62] O. A. Araromi *et al.*, "Rollable multisegment dielectric elastomer minimum energy structures for a deployable microsatellite gripper," *IEEEASME Trans. Mechatron.*, vol. 20, no. 1, pp. 438–446, 2014.
[63] A. O'Halloran, F. O'malley, and P. McHugh, "A review on dielectric elastomer actuators, technology, applications, and challenges," *J. Appl. Phys.*, vol. 104, no. 7, p. 9, 2008.
[64] A. Mardani, E. K. Zavadskas, D. Streimikiene, A. Jusoh, and M. Khoshnoudi, "A comprehensive review of data envelopment analysis (DEA) approach in energy efficiency," *Renew. Sustain. Energy Rev.*, vol. 70, pp. 1298–1322, 2017.
[65] W. D. Cook, L. Liang, and J. Zhu, "Measuring performance of two-stage network structures by DEA: a review and future perspective," *Omega*, vol. 38, no. 6, pp. 423–430, 2010.
[66] A. Poulin, S. Rosset, and H. R. Shea, "Printing low-voltage dielectric elastomer actuators," *Appl. Phys. Lett.*, vol. 107, no. 24, p. 244104, 2015.
[67] X. Ji *et al.*, "An autonomous untethered fast soft robotic insect driven by low-voltage dielectric elastomer actuators," *Sci. Robot.*, vol. 4, no. 37, 2019.
[68] B. Kussmaul *et al.*, "Enhancement of dielectric permittivity and electromechanical response in silicone elastomers: molecular grafting of organic dipoles to the macromolecular network," *Adv. Funct. Mater.*, vol. 21, no. 23, pp. 4589–4594, 2011.
[69] D. Yang *et al.*, "Dielectric elastomer actuator with excellent electromechanical performance using slide-ring materials/barium titanate composites," *J. Mater. Chem. A*, vol. 3, no. 18, pp. 9468–9479, 2015.
[70] F. B. Madsen, A. E. Daugaard, S. Hvilsted, and A. L. Skov, "The current state of silicone-based dielectric elastomer transducers," *Macromol. Rapid Commun.*, vol. 37, no. 5, pp. 378–413, 2016.
[71] G.-Y. Gu, J. Zhu, L.-M. Zhu, and X. Zhu, "A survey on dielectric elastomer actuators for soft robots," *Bioinspir. Biomim.*, vol. 12, no. 1, p. 011003, 2017.
[72] E. Acome *et al.*, "Hydraulically amplified self-healing electrostatic actuators with muscle-like performance," *Science*, vol. 359, no. 6371, pp. 61–65, 2018.
[73] X. Cheng *et al.*, "An entirely soft varifocal lens based on an electro-hydraulic actuator," *Smart Mater. Struct.*, vol. 29, no. 4, p. 045017, 2020.
[74] C. Schunk *et al.*, "System identification and closed-loop control of a hydraulically amplified self-healing electrostatic (HASEL) actuator," in *2018 IEEE/RSJ International Conference on Intelligent Robots and Systems (IROS)*, 2018, pp. 6417–6423.

[75] P. Rothemund, N. Kellaris, S. K. Mitchell, E. Acome, and C. Keplinger, “HASEL Artificial Muscles for a New Generation of Lifelike Robots—Recent Progress and Future Opportunities,” *Adv. Mater.*, p. 2003375, 2020.
[76] A. Marette, A. Poulin, N. Besse, S. Rosset, D. Briand, and H. Shea, “Flexible zinc–tin oxide thin film transistors operating at 1 kV for integrated switching of dielectric elastomer actuators arrays,” *Adv. Mater.*, vol. 29, no. 30, p. 1700880, 2017.
[77] N. Kellaris, V. G. Venkata, G. M. Smith, S. K. Mitchell, and C. Keplinger, “Peano-HASEL actuators: Muscle-mimetic, electrohydraulic transducers that linearly contract on activation,” *Sci. Robot.*, vol. 3, no. 14, 2018.
[78] K. Oguro, “Bending of an ion-conducting polymer film-electrode composite by an electric stimulus at low voltage,” *J Micromachine Soc.*, vol. 5, pp. 27–30, 1992.
[79] M. Shahinpoor and K. J. Kim, “Ionic polymer-metal composites: I. Fundamentals,” *Smart Mater. Struct.*, vol. 10, no. 4, p. 819, 2001.
[80] K. J. Kim and M. Shahinpoor, “Ionic polymer–metal composites: II. Manufacturing techniques,” *Smart Mater. Struct.*, vol. 12, no. 1, p. 65, 2003.
[81] M. Shahinpoor and K. J. Kim, “Ionic polymer–metal composites: III. Modeling and simulation as biomimetic sensors, actuators, transducers, and artificial muscles,” *Smart Mater. Struct.*, vol. 13, no. 6, p. 1362, 2004.
[82] M. Shahinpoor and K. J. Kim, “Ionic polymer–metal composites: IV. Industrial and medical applications,” *Smart Mater. Struct.*, vol. 14, no. 1, p. 197, 2004.
[83] R. Tiwari and E. Garcia, “The state of understanding of ionic polymer metal composite architecture: a review,” *Smart Mater. Struct.*, vol. 20, no. 8, p. 083001, 2011.
[84] B. Bhandari, G.-Y. Lee, and S.-H. Ahn, “A review on IPMC material as actuators and sensors: fabrications, characteristics and applications,” *Int. J. Precis. Eng. Manuf.*, vol. 13, no. 1, pp. 141–163, 2012.
[85] C. Jo, D. Pugal, I.-K. Oh, K. J. Kim, and K. Asaka, “Recent advances in ionic polymer–metal composite actuators and their modeling and applications,” *Prog. Polym. Sci.*, vol. 38, no. 7, pp. 1037–1066, 2013.
[86] M. Hao, Y. Wang, Z. Zhu, Q. He, D. Zhu, and M. Luo, “A Compact Review of IPMC as Soft Actuator and Sensor: Current Trends, Challenges, and Potential Solutions From Our Recent Work.,” *Front Robot AI 6 129 Doi 103389frobt*, 2019.
[87] K. Otsuka and C. M. Wayman, *Shape memory materials*. Cambridge university press, 1999.
[88] O. E. Ozbulut, S. Daghash, and M. M. Sherif, “Shape memory alloy cables for structural applications,” *J. Mater. Civ. Eng.*, vol. 28, no. 4, p. 04015176, 2016.
[89] H. Rodrigue, W. Wang, M.-W. Han, T. J. Kim, and S.-H. Ahn, “An overview of shape memory alloy-coupled actuators and robots,” *Soft Robot.*, vol. 4, no. 1, pp. 3–15, 2017.
[90] M. D. Hager, S. Bode, C. Weber, and U. S. Schubert, “Shape memory polymers: past, present and future developments,” *Prog. Polym. Sci.*, vol. 49, pp. 3–33, 2015.
[91] M. Behl, K. Kratz, J. Zotzmann, U. Nöchel, and A. Lendlein, “Reversible bidirectional shape-memory polymers,” *Adv. Mater.*, vol. 25, no. 32, pp. 4466–4469, 2013.
[92] W. Wang and S.-H. Ahn, “Shape memory alloy-based soft gripper with variable stiffness for compliant and effective grasping,” *Soft Robot.*, vol. 4, no. 4, pp. 379–389, 2017.

[93] Y. Yang, Y. Chen, Y. Li, M. Z. Chen, and Y. Wei, "Bioinspired robotic fingers based on pneumatic actuator and 3D printing of smart material," *Soft Robot.*, vol. 4, no. 2, pp. 147–162, 2017.
[94] A. Lendlein, M. Behl, B. Hiebl, and C. Wischke, "Shape-memory polymers as a technology platform for biomedical applications," *Expert Rev. Med. Devices*, vol. 7, no. 3, pp. 357–379, 2010.
[95] H. Meng and G. Li, "A review of stimuli-responsive shape memory polymer composites," *Polymer*, vol. 54, no. 9, pp. 2199–2221, 2013.
[96] Y. S. Krieger, S. Schiele, S. Detzel, C. Dietz, and T. C. Lueth, "Shape Memory Structures-Automated Design of Monolithic Soft Robot Structures with Pre-defined End Poses," in *2019 International Conference on Robotics and Automation (ICRA)*, 2019, pp. 9357–9362.
[97] K. Suzumori, S. Iikura, and H. Tanaka, "Development of flexible microactuator and its applications to robotic mechanisms," in *Proceedings. 1991 IEEE International Conference on Robotics and Automation*, 1991, pp. 1622–1623.
[98] M. D. Grissom *et al.*, "Design and experimental testing of the octarm soft robot manipulator," in *Unmanned Systems Technology VIII*, 2006, vol. 6230, p. 62301F.
[99] F. Ilievski, A. D. Mazzeo, R. F. Shepherd, X. Chen, and G. M. Whitesides, "Soft robotics for chemists," *Angew. Chem.*, vol. 123, no. 8, pp. 1930–1935, 2011.
[100] E. Brown *et al.*, "Universal robotic gripper based on the jamming of granular material," *Proc. Natl. Acad. Sci.*, vol. 107, no. 44, pp. 18809–18814, 2010.
[101] R. V. Martinez, C. R. Fish, X. Chen, and G. M. Whitesides, "Elastomeric origami: programmable paper-elastomer composites as pneumatic actuators," *Adv. Funct. Mater.*, vol. 22, no. 7, pp. 1376–1384, 2012.
[102] D. Yang *et al.*, "Buckling pneumatic linear actuators inspired by muscle," *Adv. Mater. Technol.*, vol. 1, no. 3, p. 1600055, 2016.
[103] W. Park, S. Seo, J. Oh, and J. Bae, "A Sensorized Hybrid Gripper to Evaluate a Grasping Quality Based on a Largest Minimum Wrench," *IEEE Robot. Autom. Lett.*, vol. 5, no. 2, pp. 3243–3250, 2020.
[104] J. Zhou, X. Chen, J. Li, Y. Tian, and Z. Wang, "A soft robotic approach to robust and dexterous grasping," in *2018 IEEE International Conference on Soft Robotics (RoboSoft)*, 2018, pp. 412–417.
[105] T. Nakajima, T. Yamaguchi, S. Wakabayashi, T. Arie, S. Akita, and K. Takei, "Transformable Pneumatic Balloon-Type Soft Robot Using Attachable Shells," *Adv. Mater. Technol.*, p. 2000201, 2020.
[106] S. Abondance, C. B. Teeple, and R. J. Wood, "A dexterous soft robotic hand for delicate in-hand manipulation," *IEEE Robot. Autom. Lett.*, vol. 5, no. 4, pp. 5502–5509, 2020.
[107] S.-H. Heo, C. Kim, T.-S. Kim, and H.-S. Park, "Human-Palm-Inspired Artificial Skin Material Enhances Operational Functionality of Hand Manipulation," *Adv. Funct. Mater.*, p. 2002360, 2020.
[108] M. Cianchetti, T. Ranzani, G. Gerboni, I. De Falco, C. Laschi, and A. Menciassi, "STIFF-FLOP surgical manipulator: mechanical design and experimental characterization of the single module," in *Intelligent Robots and Systems (IROS), 2013 IEEE/RSJ International Conference on*, 2013, pp. 3576–3581.
[109] H. Abidi *et al.*, "Highly dexterous 2-module soft robot for intra-organ navigation in minimally invasive surgery," *Int. J. Med. Robot.*, vol. 14, no. 1, p. e1875, 2018.
[110] H. K. Yap, J. H. Lim, F. Nasrallah, J. C. Goh, and R. C. Yeow, "A soft exoskeleton for hand assistive and rehabilitation application using pneumatic actuators with

variable stiffness," in *2015 IEEE international conference on robotics and automation (ICRA)*, 2015, pp. 4967–4972.
[111] H. K. Yap, H. Y. Ng, and C.-H. Yeow, "High-force soft printable pneumatics for soft robotic applications," *Soft Robot.*, vol. 3, no. 3, pp. 144–158, 2016.
[112] G. Bao *et al.*, "Soft robotics: Academic insights and perspectives through bibliometric analysis," *Soft Robot.*, vol. 5, no. 3, pp. 229–241, 2018.
[113] F. Daerden and D. Lefeber, "Pneumatic artificial muscles: actuators for robotics and automation," *Eur. J. Mech. Environ. Eng.*, vol. 47, no. 1, pp. 11–21, 2002.
[114] B. Tondu, "Modelling of the McKibben artificial muscle: A review," *J. Intell. Mater. Syst. Struct.*, vol. 23, no. 3, pp. 225–253, 2012.
[115] L. A. Al Abeach, S. Nefti-Meziani, and S. Davis, "Design of a variable stiffness soft dexterous gripper," *Soft Robot.*, vol. 4, no. 3, pp. 274–284, 2017.
[116] M. Gomez, D. E. Moulton, and D. Vella, "Critical slowing down in purely elastic 'snap-through'instabilities," *Nat. Phys.*, vol. 13, no. 2, pp. 142–145, 2017.
[117] J. T. Overvelde, T. Kloek, J. J. D'haen, and K. Bertoldi, "Amplifying the response of soft actuators by harnessing snap-through instabilities," *Proc. Natl. Acad. Sci.*, vol. 112, no. 35, pp. 10863–10868, 2015.
[118] P. Rothemund *et al.*, "A soft, bistable valve for autonomous control of soft actuators," *Sci. Robot.*, vol. 3, no. 16, 2018.
[119] H. Tsukagoshi, A. Kitagawa, and M. Segawa, "Active hose: An artificial elephant's nose with maneuverability for rescue operation," in *Proceedings 2001 ICRA. IEEE International Conference on Robotics and Automation (Cat. No. 01CH37164)*, 2001, vol. 3, pp. 2454–2459.
[120] I. D. Walker *et al.*, "Continuum robot arms inspired by cephalopods," in *Unmanned Ground Vehicle Technology VII*, 2005, vol. 5804, pp. 303–314.
[121] R. Kang, D. T. Branson, T. Zheng, E. Guglielmino, and D. G. Caldwell, "Design, modeling and control of a pneumatically actuated manipulator inspired by biological continuum structures," *Bioinspir. Biomim.*, vol. 8, no. 3, p. 036008, 2013.
[122] G. Miron, B. Bédard, and J.-S. Plante, "Sleeved bending actuators for soft grippers: A durable solution for high force-to-weight applications," in *Actuators*, 2018, vol. 7, no. 3, p. 40.
[123] B. Mosadegh *et al.*, "Pneumatic networks for soft robotics that actuate rapidly," *Adv. Funct. Mater.*, vol. 24, no. 15, pp. 2163–2170, 2014.
[124] A. J. Veale, S. Q. Xie, and I. A. Anderson, "Characterizing the Peano fluidic muscle and the effects of its geometry properties on its behavior," *Smart Mater. Struct.*, vol. 25, no. 6, p. 065013, 2016.
[125] M. T. Tolley *et al.*, "A resilient, untethered soft robot," *Soft Robot.*, vol. 1, no. 3, pp. 213–223, 2014.
[126] K. Suzumori, S. Iikura, and H. Tanaka, "Applying a flexible microactuator to robotic mechanisms," *IEEE Control Syst. Mag.*, vol. 12, no. 1, pp. 21–27, 1992.
[127] C. D. Onal, X. Chen, G. M. Whitesides, and D. Rus, "Soft mobile robots with on-board chemical pressure generation," in *Robotics Research*, Springer, 2017, pp. 525–540.
[128] R. K. Katzschmann, A. D. Marchese, and D. Rus, "Hydraulic autonomous soft robotic fish for 3D swimming," in *Experimental Robotics*, 2016, pp. 405–420.
[129] S. Sridar *et al.*, "Hydro Muscle-a novel soft fluidic actuator," in *2016 IEEE International Conference on Robotics and Automation (ICRA)*, 2016, pp. 4014–4021.

[130] H. Yuk, S. Lin, C. Ma, M. Takaffoli, N. X. Fang, and X. Zhao, "Hydraulic hydrogel actuators and robots optically and sonically camouflaged in water," *Nat. Commun.*, vol. 8, no. 1, pp. 1–12, 2017.
[131] A. Needleman, "Inflation of spherical rubber balloons," *Int. J. Solids Struct.*, vol. 13, no. 5, pp. 409–421, 1977.
[132] R. F. Shepherd, A. A. Stokes, R. M. Nunes, and G. M. Whitesides, "Soft machines that are resistant to puncture and that self seal," *Adv. Mater.*, vol. 25, no. 46, pp. 6709–6713, 2013.
[133] R. Deimel and O. Brock, "A compliant hand based on a novel pneumatic actuator," in *2013 IEEE International Conference on Robotics and Automation*, 2013, pp. 2047–2053.
[134] R. Deimel and O. Brock, "A novel type of compliant and underactuated robotic hand for dexterous grasping," *Int. J. Robot. Res.*, vol. 35, no. 1–3, pp. 161–185, 2016.
[135] A. J. Veale, S. Q. Xie, and I. A. Anderson, "Modeling the Peano fluidic muscle and the effects of its material properties on its static and dynamic behavior," *Smart Mater. Struct.*, vol. 25, no. 6, p. 065014, May 2016, doi: 10.1088/0964-1726/25/6/065014.
[136] A. J. Veale, S. Q. Xie, and I. A. Anderson, "Accurate multivariable arbitrary piecewise model regression of McKibben and Peano muscle static and damping force behavior," *Smart Mater. Struct.*, vol. 27, no. 10, p. 105048, 2018.
[137] A. J. Loeve, O. S. van de Ven, J. G. Vogel, P. Breedveld, and J. Dankelman, "Vacuum packed particles as flexible endoscope guides with controllable rigidity," *Granul. Matter*, vol. 12, no. 6, pp. 543–554, 2010.
[138] I. De Falco, M. Cianchetti, and A. Menciassi, "A soft multi-module manipulator with variable stiffness for minimally invasive surgery," *Bioinspir. Biomim.*, vol. 12, no. 5, p. 056008, 2017.
[139] M. A. Robertson and J. Paik, "New soft robots really suck: Vacuum-powered systems empower diverse capabilities," *Sci. Robot.*, vol. 2, no. 9, 2017.
[140] D. Yang, M. S. Verma, E. Lossner, D. Stothers, and G. M. Whitesides, "Negative-Pressure Soft Linear Actuator with a Mechanical Advantage," *Adv. Mater. Technol.*, vol. 2, no. 1, p. 1600164, 2017.
[141] Z. Jiao, C. Ji, J. Zou, H. Yang, and M. Pan, "Vacuum-Powered Soft Pneumatic Twisting Actuators to Empower New Capabilities for Soft Robots," *Adv. Mater. Technol.*, vol. 4, no. 1, p. 1800429, 2019.
[142] S. K. Mitchell *et al.*, "An Easy-to-Implement Toolkit to Create Versatile and High-Performance HASEL Actuators for Untethered Soft Robots," *Adv. Sci.*, vol. 6, no. 14, p. 1900178, 2019.
[143] X. Wang, S. K. Mitchell, E. H. Rumley, P. Rothemund, and C. Keplinger, "High-strain peano-HASEL actuators," *Adv. Funct. Mater.*, vol. 30, no. 7, p. 1908821, 2020.
[144] Z. Yoder *et al.*, "Design of a High-Speed Prosthetic Finger Driven by Peano-HASEL Actuators," *Front. Robot. AI*, vol. 7, p. 181, 2020.
[145] F. Hu, W. Wang, J. Cheng, and Y. Bao, "Origami spring–inspired metamaterials and robots: An attempt at fully programmable robotics," *Sci. Prog.*, vol. 103, no. 3, p. 0036850420946162, 2020.
[146] S. Li, D. M. Vogt, D. Rus, and R. J. Wood, "Fluid-driven origami-inspired artificial muscles," *Proc. Natl. Acad. Sci.*, vol. 114, no. 50, pp. 13132–13137, 2017.

[147] J. Amend, N. Cheng, S. Fakhouri, and B. Culley, “Soft robotics commercialization: Jamming grippers from research to product,” *Soft Robot.*, vol. 3, no. 4, pp. 213–222, 2016.
[148] N. Cheng *et al.*, “Prosthetic jamming terminal device: A case study of untethered soft robotics,” *Soft Robot.*, vol. 3, no. 4, pp. 205–212, 2016.
[149] S. Reitelshöfer, C. Ramer, D. Gräf, F. Matern, and J. Franke, “Combining a collaborative robot and a lightweight Jamming-Gripper to realize an intuitively to use and flexible co-worker,” in *2014 IEEE/SICE International Symposium on System Integration*, 2014, pp. 1–5.
[150] K. Harada *et al.*, “Proposal of a shape adaptive gripper for robotic assembly tasks,” *Adv. Robot.*, vol. 30, no. 17–18, pp. 1186–1198, 2016.
[151] S. Licht, E. Collins, M. L. Mendes, and C. Baxter, “Stronger at depth: Jamming grippers as deep sea sampling tools,” *Soft Robot.*, vol. 4, no. 4, pp. 305–316, 2017.
[152] J. Amend and H. Lipson, “The JamHand: Dexterous manipulation with minimal actuation,” *Soft Robot.*, vol. 4, no. 1, pp. 70–80, 2017.
[153] S. Follmer, D. Leithinger, A. Olwal, N. Cheng, and H. Ishii, “Jamming user interfaces: programmable particle stiffness and sensing for malleable and shape-changing devices,” in *Proceedings of the 25th annual ACM symposium on User interface software and technology*, 2012, pp. 519–528.
[154] A. Jiang, G. Xynogalas, P. Dasgupta, K. Althoefer, and T. Nanayakkara, “Design of a variable stiffness flexible manipulator with composite granular jamming and membrane coupling,” in *Intelligent Robots and Systems (IROS), 2012 IEEE/RSJ International Conference on*, 2012, pp. 2922–2927.
[155] S. M. Z. Sayyadan and M. M. Moniri, “Mechanical behaviors of jammable robotic structures; prediction and computation,” *Int. J. Intell. Robot. Appl.*, pp. 1–16, 2018.
[156] Y. Hao *et al.*, “A eutectic-alloy-infused soft actuator with sensing, tunable degrees of freedom, and stiffness properties,” *J. Micromechanics Microengineering*, vol. 28, no. 2, p. 024004, 2018.
[157] Y. S. Narang, J. J. Vlassak, and R. D. Howe, “Mechanically versatile soft machines through laminar jamming,” *Adv. Funct. Mater.*, vol. 28, no. 17, p. 1707136, 2018.
[158] J. Guo, K. Elgeneidy, C. Xiang, N. Lohse, L. Justham, and J. Rossiter, “Soft pneumatic grippers embedded with stretchable electroadhesion,” *Smart Mater. Struct.*, vol. 27, no. 5, p. 055006, 2018.
[159] A. Seibel and M. Yıldız, “A Gecko-Inspired Soft Passive Gripper,” *Biomimetics*, vol. 5, no. 2, p. 12, 2020.
[160] A. Pagoli, F. Chapelle, J.-A. Corrales-Ramon, Y. Mezouar, and Y. Lapusta, “Design and Optimization of a Dextrous Robotic Finger: Incorporating a Sliding, Rotating, and Soft-Bending Mechanism While Maximizing Dexterity and Minimizing Dimensions,” *IEEE Robot. Autom. Mag.*, vol. 27, no. 4, pp. 56–64, 2020.
[161] Y. Kim and Y. Cha, “Soft Pneumatic Gripper With a Tendon-Driven Soft Origami Pump,” *Front. Bioeng. Biotechnol.*, vol. 8, p. 461, 2020.
[162] M. S. Verma, A. Ainla, D. Yang, D. Harburg, and G. M. Whitesides, “A soft tube-climbing robot,” *Soft Robot.*, vol. 5, no. 2, pp. 133–137, 2018.
[163] E. D. Demaine and J. O’Rourke, *Geometric folding algorithms: linkages, origami, polyhedra*. Cambridge university press, 2007.
[164] J. Li, H. Godaba, Z. Q. Zhang, C. C. Foo, and J. Zhu, “A soft active origami robot,” *Extreme Mech. Lett.*, vol. 24, pp. 30–37, 2018.
[165] L. Paez, G. Agarwal, and J. Paik, “Design and analysis of a soft pneumatic actuator with origami shell reinforcement,” *Soft Robot.*, vol. 3, no. 3, pp. 109–119, 2016.

[166] D. Rus and M. T. Tolley, “Design, fabrication and control of origami robots,” *Nat. Rev. Mater.*, vol. 3, no. 6, pp. 101–112, 2018.
[167] Y. Yang, Y. Chen, Y. Li, Z. Wang, and Y. Li, “Novel variable-stiffness robotic fingers with built-in position feedback,” *Soft Robot.*, vol. 4, no. 4, pp. 338–352, 2017.
[168] S. Yoshida, Y. Morimoto, L. Zheng, H. Onoe, and S. Takeuchi, “Multipoint bending and shape retention of a pneumatic bending actuator by a variable stiffness endoskeleton,” *Soft Robot.*, vol. 5, no. 6, pp. 718–725, 2018.
[169] Y. Li, Y. Chen, and Y. Li, “Distributed design of passive particle jamming based soft grippers,” in *2018 IEEE International Conference on Soft Robotics (RoboSoft)*, 2018, pp. 547–552.
[170] Y. Yang, Y. Zhang, Z. Kan, J. Zeng, and M. Y. Wang, “Hybrid jamming for bioinspired soft robotic fingers,” *Soft Robot.*, vol. 7, no. 3, pp. 292–308, 2020.
[171] A. A. Stokes, R. F. Shepherd, S. A. Morin, F. Ilievski, and G. M. Whitesides, “A hybrid combining hard and soft robots,” *Soft Robot.*, vol. 1, no. 1, pp. 70–74, 2014.
[172] M. Yu, W. Yang, Y. Yu, X. Cheng, and Z. Jiao, “A Crawling Soft Robot Driven by Pneumatic Foldable Actuators Based on Miura-Ori,” in *Actuators*, 2020, vol. 9, no. 2, p. 26.
[173] Y. Li, Y. Chen, T. Ren, Y. Li, and S. H. Choi, “Precharged pneumatic soft actuators and their applications to untethered soft robots,” *Soft Robot.*, vol. 5, no. 5, pp. 567–575, 2018.
[174] “Mold Making & Casting Materials | Rubbers, Plastics, Foams & More!,” *Smooth-On, Inc.* https://www.smooth-on.com/ (accessed Nov. 05, 2020).
[175] “Silane, Silicone & Metal-Organic Materials Innovation | Gelest.” https://www.gelest.com/ (accessed Sep. 02, 2020).
[176] “SYLGARD™ 184 Silicone Elastomer Kit | Dow Inc.” https://www.dow.com/en-us/pdp.sylgard-184-silicone-elastomer-kit.01064291z.html (accessed Nov. 05, 2020).
[177] “ELASTOSIL® M 4601 A/B | Room Temperature Curing Silicone Rubber (RTV-2) | Wacker Chemie AG,” *WACKER Website*. https://www.wacker.com/h/en-us/silicone-rubber/room-temperature-curing-silicone-rubber-rtv-2/elastosil-m-4601-ab/p/000018458 (accessed Nov. 05, 2020).
[178] Y. Yang and Y. Chen, “3D printing of smart materials for robotics with variable stiffness and position feedback,” in *2017 IEEE International Conference on Advanced Intelligent Mechatronics (AIM)*, 2017, pp. 418–423.
[179] S. Pourazadi, H. Bui, and C. Menon, “Investigation on a soft grasping gripper based on dielectric elastomer actuators,” *Smart Mater. Struct.*, vol. 28, no. 3, p. 035009, 2019.
[180] M. Luo *et al.*, “A single-chamber pneumatic soft bending actuator with increased stroke-range by local electric guidance,” *IEEE Trans. Ind. Electron.*, 2020.
[181] Y. Chen, Y. Li, Y. Li, and Y. Wang, “Stiffening of soft robotic actuators—Jamming approaches,” in *2017 IEEE International Conference on Real-time Computing and Robotics (RCAR)*, 2017, pp. 17–21.
[182] S. K. Yildiz, R. Mutlu, and G. Alici, “Fabrication and characterisation of highly stretchable elastomeric strain sensors for prosthetic hand applications,” *Sens. Actuators Phys.*, vol. 247, pp. 514–521, 2016.
[183] Y.-L. Park, C. Majidi, R. Kramer, P. Bérard, and R. J. Wood, “Hyperelastic pressure sensing with a liquid-embedded elastomer,” *J. Micromechanics Microengineering*, vol. 20, no. 12, p. 125029, 2010.

[184] D. Kwon *et al.*, “Highly sensitive, flexible, and wearable pressure sensor based on a giant piezocapacitive effect of three-dimensional microporous elastomeric dielectric layer,” *ACS Appl. Mater. Interfaces*, vol. 8, no. 26, pp. 16922–16931, 2016.
[185] J. C. Yeo and C. T. Lim, “Emerging flexible and wearable physical sensing platforms for healthcare and biomedical applications,” *Microsyst. Nanoeng.*, vol. 2, no. 1, pp. 1–19, 2016.
[186] H. Mai, R. Mutlu, C. Tawk, G. Alici, and V. Sencadas, “Ultra-stretchable MWCNT–Ecoflex piezoresistive sensors for human motion detection applications,” *Compos. Sci. Technol.*, vol. 173, pp. 118–124, 2019.
[187] Y. Elsayed *et al.*, “Finite element analysis and design optimization of a pneumatically actuating silicone module for robotic surgery applications,” *Soft Robot.*, vol. 1, no. 4, pp. 255–262, 2014.
[188] M. Calisti *et al.*, “Design and development of a soft robot with crawling and grasping capabilities,” in *2012 IEEE International Conference on Robotics and Automation*, 2012, pp. 4950–4955.
[189] M. Tian, Y. Xiao, X. Wang, J. Chen, and W. Zhao, “Design and experimental research of pneumatic soft humanoid robot hand,” in *Robot Intelligence Technology and Applications 4*, Springer, 2017, pp. 469–478.
[190] H. K. Yap, J. H. Lim, F. Nasrallah, J. Cho Hong Goh, and C.-H. Yeow, “Characterisation and evaluation of soft elastomeric actuators for hand assistive and rehabilitation applications,” *J. Med. Eng. Technol.*, vol. 40, no. 4, pp. 199–209, 2016.
[191] “momentive,” *MPMSitefinityCMS*. https://www.momentive.com/en-us (accessed Nov. 05, 2020).
[192] “Shin-Etsu Silicone : Offering a variety of silicone to industrial fields.” https://www.shinetsusilicone-global.com/index.shtml (accessed Nov. 05, 2020).
[193] “Recreus Filaflex | 3D Printing | 3D filament sale,” *Recreus*. https://recreus.com/en/ (accessed Nov. 05, 2020).
[194] “NinjaTek | NinjaFlex material is the leading flexible filament in the 3D printing industry.” https://ninjatek.com/ (accessed Nov. 05, 2020).
[195] “Stratasys: 3D Printing & Additive Manufacturing,” *Stratasys*. https://www.stratasys.com (accessed Nov. 05, 2020).
[196] S. Park *et al.*, “Silicones for stretchable and durable soft devices: beyond sylgard-184,” *ACS Appl. Mater. Interfaces*, vol. 10, no. 13, pp. 11261–11268, 2018.
[197] “Dow | The Materials Science Company | Explore Products.” https://www.dow.com/en-us (accessed Sep. 02, 2020).
[198] J. Shintake, S. Rosset, B. Schubert, S. Mintchev, D. Floreano, and H. Shea, “DEA for soft robotics: 1-gram actuator picks up a 60-gram egg,” in *Electroactive Polymer Actuators and Devices (EAPAD) 2015*, 2015, vol. 9430, p. 94301S.
[199] V. Alizadehyazdi, M. Bonthron, and M. Spenko, “An Electrostatic/Gecko-Inspired Adhesives Soft Robotic Gripper,” *IEEE Robot. Autom. Lett.*, vol. 5, no. 3, pp. 4679–4686, 2020.
[200] L. Cai *et al.*, “Super-stretchable, transparent carbon nanotube-based capacitive strain sensors for human motion detection,” *Sci. Rep.*, vol. 3, p. 3048, 2013.
[201] S.-J. Woo, J.-H. Kong, D.-G. Kim, and J.-M. Kim, “A thin all-elastomeric capacitive pressure sensor array based on micro-contact printed elastic conductors,” *J. Mater. Chem. C*, vol. 2, no. 22, pp. 4415–4422, 2014.

[202] H.-K. Lee, S.-I. Chang, and E. Yoon, “A flexible polymer tactile sensor: Fabrication and modular expandability for large area deployment,” *J. Microelectromechanical Syst.*, vol. 15, no. 6, pp. 1681–1686, 2006.
[203] E. L. White, J. C. Case, and R. K. Kramer, “Multi-mode strain and curvature sensors for soft robotic applications,” *Sens. Actuators Phys.*, vol. 253, pp. 188–197, 2017.
[204] E. J. Markvicka, R. Tutika, M. D. Bartlett, and C. Majidi, “Soft electronic skin for multi-site damage detection and localization,” *Adv. Funct. Mater.*, vol. 29, no. 29, p. 1900160, 2019.
[205] W. Tang *et al.*, “Customizing a self-healing soft pump for robot,” *Nat. Commun.*, vol. 12, no. 1, pp. 1–11, 2021.
[206] T.-P. Huynh, P. Sonar, and H. Haick, “Advanced materials for use in soft self-healing devices,” *Adv. Mater.*, vol. 29, no. 19, p. 1604973, 2017.
[207] S. Terryn, G. Mathijssen, J. Brancart, G. Van Assche, B. Vanderborght, and D. Lefeber, “Investigation of self-healing compliant actuators for robotics,” in *2015 IEEE International Conference on Robotics and Automation (ICRA)*, 2015, pp. 258–263.
[208] S. Terryn, J. Brancart, D. Lefeber, G. Van Assche, and B. Vanderborght, “Self-healing soft pneumatic robots,” *Sci Robot*, vol. 2, no. 9, 2017.
[209] R. A. Bilodeau and R. K. Kramer, “Self-healing and damage resilience for soft robotics: A review,” *Front. Robot. AI*, vol. 4, p. 48, 2017.
[210] K. C. Galloway *et al.*, “Soft robotic grippers for biological sampling on deep reefs,” *Soft Robot.*, vol. 3, no. 1, pp. 23–33, 2016.
[211] M. A. Robertson, H. Sadeghi, J. M. Florez, and J. Paik, “Soft pneumatic actuator fascicles for high force and reliability,” *Soft Robot.*, vol. 4, no. 1, pp. 23–32, 2017.
[212] T. Wienzek and A. Seibel, “Elastomeric prepregs for soft robotics applications,” *Adv. Eng. Mater.*, vol. 21, no. 5, p. 1801200, 2019.
[213] A. Galley, G. K. Knopf, and M. Kashkoush, “Pneumatic Hyperelastic Actuators for Grasping Curved Organic Objects,” in *Actuators*, 2019, vol. 8, no. 4, p. 76.
[214] S. Wakimoto, K. Suzumori, and K. Ogura, “Miniature pneumatic curling rubber actuator generating bidirectional motion with one air-supply tube,” *Adv. Robot.*, vol. 25, no. 9–10, pp. 1311–1330, 2011.
[215] K. Ogura, S. Wakimoto, K. Suzumori, and Y. Nishioka, “Micro pneumatic curling actuator-Nematode actuator,” in *2008 IEEE International Conference on Robotics and Biomimetics*, 2009, pp. 462–467.
[216] V. Subramaniam, S. Jain, J. Agarwal, and P. Valdivia y Alvarado, “Design and characterization of a hybrid soft gripper with active palm pose control,” *Int. J. Robot. Res.*, p. 0278364920918918, 2020.
[217] J. Goff, S. Sulaiman, B. Arkles, and J. P. Lewicki, “Soft materials with recoverable shape factors from extreme distortion states,” *Adv. Mater.*, vol. 28, no. 12, pp. 2393–2398, 2016.
[218] W. Hu and G. Alici, “Bioinspired Three-Dimensional-Printed Helical Soft Pneumatic Actuators and Their Characterization,” *Soft Robot.*, vol. 7, no. 3, pp. 267–282, 2020.
[219] C. Du Pasquier, T. Chen, S. Tibbits, and K. Shea, “Design and computational modeling of a 3D printed pneumatic toolkit for soft robotics,” *Soft Robot.*, vol. 6, no. 5, pp. 657–663, 2019.
[220] Y. Chen, Z. Xia, and Q. Zhao, “Optimal design of soft pneumatic bending actuators subjected to design-dependent pressure loads,” *IEEEASME Trans. Mechatron.*, 2019.

[221] K.-J. Cho, J.-S. Koh, S. Kim, W.-S. Chu, Y. Hong, and S.-H. Ahn, "Review of manufacturing processes for soft biomimetic robots," *Int. J. Precis. Eng. Manuf.*, vol. 10, no. 3, pp. 171–181, 2009.
[222] G. Alici, T. Canty, R. Mutlu, W. Hu, and V. Sencadas, "Modeling and experimental evaluation of bending behavior of soft pneumatic actuators made of discrete actuation chambers," *Soft Robot.*, vol. 5, no. 1, pp. 24–35, 2018.
[223] S. A. Morin, R. F. Shepherd, S. W. Kwok, A. A. Stokes, A. Nemiroski, and G. M. Whitesides, "Camouflage and display for soft machines," *Science*, vol. 337, no. 6096, pp. 828–832, 2012.
[224] F. Schmitt, O. Piccin, L. Barbé, and B. Bayle, "Soft robots manufacturing: a review," *Front. Robot. AI*, vol. 5, p. 84, 2018.
[225] R. Mutlu, C. Tawk, G. Alici, and E. Sariyildiz, "A 3D printed monolithic soft gripper with adjustable stiffness," in *IECON 2017-43rd Annual Conference of the IEEE Industrial Electronics Society*, 2017, pp. 6235–6240.
[226] B. N. Peele, T. J. Wallin, H. Zhao, and R. F. Shepherd, "3D printing antagonistic systems of artificial muscle using projection stereolithography," *Bioinspir. Biomim.*, vol. 10, no. 5, p. 055003, 2015.
[227] F. Liravi and E. Toyserkani, "Additive manufacturing of silicone structures: A review and prospective," *Addit. Manuf.*, vol. 24, pp. 232–242, 2018.
[228] T. J. Wallin, J. Pikul, and R. F. Shepherd, "3D printing of soft robotic systems," *Nat. Rev. Mater.*, vol. 3, no. 6, pp. 84–100, 2018.
[229] J. Z. Gul *et al.*, "3D printing for soft robotics–a review," *Sci. Technol. Adv. Mater.*, vol. 19, no. 1, pp. 243–262, 2018.
[230] Y. Shapiro, A. Wolf, and K. Gabor, "Bi-bellows: Pneumatic bending actuator," *Sens. Actuators Phys.*, vol. 167, no. 2, pp. 484–494, 2011.
[231] T. Shao, L. Zhang, G. Bao, X. Luo, and Q. Yang, "Basic characteristics of a new flexible pneumatic bending joint," *Chin. J. Mech. Eng.*, vol. 27, no. 6, pp. 1143–1149, 2014.
[232] J. Shintake, V. Cacucciolo, H. Shea, and D. Floreano, "Soft biomimetic fish robot made of dielectric elastomer actuators," *Soft Robot.*, vol. 5, no. 4, pp. 466–474, 2018.
[233] K. M. de Payrebrune and O. M. O'Reilly, "On constitutive relations for a rod-based model of a pneu-net bending actuator," *Extreme Mech. Lett.*, vol. 8, pp. 38–46, 2016.
[234] G. S. Chirikjian and J. W. Burdick, "A modal approach to hyper-redundant manipulator kinematics," *IEEE Trans. Robot. Autom.*, vol. 10, no. 3, pp. 343–354, 1994.
[235] D. Trivedi, A. Lotfi, and C. D. Rahn, "Geometrically exact models for soft robotic manipulators," *IEEE Trans. Robot.*, vol. 24, no. 4, pp. 773–780, 2008.
[236] P. Polygerinos *et al.*, "Modeling of soft fiber-reinforced bending actuators," *IEEE Trans. Robot.*, vol. 31, no. 3, pp. 778–789, 2015.
[237] Z. Wang and S. Hirai, "Soft gripper dynamics using a line-segment model with an optimization-based parameter identification method," *IEEE Robot. Autom. Lett.*, vol. 2, no. 2, pp. 624–631, 2017.
[238] G. Decroly, B. Mertens, P. Lambert, and A. Delchambre, "Design, characterization and optimization of a soft fluidic actuator for minimally invasive surgery," *Int. J. Comput. Assist. Radiol. Surg.*, vol. 15, no. 2, pp. 333–340, 2020.
[239] P. Moseley, J. M. Florez, H. A. Sonar, G. Agarwal, W. Curtin, and J. Paik, "Modeling, design, and development of soft pneumatic actuators with finite element method," *Adv. Eng. Mater.*, vol. 18, no. 6, pp. 978–988, 2016.

[240] O. H. Yeoh, “Some forms of the strain energy function for rubber,” *Rubber Chem. Technol.*, vol. 66, no. 5, pp. 754–771, 1993.
[241] M. Mooney, “A theory of large elastic deformation,” *J. Appl. Phys.*, vol. 11, no. 9, pp. 582–592, 1940.
[242] R. W. Ogden, “Large deformation isotropic elasticity–on the correlation of theory and experiment for incompressible rubberlike solids,” *Proc. R. Soc. Lond. Math. Phys. Sci.*, vol. 326, no. 1567, pp. 565–584, 1972.
[243] O. H. Yeoh, “Characterization of elastic properties of carbon-black-filled rubber vulcanizates,” *Rubber Chem. Technol.*, vol. 63, no. 5, pp. 792–805, 1990.
[244] L. Marechal, P. Balland, L. Lindenroth, F. Petrou, C. Kontovounisios, and F. Bello, “Toward a Common Framework and Database of Materials for Soft Robotics,” *Soft Robot.*, 2020.
[245] J. L. Sparks *et al.*, “Use of silicone materials to simulate tissue biomechanics as related to deep tissue injury,” *Adv. Skin Wound Care*, vol. 28, no. 2, pp. 59–68, 2015.
[246] G. Agarwal, N. Besuchet, B. Audergon, and J. Paik, “Stretchable materials for robust soft actuators towards assistive wearable devices,” *Sci. Rep.*, vol. 6, no. 1, pp. 1–8, 2016.
[247] R. V. Martinez *et al.*, “Robotic tentacles with three-dimensional mobility based on flexible elastomers,” *Adv. Mater.*, vol. 25, no. 2, pp. 205–212, 2013.
[248] S. Sareh *et al.*, “Anchoring like octopus: biologically inspired soft artificial sucker,” *J. R. Soc. Interface*, vol. 14, no. 135, p. 20170395, 2017.
[249] D. Steck, J. Qu, S. B. Kordmahale, D. Tscharnuter, A. Muliana, and J. Kameoka, “Mechanical responses of Ecoflex silicone rubber: Compressible and incompressible behaviors,” *J. Appl. Polym. Sci.*, vol. 136, no. 5, p. 47025, 2019.
[250] G. Runge, M. Wiese, L. Günther, and A. Raatz, “A framework for the kinematic modeling of soft material robots combining finite element analysis and piecewise constant curvature kinematics,” in *2017 3rd International Conference on Control, Automation and Robotics (ICCAR)*, 2017, pp. 7–14.
[251] A. M. Nasab, A. Sabzehzar, M. Tatari, C. Majidi, and W. Shan, “A soft gripper with rigidity tunable elastomer strips as ligaments,” *Soft Robot.*, vol. 4, no. 4, pp. 411–420, 2017.
[252] F. Pineda, F. Bottausci, B. Icard, L. Malaquin, and Y. Fouillet, “Using electrofluidic devices as hyper-elastic strain sensors: Experimental and theoretical analysis,” *Microelectron. Eng.*, vol. 144, pp. 27–31, 2015.
[253] J. K. Lee, N. Stoffel, and K. Fite, “Electronic packaging of sensors for lower limb prosthetics,” in *2012 IEEE 62nd Electronic Components and Technology Conference*, 2012, pp. 86–91.
[254] O. Byrne *et al.*, “Additive manufacture of composite soft pneumatic actuators,” *Soft Robot.*, vol. 5, no. 6, pp. 726–736, 2018.
[255] K. Batsuren and D. Yun, “Soft robotic gripper with chambered fingers for performing in-hand manipulation,” *Appl. Sci.*, vol. 9, no. 15, p. 2967, 2019.
[256] J.-H. Low, M. H. Ang, and C.-H. Yeow, “Customizable soft pneumatic finger actuators for hand orthotic and prosthetic applications,” in *2015 IEEE International Conference on Rehabilitation Robotics (ICORR)*, 2015, pp. 380–385.
[257] K. H. Heung, R. K. Tong, A. T. Lau, and Z. Li, “Robotic glove with soft-elastic composite actuators for assisting activities of daily living,” *Soft Robot.*, vol. 6, no. 2, pp. 289–304, 2019.

[258] M. Al-Rubaiai, T. Pinto, C. Qian, and X. Tan, “Soft actuators with stiffness and shape modulation using 3D-printed conductive polylactic acid material,” *Soft Robot.*, vol. 6, no. 3, pp. 318–332, 2019.
[259] Z. Zhang, X. Wang, H. Liu, B. Liang, and S. Wang, “Kinematic Analysis of Novel Soft Robotic Arm Based on Virtual Work Principle,” in *2018 IEEE International Conference on Robotics and Biomimetics (ROBIO)*, 2018, pp. 984–990.
[260] C. Yang, R. Kang, D. T. Branson, L. Chen, and J. S. Dai, “Kinematics and statics of eccentric soft bending actuators with external payloads,” *Mech. Mach. Theory*, vol. 139, pp. 526–541, 2019.
[261] T. Wang, L. Ge, and G. Gu, “Programmable design of soft pneu-net actuators with oblique chambers can generate coupled bending and twisting motions,” *Sens. Actuators Phys.*, vol. 271, pp. 131–138, 2018.
[262] W. Hu, R. Mutlu, W. Li, and G. Alici, “A structural optimisation method for a soft pneumatic actuator,” *robotics*, vol. 7, no. 2, p. 24, 2018.
[263] Y. Zhang *et al.*, “A Mechatronics-Embedded Pneumatic Soft Modular Robot Powered via Single Air Tube,” *Appl. Sci.*, vol. 9, no. 11, p. 2260, 2019.
[264] C. Tawk, G. M. Spinks, M. in het Panhuis, and G. Alici, “3D Printable Linear Soft Vacuum Actuators: Their Modeling, Performance Quantification and Application in Soft Robotic Systems,” *IEEEASME Trans. Mechatron.*, vol. 24, no. 5, pp. 2118–2129, 2019.
[265] C. Tawk, A. Gillett, M. in het Panhuis, G. M. Spinks, and G. Alici, “A 3D-printed omni-purpose soft gripper,” *IEEE Trans. Robot.*, vol. 35, no. 5, pp. 1268–1275, 2019.
[266] J. Allard *et al.*, “Sofa-an open source framework for medical simulation,” 2007.
[267] Y. Payan, *Soft tissue biomechanical modeling for computer assisted surgery*, vol. 11. Springer, 2012.
[268] M. Thieffry, A. Kruszewski, T.-M. Guerra, and C. Duriez, “Reduced order control of soft robots with guaranteed stability,” in *2018 European Control Conference (ECC)*, 2018, pp. 635–640.
[269] E. Coevoet *et al.*, “Software toolkit for modeling, simulation, and control of soft robots,” *Adv. Robot.*, vol. 31, no. 22, pp. 1208–1224, 2017.
[270] K. Wu and G. Zheng, “Simulation and control co-design methodology for soft robotics”.
[271] M. Pozzi *et al.*, “Efficient fem-based simulation of soft robots modeled as kinematic chains,” in *2018 IEEE international conference on robotics and automation (ICRA)*, 2018, pp. 1–8.
[272] F. S. Sin, D. Schroeder, and J. Barbič, “Vega: non-linear FEM deformable object simulator,” in *Computer Graphics Forum*, 2013, vol. 32, no. 1, pp. 36–48.
[273] J. Sanchez, C. M. Mateo, J. A. Corrales, B.-C. Bouzgarrou, and Y. Mezouar, “Online shape estimation based on tactile sensing and deformation modeling for robot manipulation,” in *2018 IEEE/RSJ International Conference on Intelligent Robots and Systems (IROS)*, 2018, pp. 504–511.
[274] J. Hiller and H. Lipson, “Dynamic simulation of soft multimaterial 3d-printed objects,” *Soft Robot.*, vol. 1, no. 1, pp. 88–101, 2014.
[275] N. Cheney, R. MacCurdy, J. Clune, and H. Lipson, “Unshackling evolution: evolving soft robots with multiple materials and a powerful generative encoding,” in *Proceedings of the 15th annual conference on Genetic and evolutionary computation*, 2013, pp. 167–174.
[276] S. Kriegman, C. Cappelle, F. Corucci, A. Bernatskiy, N. Cheney, and J. C. Bongard, “Simulating the evolution of soft and rigid-body robots,” in *Proceedings*

of the Genetic and Evolutionary Computation Conference Companion, 2017, pp. 1117–1120.

[277] K.-H. Lee *et al.*, "Nonparametric online learning control for soft continuum robot: An enabling technique for effective endoscopic navigation," *Soft Robot.*, vol. 4, no. 4, pp. 324–337, 2017.

[278] T. G. Thuruthel, B. Shih, C. Laschi, and M. T. Tolley, "Soft robot perception using embedded soft sensors and recurrent neural networks," *Sci. Robot.*, vol. 4, no. 26, 2019.

[279] M. Giorelli, F. Renda, M. Calisti, A. Arienti, G. Ferri, and C. Laschi, "Learning the inverse kinetics of an octopus-like manipulator in three-dimensional space," *Bioinspir. Biomim.*, vol. 10, no. 3, p. 035006, 2015.

[280] M. Li, R. Kang, D. T. Branson, and J. S. Dai, "Model-free control for continuum robots based on an adaptive Kalman filter," *IEEEASME Trans. Mechatron.*, vol. 23, no. 1, pp. 286–297, 2017.

[281] Z. Zhang, T. M. Bieze, J. Dequidt, A. Kruszewski, and C. Duriez, "Visual servoing control of soft robots based on finite element model," in *2017 IEEE/RSJ International Conference on Intelligent Robots and Systems (IROS)*, 2017, pp. 2895–2901.

[282] P. Hyatt, D. Kraus, V. Sherrod, L. Rupert, N. Day, and M. D. Killpack, "Configuration estimation for accurate position control of large-scale soft robots," *IEEEASME Trans. Mechatron.*, vol. 24, no. 1, pp. 88–99, 2018.

[283] T. Watanabe, K. Yamazaki, and Y. Yokokohji, "Survey of robotic manipulation studies intending practical applications in real environments-object recognition, soft robot hand, and challenge program and benchmarking," *Adv. Robot.*, vol. 31, no. 19–20, pp. 1114–1132, 2017.

[284] S. Rosset and H. R. Shea, "Flexible and stretchable electrodes for dielectric elastomer actuators," *Appl. Phys. A*, vol. 110, no. 2, pp. 281–307, 2013.

[285] C. Wang *et al.*, "Soft ultrathin electronics innervated adaptive fully soft robots," *Adv. Mater.*, vol. 30, no. 13, p. 1706695, 2018.

[286] Y. Hu *et al.*, "A bioinspired multi-functional wearable sensor with an integrated light-induced actuator based on an asymmetric graphene composite film," *J. Mater. Chem. C*, vol. 7, no. 23, pp. 6879–6888, 2019.

[287] R. Tabassian *et al.*, "Graphene Mesh for Self-Sensing Ionic Soft Actuator Inspired from Mechanoreceptors in Human Body," *Adv. Sci.*, vol. 6, no. 23, p. 1901711, 2019.

[288] E. Sachyani Keneth *et al.*, "Pre-programmed Tri-layer Electro-Thermal Actuators Composed of Shape Memory Polymer and Carbon Nanotubes," *Soft Robot.*, vol. 7, no. 2, pp. 123–129, 2020.

[289] M. Amjadi and M. Sitti, "Self-Sensing Paper Actuators Based on Graphite–Carbon Nanotube Hybrid Films," *Adv. Sci.*, vol. 5, no. 7, p. 1800239, 2018.

[290] D. McCoul, W. Hu, M. Gao, V. Mehta, and Q. Pei, "Recent advances in stretchable and transparent electronic materials," *Adv. Electron. Mater.*, vol. 2, no. 5, p. 1500407, 2016.

[291] T. H. Yang, J. Shintake, R. Kanno, C. R. Kao, and J. Mizuno, "Low-Cost Sensor-Rich Fluidic Elastomer Actuators Embedded with Paper Electronics," *Adv. Intell. Syst.*, p. 2000025.

[292] S. S. Robinson *et al.*, "Integrated soft sensors and elastomeric actuators for tactile machines with kinesthetic sense," *Extreme Mech. Lett.*, vol. 5, pp. 47–53, 2015.

[293] H. Zhao, K. O'Brien, S. Li, and R. F. Shepherd, "Optoelectronically innervated soft prosthetic hand via stretchable optical waveguides," *Sci. Robot.*, vol. 1, no. 1, 2016.

[294] S. Ozel, N. A. Keskin, D. Khea, and C. D. Onal, "A precise embedded curvature sensor module for soft-bodied robots," *Sens. Actuators Phys.*, vol. 236, pp. 349–356, 2015.
[295] Z. Wang and S. Hirai, "A 3D printed soft gripper integrated with curvature sensor for studying soft grasping," in *2016 IEEE/SICE International Symposium on System Integration (SII)*, 2016, pp. 629–633.
[296] D. H. Kim, S. W. Lee, and H.-S. Park, "Sensor evaluation for soft robotic hand rehabilitation devices," in *2016 6th IEEE International Conference on Biomedical Robotics and Biomechatronics (BioRob)*, 2016, pp. 1220–1223.
[297] J. Jung, M. Park, D. Kim, and Y.-L. Park, "Optically sensorized elastomer air chamber for proprioceptive sensing of soft pneumatic actuators," *IEEE Robot. Autom. Lett.*, vol. 5, no. 2, pp. 2333–2340, 2020.
[298] S. Ozel *et al.*, "A composite soft bending actuation module with integrated curvature sensing," in *2016 IEEE International Conference on Robotics and Automation (ICRA)*, 2016, pp. 4963–4968.
[299] W. Tao, E. H. Skorina, F. Chen, J. McInnis, M. Luo, and C. D. Onal, "Bioinspired design and fabrication principles of reliable fluidic soft actuation modules," in *2015 IEEE International Conference on Robotics and Biomimetics (ROBIO)*, 2015, pp. 2169–2174.
[300] M. Luo *et al.*, "Toward modular soft robotics: Proprioceptive curvature sensing and sliding-mode control of soft bidirectional bending modules," *Soft Robot.*, vol. 4, no. 2, pp. 117–125, 2017.
[301] B. E. Schubert and D. Floreano, "Variable stiffness material based on rigid low-melting-point-alloy microstructures embedded in soft poly (dimethylsiloxane)(PDMS)," *Rsc Adv.*, vol. 3, no. 46, pp. 24671–24679, 2013.
[302] Y. Elsayed, C. Lekakou, T. Geng, and C. M. Saaj, "Design optimisation of soft silicone pneumatic actuators using finite element analysis," in *2014 IEEE/ASME International Conference on Advanced Intelligent Mechatronics*, 2014, pp. 44–49.
[303] K. Deb, A. Pratap, S. Agarwal, and T. Meyarivan, "A fast and elitist multiobjective genetic algorithm: NSGA-II," *IEEE Trans. Evol. Comput.*, vol. 6, no. 2, pp. 182–197, 2002.
[304] A. F. Release, "16.2, ANSYS® Academic Research, Help System," *Fluent Theory User's Guide*, 2016.
[305] R. R. Ma and A. M. Dollar, "On dexterity and dexterous manipulation," in *2011 15th International Conference on Advanced Robotics (ICAR)*, 2011, pp. 1–7.
[306] N. C. Dafle *et al.*, "Extrinsic dexterity: In-hand manipulation with external forces," in *2014 IEEE International Conference on Robotics and Automation (ICRA)*, 2014, pp. 1578–1585.
[307] R. R. Ma and A. M. Dollar, "An underactuated hand for efficient finger-gaiting-based dexterous manipulation," in *2014 IEEE International Conference on Robotics and Biomimetics (ROBIO 2014)*, 2014, pp. 2214–2219.
[308] B. Sundaralingam and T. Hermans, "Geometric in-hand regrasp planning: Alternating optimization of finger gaits and in-grasp manipulation," in *2018 IEEE International Conference on Robotics and Automation (ICRA)*, 2018, pp. 231–238.
[309] N. Chavan-Dafle and A. Rodriguez, "Prehensile pushing: In-hand manipulation with push-primitives," in *2015 IEEE/RSJ International Conference on Intelligent Robots and Systems (IROS)*, 2015, pp. 6215–6222.
[310] Z. Doulgeri and L. Droukas, "On rolling contact motion by robotic fingers via prescribed performance control," in *2013 IEEE International Conference on Robotics and Automation*, 2013, pp. 3976–3981.

[311] J. Shi, J. Z. Woodruff, P. B. Umbanhowar, and K. M. Lynch, "Dynamic in-hand sliding manipulation," *IEEE Trans. Robot.*, vol. 33, no. 4, pp. 778–795, 2017.
[312] "Dexterous Hand Series – Shadow Robot Company." https://www.shadowrobot.com/dexterous-hand-series/ (accessed Dec. 02, 2020).
[313] O. M. Andrychowicz *et al.*, "Learning dexterous in-hand manipulation," *Int. J. Robot. Res.*, vol. 39, no. 1, pp. 3–20, 2020.
[314] J. Zhou *et al.*, "A soft-robotic approach to anthropomorphic robotic hand dexterity," *IEEE Access*, vol. 7, pp. 101483–101495, 2019.
[315] B. Shih *et al.*, "Custom soft robotic gripper sensor skins for haptic object visualization," in *2017 IEEE/RSJ international conference on intelligent robots and systems (IROS)*, 2017, pp. 494–501.
[316] J. Zhou, J. Yi, X. Chen, Z. Liu, and Z. Wang, "BCL-13: A 13-DOF Soft Robotic Hand for Dexterous Grasping and In-Hand Manipulation," *IEEE Robot. Autom. Lett.*, vol. 3, no. 4, pp. 3379–3386, Oct. 2018, doi: 10.1109/LRA.2018.2851360.
[317] C. Della Santina, G. Grioli, M. Catalano, A. Brando, and A. Bicchi, "Dexterity augmentation on a synergistic hand: the Pisa/IIT SoftHand+," in *2015 IEEE-RAS 15th International Conference on Humanoid Robots (Humanoids)*, 2015, pp. 497–503.
[318] H. Liu *et al.*, "Multisensory five-finger dexterous hand: The DLR/HIT Hand II," in *2008 IEEE/RSJ international conference on intelligent robots and systems*, 2008, pp. 3692–3697.
[319] A. M. Okamura, N. Smaby, and M. R. Cutkosky, "An overview of dexterous manipulation," in *Proceedings 2000 ICRA. Millennium Conference. IEEE International Conference on Robotics and Automation. Symposia Proceedings (Cat. No. 00CH37065)*, 2000, vol. 1, pp. 255–262.
[320] S. M. Mustaza, Y. Elsayed, C. Lekakou, C. Saaj, and J. Fras, "Dynamic modeling of fiber-reinforced soft manipulator: A visco-hyperelastic material-based continuum mechanics approach," *Soft Robot.*, vol. 6, no. 3, pp. 305–317, 2019.
[321] C. Lekakou, Y. Elsayed, T. Geng, and C. M. Saaj, "Skins and sleeves for soft robotics: inspiration from nature and architecture," *Adv. Eng. Mater.*, vol. 17, no. 8, pp. 1180–1188, 2015.
[322] Z. Kappassov, J.-A. Corrales, and V. Perdereau, "Tactile sensing in dexterous robot hands," *Robot. Auton. Syst.*, vol. 74, pp. 195–220, 2015.
[323] Y. L. Yap, S. L. Sing, and W. Y. Yeong, "A review of 3D printing processes and materials for soft robotics," *Rapid Prototyp. J.*, 2020.
[324] S. Li, H. Zhao, and R. F. Shepherd, "Flexible and stretchable sensors for fluidic elastomer actuated soft robots," *Mrs Bull.*, vol. 42, no. 2, pp. 138–142, 2017.
[325] H. Yousef, M. Boukallel, and K. Althoefer, "Tactile sensing for dexterous in-hand manipulation in robotics—A review," *Sens. Actuators Phys.*, vol. 167, no. 2, pp. 171–187, 2011.
[326] A. Koivikko, E. S. Raei, M. Mosallaei, M. Mäntysalo, and V. Sariola, "Screen-printed curvature sensors for soft robots," *IEEE Sens. J.*, vol. 18, no. 1, pp. 223–230, 2017.
[327] D. J. Lipomi, J. A. Lee, M. Vosgueritchian, B. C.-K. Tee, J. A. Bolander, and Z. Bao, "Electronic properties of transparent conductive films of PEDOT: PSS on stretchable substrates," *Chem. Mater.*, vol. 24, no. 2, pp. 373–382, 2012.
[328] S. Y. Kim, S. Park, H. W. Park, D. H. Park, Y. Jeong, and D. H. Kim, "Highly sensitive and multimodal all-carbon skin sensors capable of simultaneously detecting tactile and biological stimuli," *Adv. Mater.*, vol. 27, no. 28, pp. 4178–4185, 2015.

[329] J. Gafford *et al.*, “Shape deposition manufacturing of a soft, atraumatic, deployable surgical grasper,” *J. Med. Devices*, vol. 8, no. 3, 2014.
[330] M.-Y. Cheng, C.-M. Tsao, and Y.-J. Yang, “An anthropomorphic robotic skin using highly twistable tactile sensing array,” in *2010 5th IEEE Conference on Industrial Electronics and Applications*, 2010, pp. 650–655.
[331] V. Ho and S. Hirai, “Design and analysis of a soft-fingered hand with contact feedback,” *IEEE Robot. Autom. Lett.*, vol. 2, no. 2, pp. 491–498, 2016.
[332] A. Ramadan Suleiman and M. L. Nehdi, “Modeling self-healing of concrete using hybrid genetic algorithm–artificial neural network,” *Materials*, vol. 10, no. 2, p. 135, 2017.
[333] R. Wei, K. Ouyang, X. Bao, X. Gao, and C. Chen, “High-precision smart calibration system for temperature sensors,” *Sens. Actuators Phys.*, vol. 297, p. 111561, 2019.
[334] A. M. Almassri, W. Z. Wan Hasan, S. A. Ahmad, S. Shafie, C. Wada, and K. Horio, “Self-calibration algorithm for a pressure sensor with a real-time approach based on an artificial neural network,” *Sensors*, vol. 18, no. 8, p. 2561, 2018.
[335] J. Ye, Z. Lin, J. You, S. Huang, and H. Wu, “Inconsistency calibrating algorithms for large scale piezoresistive electronic skin,” *Micromachines*, vol. 11, no. 2, p. 162, 2020.
[336] N. Ni and L. Zhang, “Dielectric elastomer sensors,” *Elastomers Intechopen Publ. Lond. UK*, pp. 231–253, 2017.
[337] “Bare Conductive.” https://www.bareconductive.com/ (accessed Aug. 30, 2021).
[338] M. Teyssier, G. Bailly, C. Pelachaud, E. Lecolinet, A. Conn, and A. Roudaut, “Skin-on interfaces: A bio-driven approach for artificial skin design to cover interactive devices,” in *Proceedings of the 32nd Annual ACM Symposium on User Interface Software and Technology*, 2019, pp. 307–322.
[339] A. Pagoli, F. Chapelle, J. A. C. Ramon, Y. Mezouar, and Y. Lapusta, “A Soft Robotic Gripper with an Active Palm and Reconfigurable Fingers for Fully Dexterous In-Hand Manipulation,” *IEEE Robot. Autom. Lett.*, 2021.
[340] R. Hecht-Nielsen, “Theory of the backpropagation neural network,” in *Neural networks for perception*, Elsevier, 1992, pp. 65–93.
[341] K. Elsayed and C. Lacor, “Modeling, analysis and optimization of aircyclones using artificial neural network, response surface methodology and CFD simulation approaches,” *Powder Technol.*, vol. 212, no. 1, pp. 115–133, 2011.
[342] J. Fras and K. Althoefer, “Soft fiber-reinforced pneumatic actuator design and fabrication: Towards robust, soft robotic systems,” in *Annual Conference Towards Autonomous Robotic Systems*, 2019, pp. 103–114.
[343] F. Schmitt, O. Piccin, B. Bayle, P. Renaud, and L. Barbé, “Inverted Honeycomb Cell as a Reinforcement Structure for Building Soft Pneumatic Linear Actuators,” *J. Mech. Robot.*, vol. 13, no. 1, p. 011020, 2021.
[344] S. Sun *et al.*, “A compact variable stiffness and damping shock absorber for vehicle suspension,” *IEEEASME Trans. Mechatron.*, vol. 20, no. 5, pp. 2621–2629, 2015.
[345] M. Eshaghi, R. Sedaghati, and S. Rakheja, “Dynamic characteristics and control of magnetorheological/electrorheological sandwich structures: a state-of-the-art review,” *J. Intell. Mater. Syst. Struct.*, vol. 27, no. 15, pp. 2003–2037, 2016.